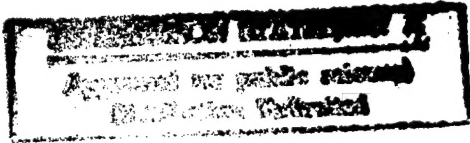



REPORT DOCUMENTATION PAGE			Form Approved OMB No. 0704-0188	
Public reporting burden for this collection of information is estimated to average 1 hour per response, including the time for reviewing instructions, searching existing data sources, gathering and maintaining the data needed, and completing and reviewing the collection of information. Send comments regarding this burden estimate or any other aspect of this collection of information, including suggestions for reducing this burden, to Washington Headquarters Services, Directorate for Information Operations and Reports, 1215 Jefferson Davis Highway, Suite 1204, Arlington, VA 22202-4302, and to the Office of Management and Budget, Paperwork Reduction Project (0704-0188), Washington, DC 20503.				
1. AGENCY USE ONLY (Leave blank)		2. REPORT DATE 11 September 1998		3. REPORT TYPE AND DATES COVERED
4. TITLE AND SUBTITLE THE DEVELOPEMENT OF A SEASONAL CLIMATE FORECAST METHODOLOGY FOR ITCZ ASSOCIATED RAINFALL APPLIED TO EASTERN AFRICA			5. FUNDING NUMBERS	
6. AUTHOR(S) RONALD PAUL LOWTHER				
7. PERFORMING ORGANIZATION NAME(S) AND ADDRESS(ES) TEXAS A&M UNIVERSITY			8. PERFORMING ORGANIZATION REPORT NUMBER 98-030D	
9. SPONSORING/MONITORING AGENCY NAME(S) AND ADDRESS(ES) THE DEPARTMENT OF THE AIR FORCE AFIT/CIA, BLDG 125 2950 P STREET WPAFB OH 45433			10. SPONSORING/MONITORING AGENCY REPORT NUMBER	
11. SUPPLEMENTARY NOTES				
12a. DISTRIBUTION AVAILABILITY STATEMENT Unlimited distribution In Accordance With 35-205/AFIT Sup 1			12b. DISTRIBUTION CODE	
13. ABSTRACT (Maximum 200 words)				
 				
14. SUBJECT TERMS			15. NUMBER OF PAGES 161	
			16. PRICE CODE	
17. SECURITY CLASSIFICATION OF REPORT	18. SECURITY CLASSIFICATION OF THIS PAGE	19. SECURITY CLASSIFICATION OF ABSTRACT	20. LIMITATION OF ABSTRACT	

THE DEVELOPMENT OF A
SEASONAL CLIMATE FORECAST METHODOLOGY FOR
ITCZ ASSOCIATED RAINFALL APPLIED TO EASTERN AFRICA

A Dissertation

by

RONALD PAUL LOWTHER

Submitted to the Office of Graduate Studies of
Texas A&M University
in partial fulfillment of the requirements for the degree of
DOCTOR OF PHILOSOPHY

December 1998

Major Subject: Meteorology

19980915 022

THE DEVELOPMENT OF A
SEASONAL CLIMATE FORECAST METHODOLOGY FOR
ITCZ ASSOCIATED RAINFALL APPLIED TO EASTERN AFRICA

A Dissertation

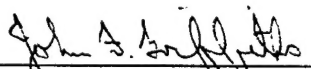
by


RONALD PAUL LOWTHER

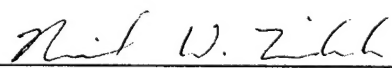
Submitted to Texas A&M University
in partial fulfillment of the requirements
for the degree of


DOCTOR OF PHILOSOPHY


Approved as to style and content by:


Joan F. Griffiths
(Chair of Committee)


Gerald R. North
(Member)


Neil W. Tindale
(Member)


Bakama B. Bakama
(Member)


Gerald R. North
(Head of Department)

December 1998

Major Subject: Meteorology

ABSTRACT

The Development of a Seasonal Climate Forecast Methodology for
ITCZ Associated Rainfall Applied to Eastern Africa. (December 1998)

Ronald Paul Lowther, B.S., Chapman College;

M.S., Texas A&M University

Chair of Advisory Committee: Prof. John F. Griffiths

A detailed examination is performed of Inter-Tropical Convergence Zone (ITCZ) associated rainfall over Eastern Africa. A methodology is developed for seasonal climate forecasting of ITCZ-associated rainfall which shows reasonably dependable predictability. Using this methodology, rainfall probability decision flowcharts are produced which are simple enough to use in seasonal forecast efforts by a variety of users. Their purpose is to provide improved predictive guidelines for forecasting either actual rainfall amounts or for an indication of rainfall trends three months in advance.

Also explored is whether rainfall trends during the passage of the ITCZ can be determined by examining rainfall trends which occur earlier as the ITCZ traverses a region. The area of research is divided into four seasonal rainfall patterns, within four regions, corresponding to the latitudinal displacement of the ITCZ. The data are examined based on preceding conditions and minimal statistical assumptions and relationships are formulated within regions and between seasons.

A time series visualization of ITCZ-associated rainfall data is created by combining the regional indices for all four regions in sequential order through the period of study. Key relationships are found after examining the first-difference transformation of this seasonal time series. By examining the change (or first-difference transformation) between the rainfall indices of two regions, as they are traversed by the ITCZ, it is found that a forecast for the next region traversed can be

made. It is further found that these predictive relationships can be improved upon towards the extremes of the data distributions and, during certain periods, associated with known teleconnections. Also explored is whether ITCZ-associated rainfall is influenced by insolation forcing and, whether or not any trends are evident in the rainfall record that may be attributable to climate change.

This methodology may be used in rainfall forecast efforts to reduce risks in potentially "poor" years and maximize gains in potentially "good" years. The predictive results have direct relevance to many endeavors such as agricultural production and economics; and, the same methodology may be applicable to other tropical areas with similar monsoonal-type regimes.

DEDICATION

This dissertation is dedicated to my wife, Sue, for all her love and devotion. For without her, I would have no dreams or aspirations. She is the reason for all the successes in my life and, for this reason, this dissertation is really the result of her work.

ACKNOWLEDGEMENTS

I would like to thank the members of my research committee, Professor John Griffiths, Dr. Gerald North, Dr. Neil Tindale, and Dr. Bakama BakamaNume, for the help and encouragement that they have given over the course of this study. I give especial thanks to my committee chair, Prof. John Griffiths, who is the reason I returned to Texas A&M to further my studies. His assistance as my mentor and friendship as my friend will always be cherished. I wish him all the best in his retirement years.

Thanks are also due to the United States Air Force for funding my studies and career. I thank Dr. Kwang-Yul Kim for his assistance during my defense and I thank Mr. Robert White for his invaluable computer and network assistance. I am also very much appreciative of the Meteorology Department staff and faculty for their help and support and the creation of a great learning environment.

TABLE OF CONTENTS

	Page
ABSTRACT.....	iii
DEDICATION.....	v
ACKNOWLEDGMENTS.....	vi
TABLE OF CONTENTS	vii
LIST OF TABLES.....	ix
LIST OF FIGURES.....	xii
CHAPTER	Page
I INTRODUCTION	1
Problem Statement.....	1
Research Objectives.....	4
II DESCRIPTIVES AND LITERATURE REVIEW.....	6
Research Location and Geography.....	6
Regional Climate	6
General Circulation Climatic Controls.....	10
Regional Climatic Controls.....	19
Teleconnections	30
Sea Surface Temperature Effects	32
Problem: ENSO Events.....	34
Interannual Variability	36
Solar Forcing Factors	37
Atmospheric Aerosol Factors.....	39
III DATA COLLECTION.....	41
Rainfall Data	41
Radiational Forcing Data	41
Teleconnection Indices.....	44
ENSO Events	45
IV PROCEDURES AND METHODS OF ANALYSIS	46
Determining Rainfall Seasonality.....	46
The Development of Rainfall Seasons.....	50
Creating Geographical Regions.....	55
Cornu Criterion Normality Test.....	58

CHAPTER		Page
	The Creation of Regional Indices.....	65
	Time Series Analysis of the Regional Indices	67
	Spectral Analysis of the Regional Indices.....	75
	Time Series Analysis of the ITCZ-associated Rainfall Data	76
	Spectral Analysis of the ITCZ-associated Rainfall Data	81
V	FORECAST METHODOLOGY.....	86
	Methodology Reasoning	86
	Methodology Development.....	89
	Improvement of the Results	94
VI	FORECASTING TOOLS	100
	Regression Tool and Decision Flowchart.....	100
	Trend Tool with Probability Table	105
	Trend Tool with Decision Flowchart for Probabilities.....	106
	Improvement Tools Using Teleconnections.....	111
VII	USER FORECASTING DECISION FLOWCHARTS	122
VIII	CONCLUSIONS AND RECOMMENDATIONS.....	136
	Conclusions	136
	Recommendations.....	140
	REFERENCES.....	142
	APPENDIX A	147
	APPENDIX B.....	157
	APPENDIX C.....	158
	VITA.....	161

LIST OF TABLES

Table		Page
1	Warm episode (El Nino) years in the eastern equatorial Pacific as identified by Rasmusson and Carpenter (1982); and Quinn et al. (1978).....	45
2	A visualization of seasonal rainfall patterns for stations near the equator.....	51
3	Same as Table 2 except that it represents the most northern extreme of stations in the research area.	52
4	Same as Table 2 except that it represents the most southern extreme of stations in the research area.....	53
5	The percent of stations within each region whose observations failed the Cornu Criterion at the 5 and 1% probability levels.....	64
6	Regional means and indices for the LR region.....	66
7	Descriptive statistics of the SR regional indices.	78
8	Seasonal rainfall indices for each rainfall season over Eastern Africa.....	80
9	Changes between rainfall indices.....	84
10	Results of correlation analyses between sets of changes including all years of data..	89
11	Coefficients of regression analyses for use in seasonal rainfall climate forecasts using all years of data.....	91
12	Example of a 2x2 contingency table representing the number of occurrences by quadrant found in Fig. 51a.	93
13	Significance of observation counts using the χ^2 test and the probabilities of making a correct forecast using the trend method when the first change is known.....	93

Table		Page
14	Same as Table 10 except only when the absolute value of the first change was greater than the probable error.....	96
15	Same as Table 11 except only when the absolute value of the first change was greater than the probable error.....	96
16	Same as Table 12 except only when the absolute value of the first change was greater than the probable error.....	96
17	Same as Table 13 except only when the absolute value of the first change was greater than the probable error.....	96
18	Same as Table 10 except only when the absolute value of the first change was greater than one standard deviation.....	99
19	Same as Table 11 except only when the absolute value of the first change was greater than one standard deviation.....	99
20	Same as Table 12 except only when the absolute value of the first change was greater than one standard deviation.....	99
21	Same as Table 13 except only when the absolute value of the first change was greater than one standard deviation.....	99
22	Example seasonal rainfall indices and changes between them for the rainfall seasons of 1934 and 1956.....	102
23	Results of the regression forecasting flowchart tool (Fig. 54) for the two example periods.....	102
24	Overall probability of receiving a correct trend forecast for each of the three sets of observations.....	105
25	Example results using the trend tool decision flowchart showing the probabilities of getting a second change of opposite sign and, whether or not, the change was of opposite sign for the two example periods.....	111

Table		Page
26	Correlation values between the $SR \rightarrow AR$ and $AR \rightarrow LR$ changes using selected sets of observations and phases of the SOI.....	114
27	Correlation values between the $LR \rightarrow BR$ and $BR \rightarrow SR$ changes using selected sets of observations and phases of the ASP.....	119

LIST OF FIGURES

Figure		Page
1	Topographical map of the African continent.....	7
2	Map of Eastern Africa as defined in this research which is bounded by 23.5°S-23.5°N latitude and 30-40°E longitude.....	8
3	Four specific seasonal rainfall climatic regions in Eastern Africa each bounded by 30-40°E longitude.....	9
4	Mean monthly maximum temperatures of the African continent for July.....	11
5	Mean monthly maximum temperatures of the African continent for January.....	12
6	The most northern extent and the most southern extent of the ITCZ.....	13
7	Mean monthly rainfall of the African continent for July.....	14
8	Mean monthly rainfall of the African continent for January.....	15
9	Meridional cross-sections of the mean meridional circulation in the tropics in the form of mass-flow streamlines.....	16
10	Tropical stations making radiosonde and RAWIN/PIBAL observations at the beginning of 1991.	18
11	Zonal circulation cells along the equator known as the Walker Circulation.....	18
12	Sea level pressure patterns for January and July.....	21
13	General patterns of wind, pressure, and convergence over Africa.....	22
14	Schematic of the subtropical highs, associated ocean currents, and mean annual precipitation amounts.....	23

Figure		Page
15	Recorded tropical cyclone tracks over a 15-year period for the northwestern Indian Ocean and the southwestern Indian Ocean and the southwestern Indian Ocean.....	25
16	Successive positions of the Somali Jet 20-knot isotach at 1km AGL between April and July.....	27
17	Meridional cross-section of the troposphere depicting air mass features associated with the ITCZ front as it moves northward into the BR region.....	29
18	Schematic diagram illustrating the effect of planetary forces on the earth's axis and orbit.....	40
19	Number of locations within the research area with available monthly observations.....	42
20	Time series of the global means of climate forcings....	43
21	Comparison of annual seasonal rainfall patterns for three stations located within Nairobi, Kenya.....	47
22	Correlation coefficients between data from stations within the Nairobi, Kenya area.....	47
23	Comparison of annual seasonal rainfall patterns for stations in northeastern Kenya and western Somalia.	48
24	Comparison of annual seasonal rainfall patterns for two inland stations and two coastal stations in Kenya.	49
25	Comparison of yearly rainfall patterns for (a) a BR station and (b) a LR/SR station.....	56
26	Comparison of yearly rainfall patterns for a NH buffer zone station.....	57
27	Graph of the Long Rains (LR) region.....	59
28	Same as Figure 27 except for Boreal Rains (BR) region.....	60
29	Same as Figure 27 except for Short Rains (SR) region.	61
30	Same as Figure 27 except for Austral Rains (AR) region.....	62

Figure		Page
31	Cornu Criterion probability levels for n=10 through n=41.....	64
32	Histogram of the LR regional indices expressed in terms of standard deviations from the mean.....	68
33	Same as Figure 32 except for the BR region.....	68
34	Same as Figure 32 except for the SR region.....	69
35	Same as Figure 32 except for the AR region.....	69
36	Histogram of the SR regional indices expressed in terms of standard deviations from the mean with the outlier years removed.....	70
37	Same as Figure 36 except only data from the year 1961 is removed.....	70
38	Time series record of LR rainfall in terms of standard deviations from the mean.....	72
39	Time series record of BR rainfall in terms of standard deviations from the mean.....	72
40	Time series record of SR rainfall in terms of standard deviations from the mean.....	73
41	Time series record of AR rainfall in terms of standard deviations from the mean.....	73
42	Autocorrelation coefficients at different lags for each of the four regions.....	74
43	Times series of ITCZ-associated rainfall which includes all four seasons.....	77
44	Histogram of ITCZ-associated rainfall data expressed in terms of standard deviations from the mean.....	77
45	Same as in Figure 43 except with the 1961 SR datum and its influence on the remaining SR indices removed.....	79
46	Autocorrelation coefficients at different lags for the ITCZ-associated rainfall data.....	82
47	Times series of the first-difference transformation of the ITCZ-associated rainfall data.....	83

Figure		Page
48	Histogram of the first-difference transformation of the ITCZ-associated rainfall data.....	83
49	Autocorrelation coefficients (r) at different lags for the first-difference transformation of the ITCZ-associated rainfall data.....	85
50	Proposed meridional cross-section of the troposphere depicting air mass features associated with the ITCZ as it resides over the BR region.....	88
51	Using all years with data, scatter graphs with linear regression lines are shown for predicting the seasonal rainfall of the (a) BR, (b) SR, (c) AR, and (d) LR rainy seasons.....	90
52	Same as Figure 51 except using only years where the absolute value of the first change is greater than the probable error.....	95
53	Same as Figure 51 except using only years where the absolute value of the first change is greater than one standard deviation.....	98
54	Predictive flowchart tool for the regression forecasting method to predict the third region's seasonal rainfall index.....	101
55	Same as Figure 54 except showing the paths taken through the flowchart while producing the example forecasts listed in Table 24 for the year 1934.....	103
56	Same as Figure 54 except showing the paths taken through the flowchart while producing the example forecasts listed in Table 24 for the year 1956.....	104
57	Predictive flowchart to determine the probability of the trend of the second change when the first change is already known.....	107
58	Same as Figure 57 except showing the paths taken through the flowchart to determine the probabilities of the trend (or sign) of the second change for the example data of 1956 in Table 22.....	109

Figure		Page
59	Insolation forcing effects from solar parameters, stratospheric aerosols, greenhouse gases, and the combined effects of all three overlaid on top of the annual BR regional rainfall indices.....	115
60	Scatter graphs depicting the relationship between the LR→BR and BR→SR changes when the ASP index is higher than its mean during the BR season and when both the ASP index is higher than its mean and the absolute value of the LR→BR change is greater than its probable error.....	120
61	Steps to produce a seasonal rainfall forecast.....	123
62	Forecast decision flowchart for the LR region.....	124
63	Forecast decision flowchart for the BR region.....	127
64	Forecast decision flowchart for the SR region.....	130
65	Forecast decision flowchart for the AR region.....	133

CHAPTER I

INTRODUCTION

Problem Statement

While there is considerable work done on global-scale assessments of climate change and interannual variability of climatic factors, the confidence level in regional-scale assessments is still low (Kulshrestha, 1995). However, it is at the regional and country level where cost-effective response strategies and policies are formulated and implemented. Due to this, a transition from global generalities to regional specifics is needed to refocus attention on the regional climate and its impacts. This study performs a detailed examination of regional aspects of the Inter-Tropical Convergence Zone (ITCZ) associated rainfall over Eastern Africa (a monsoon related system) with the hope of showing reasonably dependable predictability.

Food production and water resources in Eastern Africa depend fundamentally on the strength and duration of the ITCZ's rainfall. Therefore, the ability to understand and predict variations of this are of paramount importance to the large agrarian populations of the region (Waterbury, 1979). It is also of strategic interest to the world community and even military deployments in these regions. For example, water allocation in the Nile Valley is critically important due to the economic growth of the region and agricultural expansion needed to meet the needs of population growth. Egypt is currently totally dependent on the Nile River for its dwindling fresh water resources. Of the Nile's two major tributaries, the White and the Blue, the latter contributes about 85% of the total volume of the main stream. The bulk of this discharge occurs in August and September following the summer rains in Ethiopia

This dissertation follows the style and format of the *Journal of Climate*.

(Adams, 1983). Except for Egypt, the development of infrastructure in nations of the Nile River Basin has not occurred on a large scale due to instability and sustained poverty in the region. When development does occur, the water resources available for downstream users may reach a crisis stage. The countries of Eastern Africa are now at a crossroads and must decide to cooperate with each other or risk conflict concerning water resources. In the meantime, scientists must provide additional knowledge and understanding, as well as rainfall forecasting mechanisms, to enable these countries to maximize their use of available water resources.

While the economy and many societal activities of the region are vitally linked to seasonal rainfall expectations (Ogallo, 1979), rainfall is the climatic element with the highest variability in both space and time. Anomalies in rainfall expectations have therefore been associated with many socio-economic miseries, and, the primary factor linked to these anomalies is the influence of the ITCZ.

Improved prediction of the seasonal rainfall would lead to better management of water resources available for agricultural production, as well as the improvement of such production with less risks. The methodology described in this research provides a means to forecast regional rainfall trends three months in advance for various regions in Eastern Africa. It is simple enough to be incorporated into forecast management systems for both agricultural production and market commodities. It may be used in climate forecast systems to reduce risks in potentially "poor" years and maximize gains in potentially "good" years (Stone et al., 1996). Further research may also deem this methodology to be applicable to other regions around the globe that experience a monsoonal regime.

In recent years, major advances in the simulation of monsoons using general circulation models (GCMs) have occurred; however, the prediction of regional effects remains elusive. Improved seasonal prediction capabilities are awaited by many disciplines, especially agricultural. Viewed from a hydrologic perspective, the purpose of river basin development is to improve the distribution and utilization of

surface water (United Nations, 1970). Since nearly all of Eastern Africa is part of some river basin system, climatologists can play a crucial role if they are able to understand and predict variations in seasonal rainfall affecting the basins.

Using annual data, Nicholson (1981) found a continental coherence of rainfall anomalies between hemispheres on the continent. These were difficult to explain because the seasonality of rainfall differs considerably between hemispheres. However, the findings seem to imply that causal factors of rainfall anomalies may persist over several seasons. Other studies of interannual variability have either failed to distinguish between the annual and seasonal nature of rainfall data distributions; or used monthly means to indicate seasonal distributions. Using monthly means leads to several disadvantages (Nieuwolt, 1977). First, monthly and annual means are inflated by a few heavy rainfalls or periods, particularly in relatively dry months (Riehl, 1954). Secondly, events which do not occur every year during the same month are not shown by monthly means, because they are averaged out.

Most previous studies were accomplished with relatively small datasets or focused on small regions. Other studies examined continental scale analyses as a whole (Nicholson, 1986b), but no studies have selectively chosen stations to specifically examine interseasonal variability or to limit signal contamination by coastal and other synoptic influences. Neither have they examined regional rainfall based solely on preceding conditions in regions recently traversed by the same ITCZ system and, most important, all studies assumed normality of the data when it is in fact not normally distributed by nature. So, the question remains as to whether or not rainfall trends during the passage of the ITCZ can be determined and predicted by examining seasonal trends which occurred earlier as the ITCZ traversed other regions.

A secondary hypothesis of this research is that ITCZ-associated rainfall is influenced by solar insolation amounts and these influences may be detectable on seasonal scales. For example, reduced solar insolation near the northward extremes of the solar declination's path

or over the vast expanse of the Asian continent may lead to weaker forcing, causing less rainfall in the northern extremity of the ITCZ's path but perhaps more rainfall in regions equatorward where the ITCZ is held over a region longer than it is on average. Such relationships, if found, may be feasible to use in seasonal climate prediction efforts.

Research Objectives

In the absence of credible climate prediction capabilities, the expectations of future climate conditions must be based on analyses of historical records (Winstanley, 1985). This study examined the interseasonal variability of Eastern Africa rainfall on the hypothesis that it is a major climatic phenomenon exhibiting large scale, well-organized characteristics which occur fairly regularly. Such systems should therefore be susceptible to a reasonable degree of empirical analysis for predictability purposes (Bhatt, 1989).

Since the term prediction should refer to a statement about an event from information on antecedent conditions (Hastenrath, 1986), seasonal rainfall prediction is therefore a statement on the quality of a rainy season as a whole, based on preceding conditions. Using a time series analysis approach, this work examines regional rainfall based on preceding conditions and detects patterns of variability. The specific tasks necessary to achieve this goal are:

1. to divide the area of Eastern Africa, very selectively, into regions of seasonal rainfall patterns by choosing only research-quality data for stations which, on average, exhibit rainy seasons conforming to expected ITCZ-associated mechanisms;
2. to analyze the data using minimal statistical assumptions and, to formulate relationships between rainy seasons among regions by using both spatial and temporal methods and, also, by indexing and compositing techniques;
3. to create a time series visualization of each region's rainfall and of ITCZ-associated rainfall as the ITCZ traverses over different regions and to determine any trends in the rainfall data time series for the entire period of record (POR) that may be attributable to climate change;

4. to formulate predictive relationships among the time series data by the detection of any recurring patterns;

5. to improve upon the predictive relationships found by examining those relationships towards the extremes of the data distributions;

6. to improve upon the predictive relationships found by examining those relationships during periods of El-Nino Southern Oscillation (ENSO) events, phases of the Southern Oscillation, and other teleconnected phenomena;

7. to compare regional rainfall with modeled insolation forcing data in the Northern Hemisphere to determine any effects on the poleward progression of the ITCZ;

8. to develop predictive guidelines for forecasting seasonal rainfall based on relationships found and, to use only data and indices of teleconnected phenomena that are accessible by world-wide users.

CHAPTER II

DESCRIPTIVES AND LITERATURE REVIEW

Research Location and Geography

Figure 1 depicts surface elevations of the African continent which allow terrain features and major river basins to be easily seen. In this research, the term Eastern Africa refers to the area bounded by 23.5°S-23.5°N latitude and 30-40°E longitude (Fig. 2). The area was chosen to minimize coastal and sea surface temperature (SST) effects on the regional climate that have inhibited previous work and to encompass the full extent of the latitudinal movement of the ITCZ. In addition, the area is divided into four specific rainfall climatic seasons, each within the geographical areas depicted in Figure 3. For terminology purposes, these are referred to as the Long Rains (LR), which occur during the Northern Hemisphere (NH) spring; the Boreal Rains (BR), which occur during the NH summer; the Short Rains (SR), which occur during the NH autumn; and the Austral Rains (AR), which occur during the NH winter.

Regional Climate

The climate of any region is defined as the synthesis of weather, therefore, it is essential that both climatology and relevant synoptic features be considered when identifying the weather of a region (Griffiths, 1962). While all factors that combine to produce the weather of Eastern Africa are not completely understood, the fundamental major climatic controls are well known, as is the geography of the area.

The path of the solar declination on the surface of the earth covers 94° of latitude as it traverses its annual cycle and moves at a speed of roughly 25 km per day. The band of maximum surface heating moves with the solar declination, lagging a little (Griffiths, 1972). The solar declination reaches its most northern extent on the solstice in June and

Elevation and Topography

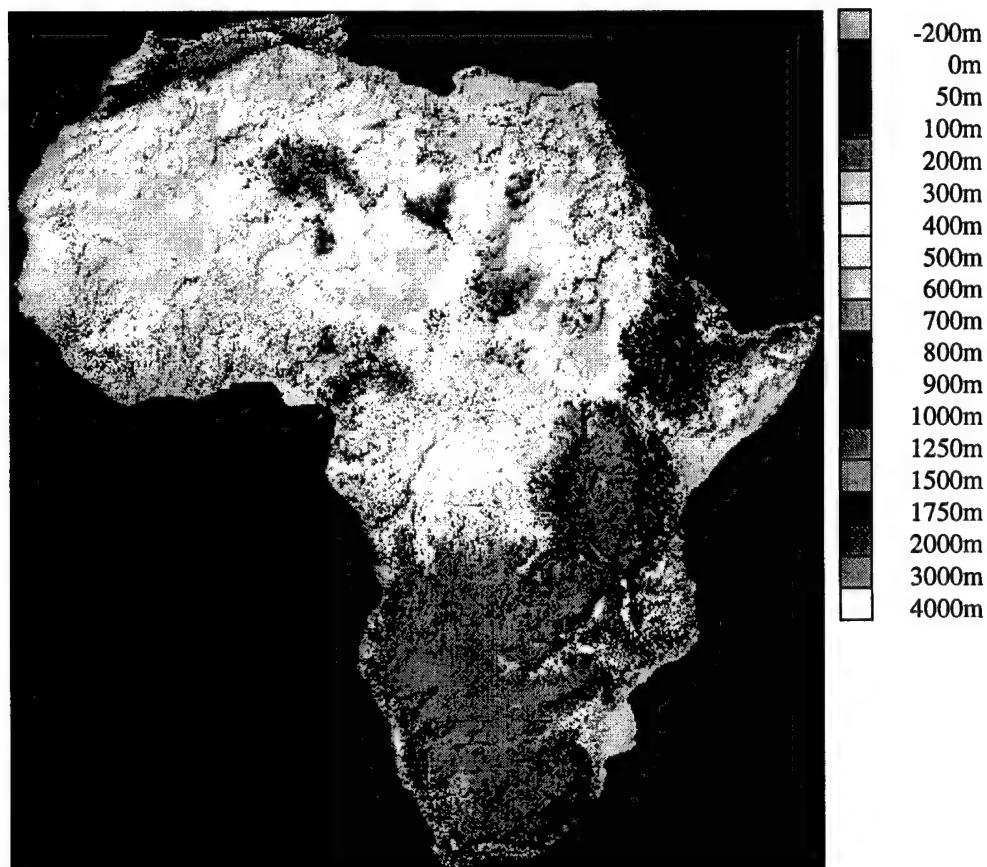


Fig. 1. Topographical map of the African continent (modified from Hutchinson et al., 1995).

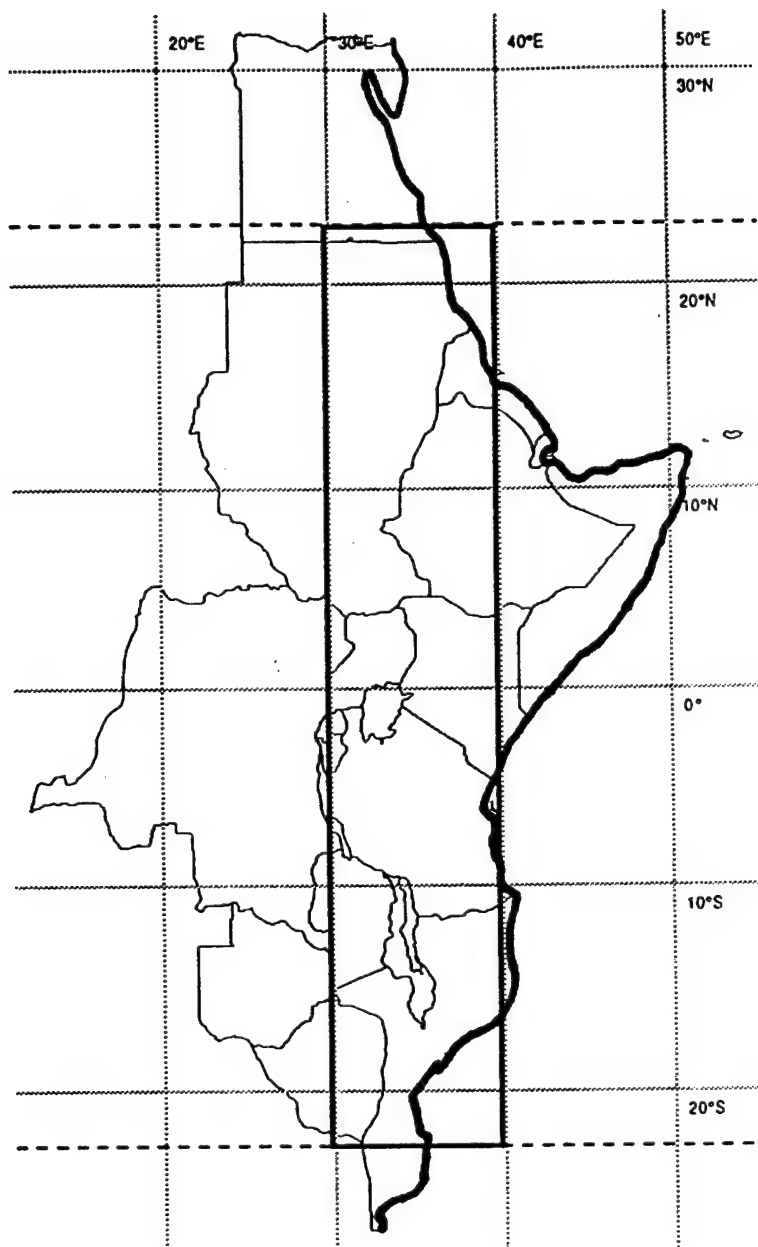


Fig. 2. Map of Eastern Africa as defined in this research which is bounded by 23.5°S-23.5°N latitude and 30-40°E longitude.

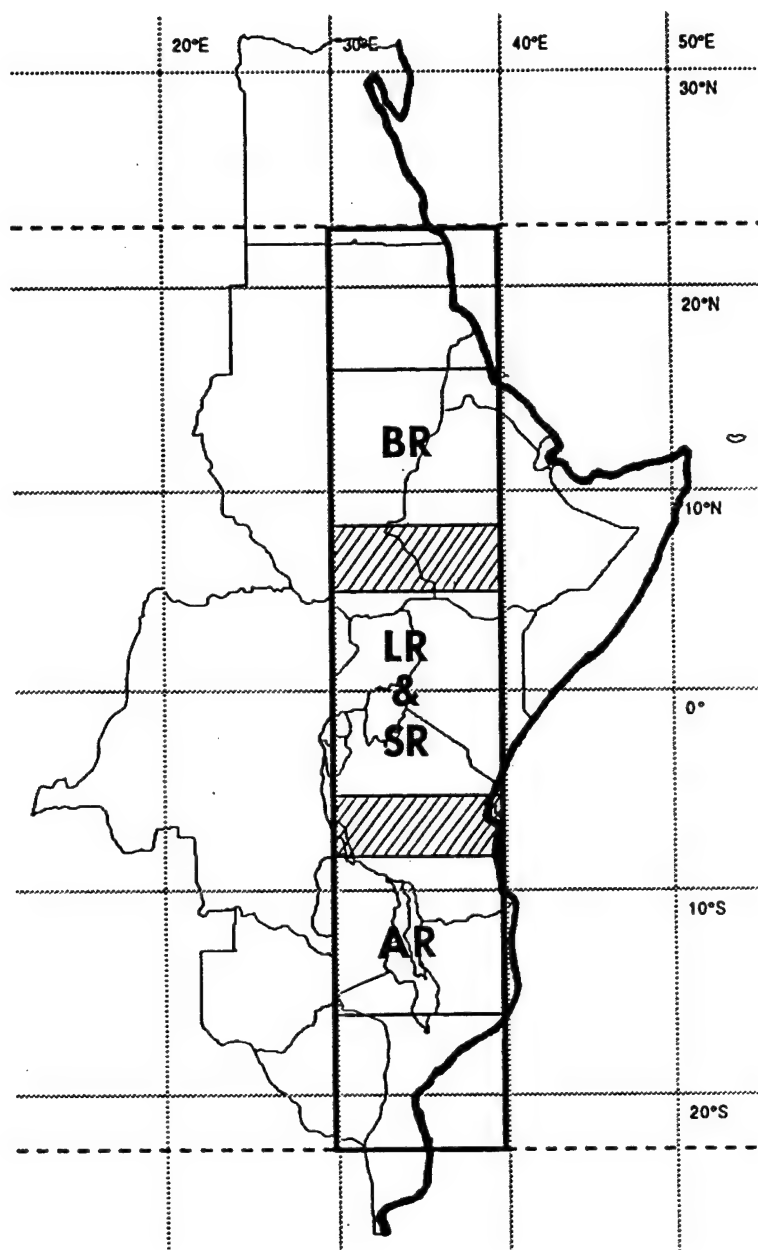


Fig. 3. Four specific seasonal rainfall climatic regions in Eastern Africa each bounded by 30-40°E longitude. They are referred to as the Long Rains (LR) region whose rainy season is during the NH spring; the Boreal Rains (BR) region, whose rainy season is during the NH summer; the Short Rains (SR) region, whose rainy season is during the NH autumn; and the Austral Rains (AR) region, whose rainy season is during the NH winter.

its most southern extent on the solstice in December. Therefore, the mean monthly maximum temperature for the northern extent of the continent is greatest in July (Fig. 4) and least in January (Fig. 5). In the zone of maximum surface heating, the air is warmed and rises, and the surface pressure is decreased which forces the Inter-tropical Convergence Zone (ITCZ) to transit north and south over the continent. The mean positions of the ITCZ in July and January are depicted in Figure 6.

The climatic feature of most significance in Africa is undoubtedly rainfall associated with the ITCZ (Griffiths, 1962). The ITCZ is defined in many ways but to the layman in Africa it is none other than the practical definition of "the rainy season." Since this zone follows the solar declination with a lag of about one month, a rough estimation of the bands of maximum rainfall can be easily followed. The most northern extent of maximum rainfall occurs in July (Fig. 7) and the most southern extent occurs in January (Fig. 8) (Hutchinson et al., 1995). A comparison of African terrain in Figure 1 with Figure 6 illustrates that the areas of heaviest rainfall over Eastern Africa correspond with topographical features of the continent.

General Circulation Climatic Controls

The term "general circulation" refers to a statistical description of the mean large-scale atmospheric motions over the entire planet. These statistics are mainly derived from daily observations and include not only the mean conditions but also the variability of the flow resulting from seasonal changes and transient synoptic features (Huschke, 1959). Many general circulation studies have been made, especially since the worldwide expansion of upper-air networks during World War II. While Lorenz (1967) made an excellent survey, a group of Massachusetts Institute of Technology (MIT) researchers concentrated on the general circulation of the tropics using upper-air data and assembled mean meridional cross-sections (Fig. 9) (Newell et al., 1972). One must use caution in interpreting their work though since the MIT study only used eight years of data and there is a serious problem both then and

July Mean Maximum Temperature

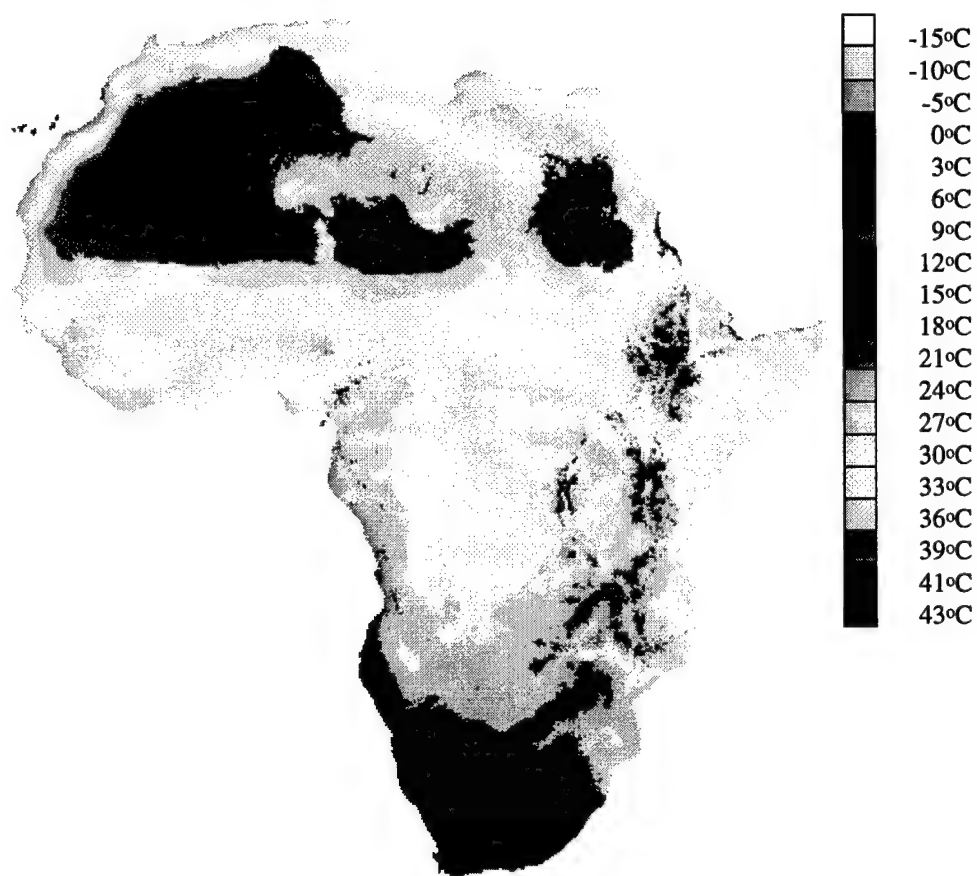


Fig. 4. Mean monthly maximum temperatures of the African continent for July (modified from Hutchinson et al., 1995).

January Mean Maximum Temperature

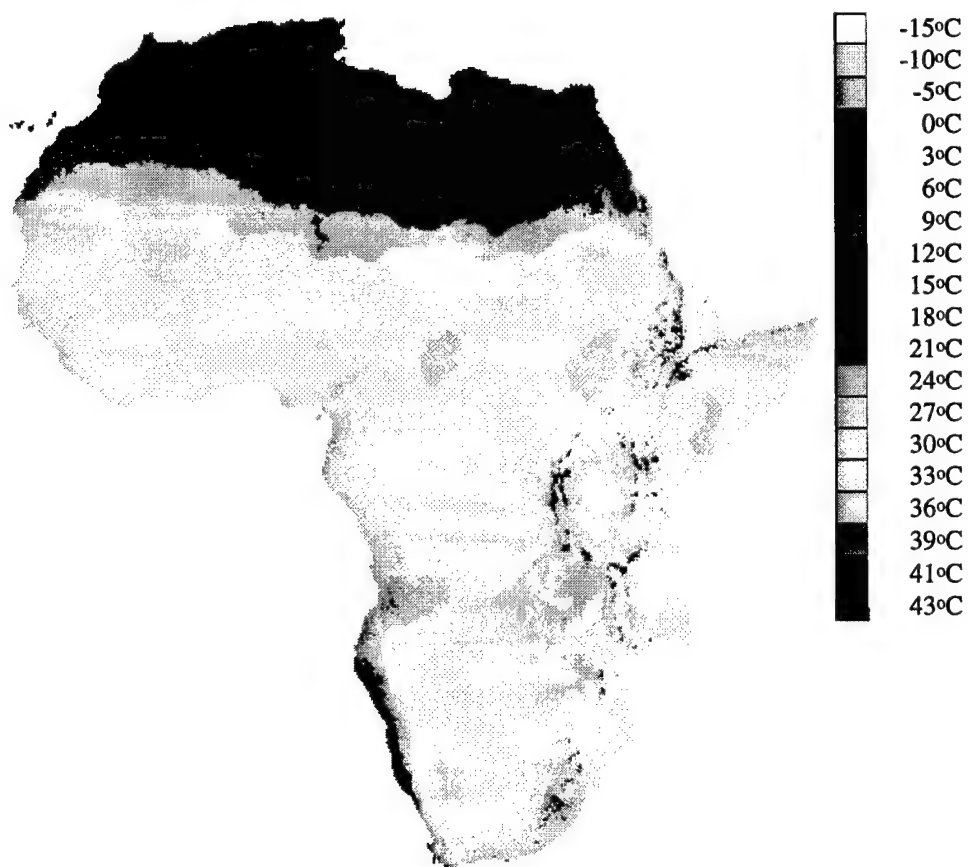


Fig. 5. Mean monthly maximum temperatures of the African continent for January (modified from Hutchinson et al., 1995).

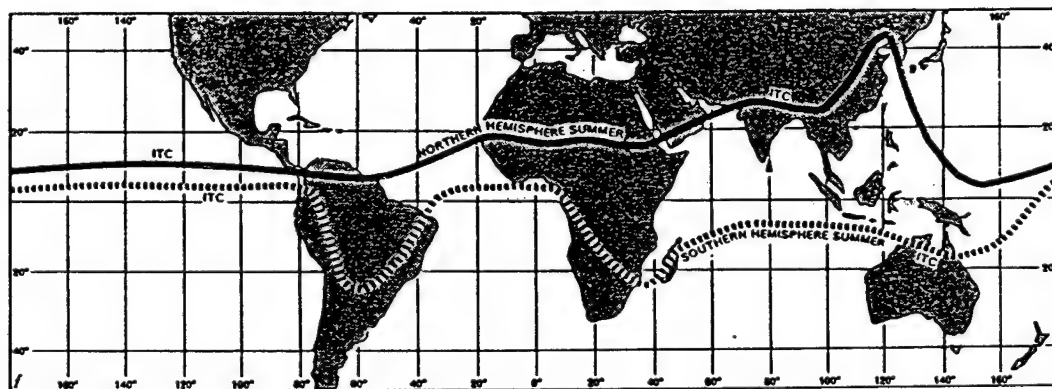


Fig. 6. The most northern extent (in July) and the most southern extent (in January) of the ITCZ (adapted from Van Riper, 1971). Over South America (in January) and Eastern Asia (in July), the boundary represents, not the classical definition of the ITCZ but rather, the poleward extent of the seasonal monsoonal regime.

July Mean Rainfall

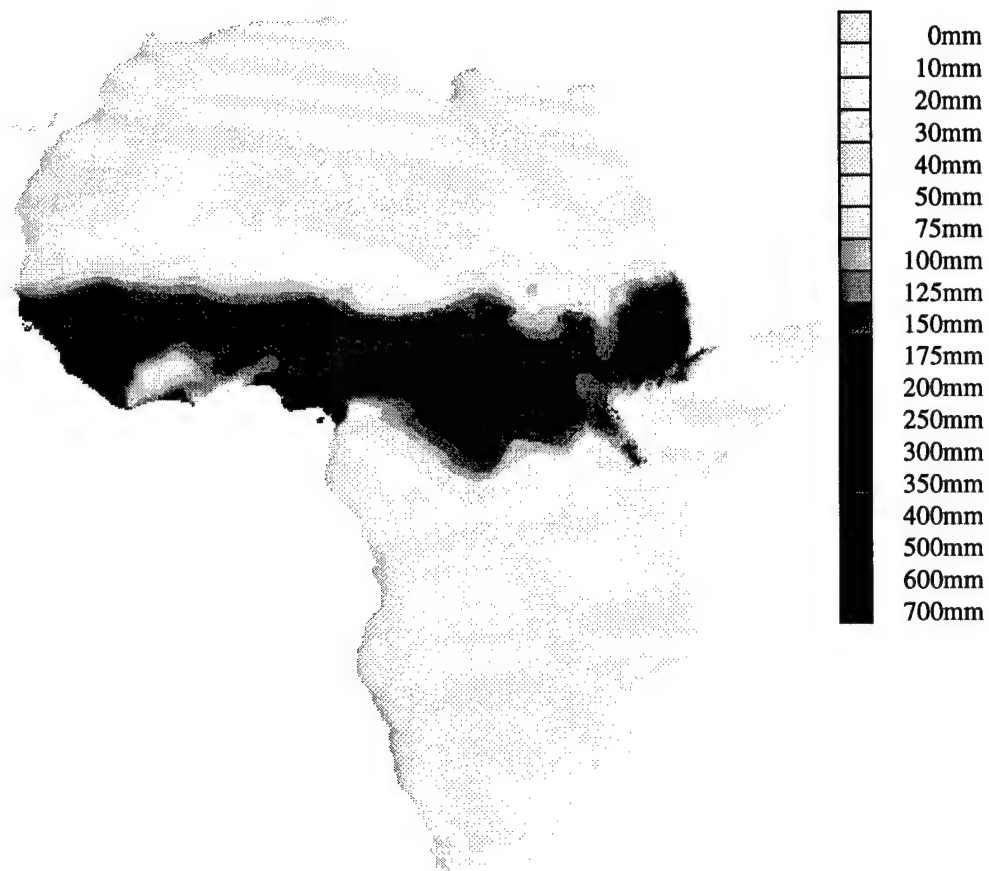


Fig. 7. Mean monthly rainfall of the African continent for July
(modified from Hutchinson et al., 1995).

January Mean Rainfall

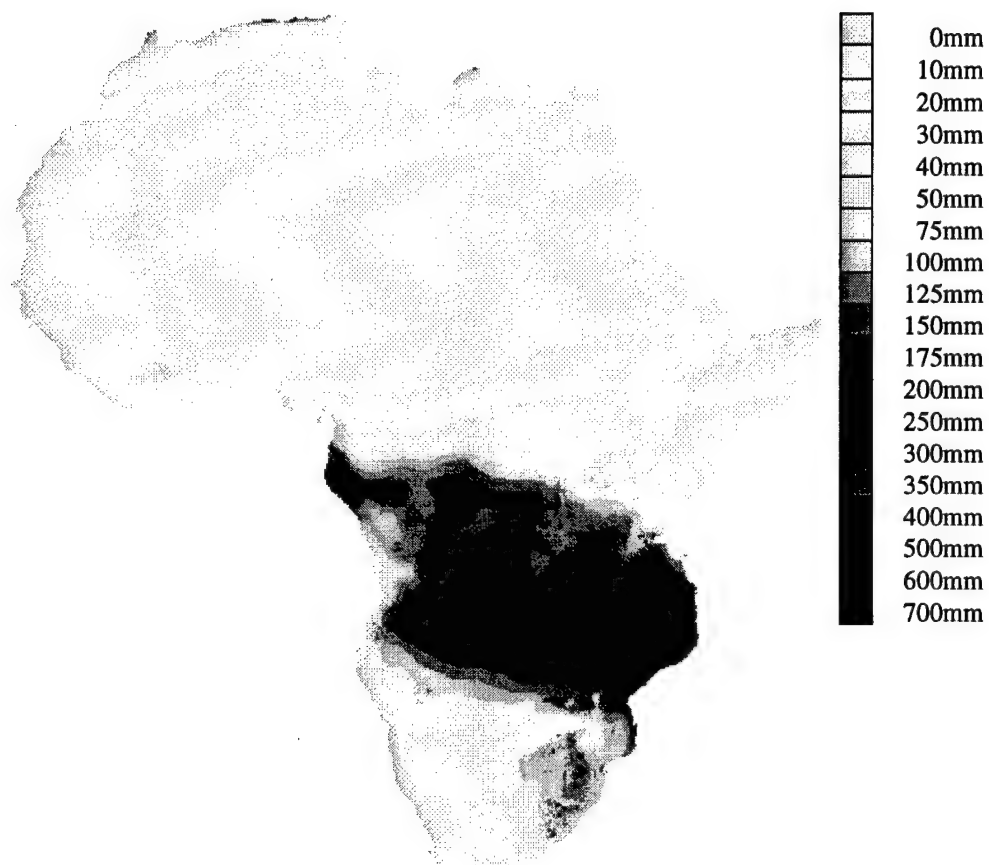


Fig. 8. Mean monthly rainfall of the African continent for January
(modified from Hutchinson et al., 1995).

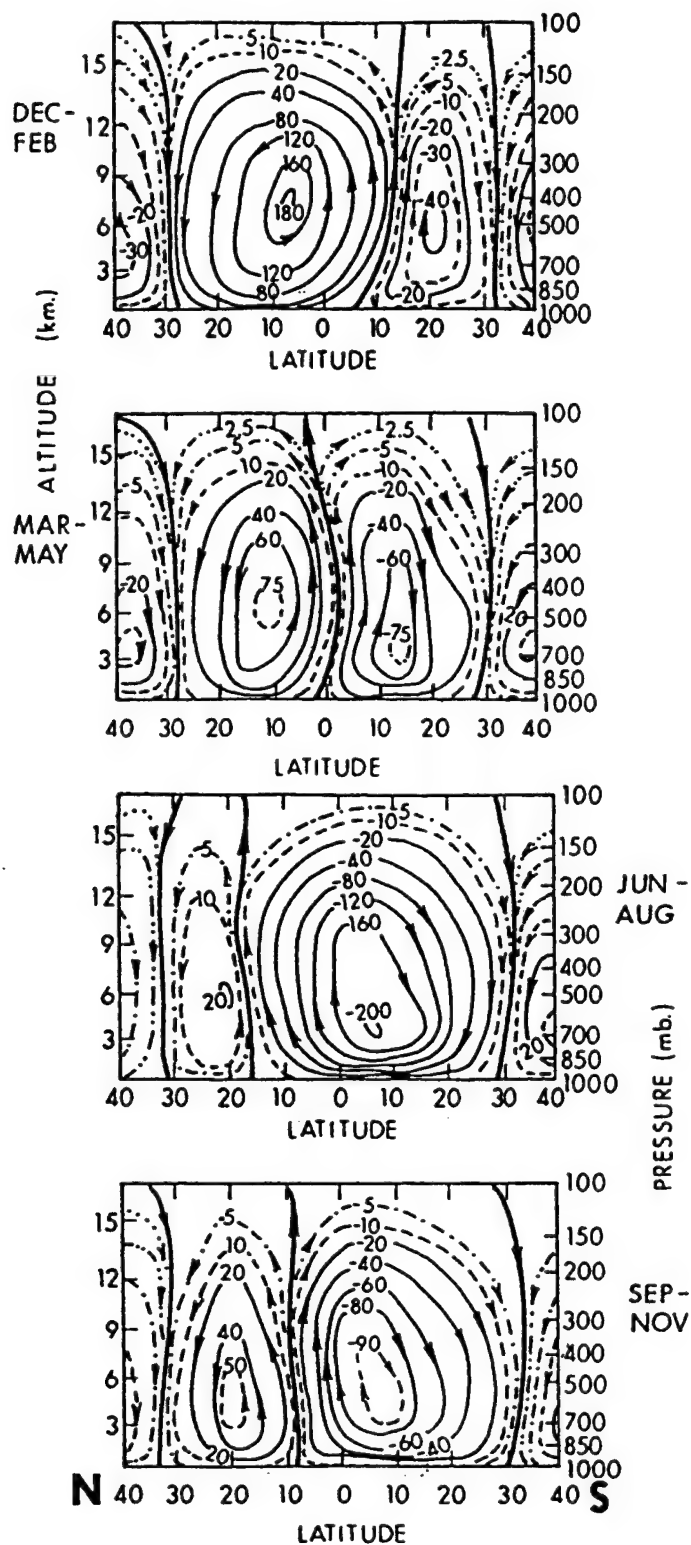


Fig. 9. Meridional cross-sections of the mean meridional circulation in the tropics in the form of mass-flow streamlines (Units 10^{12} g/s) (adapted from Newell et al., 1972).

now with the lack of sufficient tropical upper air observations, as shown in Figure 10 (Ramage, 1995). In fact, only 4 upper air observation sites are currently located in the defined research area and all are in the Southern Hemisphere (SH). Therefore, even though there is a current conception of what the generalized mean meridional circulation (MMC) looks like, there is plenty of room for error in this assumption, especially over data-sparse Africa. In addition, due to a relatively adequate distribution of observations in the tropical western Pacific and an intense interest in the ENSO phenomenon, it is the opinion of many that the view of the MMC is skewed to that of the Pacific region and may not represent the circulation over Africa at all. It must also be remembered that the circulation at any one time may differ greatly from the long-term average.

In Figure 9, the cellular patterns of the Hadley Cells are evident with rising motion near the equator and sinking motion in the subtropics. Hadley (1735) discovered that these cellular circulations accounted for the trade winds, and more recent studies have found that the Hadley Cell is strongest in the winter hemisphere (Grotjahn, 1993). The Hadley Cells are fueled initially by solar insolation and maintain the equatorward latent-heat transport in the lower troposphere. They are referred to as "direct" circulations, with warmer air rising and cooler air sinking and their primary energy source is the latent heat of condensation released in the rising branches of the cells. Other than directly beneath the rising branches of the Hadley Cells, the overturning of the cells results in large scale subsidence elsewhere. This results in a very shallow (about 500 meters) trade wind inversion layer over the oceans and neighboring land areas to which moisture transport by the trade winds is limited.

However, the Hadley Cell is a conceptualized model and the mean vertical motion can vary greatly around latitude circles. Over latitude circles near the equator, centers of upward motion tend to form over the continent with centers of downward motion over the oceans. The thermal drivers of these motions are the heat sources from the continents (and regions) of South America, Africa, and Indonesia; and

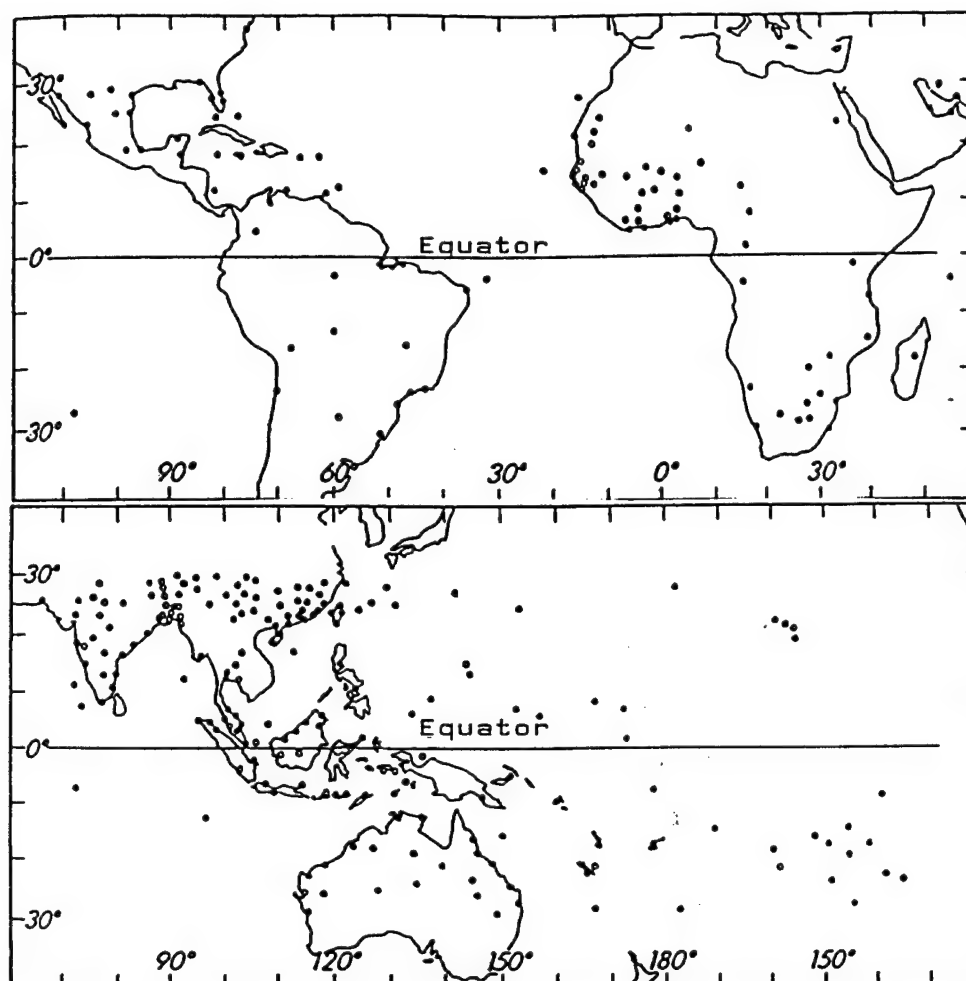


Fig. 10. Tropical stations making radiosonde (o) and RAWIN/PIBAL (o) observations at the beginning of 1991 (adapted from Ramage, 1995).

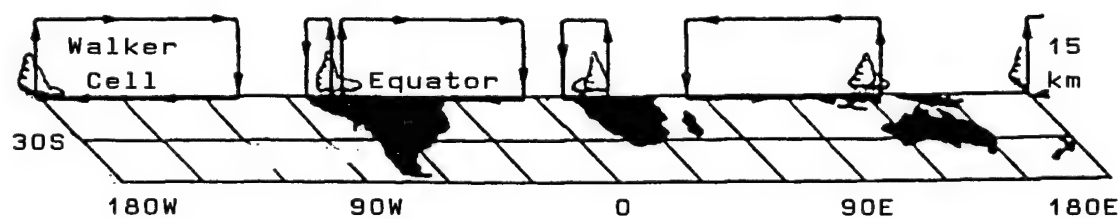


Fig. 11. Zonal circulation cells along the equator known as the Walker Circulation (adapted from Ramage, 1995).

from longitudinal variations in SST due mainly to the effects of wind-driven ocean currents (Holton, 1992). They exist under the premise that due to diabatic heating, zonal temperature differences are not negligible in comparison to meridional differences. Of particular interest is the east-west overturning circulation along the equator (Fig. 11), with the dominant cell being that in the equatorial Pacific. This cell alone is often referred to as the Walker circulation, after G. T. Walker who first discovered the surface pressure pattern associated with it (Walker, 1924) and, the ENSO phenomenon is thought to be the result of changes within it. However, the meridional overturning of the Hadley circulation dwarfs the zonal overturning of the Walker circulation to the extent that the actual existence of the Walker Circulation is questioned by some (in other words, we cannot track a balloon around it). And as before, with the MMC in general, due to the relatively adequate distribution of observations in the tropical western Pacific and an intense interest in the ENSO phenomenon, it is also the opinion of many that the view of the Walker circulation is skewed to that of the one cell over the Pacific region and may not represent the circulation over other equatorial regions at all.

Regional Climatic Controls

The distribution of land and water affects all scales of motion in the tropics, especially over the large land mass of Africa. The continent experiences a much larger annual cycle of radiational heating and cooling than nearby oceans where the specific heat is higher. Consequently, the ITCZ and seasonal wind regimes dominate the Eastern African climate, and large variations are seen in both rainfall amounts and the time of year when the rain falls over the region. While the ITCZ is the main climatic rainfall control, various synoptic weather features also affect regional rainfall. These must be considered in order to narrow the study to regions where rainfall is mostly affected by ITCZ forcing and not by synoptic scale factors.

While the main rainfall control of Eastern Africa is associated with the passage of the ITCZ, Griffiths (1972) concluded that large areas of the

region cannot be categorized into classical distribution patterns since mountains, high plateaus and large lake basins distort the flow to modify the distributions. Johnson (1962) pointed out the complicated nature of rainfall distribution in the region and found the evolution and decay of some systems took many days but seemed to be independent of the ITCZ rain belts. Such a conclusion is difficult to envision though because the same paper concluded that the ITCZ itself cannot be tracked on daily synoptic weather charts.

In addition, Grotjahn (1993) points out the difficulties of interpreting the tropospheric structure over tropical Africa to match the classical ITCZ concepts. Eastern Africa borders the western extremity of the Indian Ocean where synoptic variability consists primarily of day-to-day variations in the position and intensity of large scale features. He points out that from near 35°E and westward, regional forcing caused by the topography of the region may become a dominant forcing factor. Unless regional effects are considered, it is likely that any explanations of the mean flow and rainfall distribution will be incomplete and misleading. Regional features which may influence the climate are the subtropical anticyclones, tropical cyclones, easterly waves, jet streams, extra-tropical weather systems, the structure of ITCZ fronts, global teleconnections, and SSTs.

The two major anticyclones which significantly influence the monsoonal flow over the region are the Arabian and Mascarene high pressure systems (Fig. 12 and 14). The intensity and orientation of these systems have a major impact on the orientation and latitudinal displacement of the ITCZ. Figure 12 depicts the sea level pressure patterns for both January and July, and Figure 13 depicts the general pattern of winds and convergence zones over Africa as a result of these patterns. Figure 14 is a conceptualized model of the high pressure cells which exist continuously over the oceans and their associated ocean currents and rainfall effects. The intensity of the Saint Helena high pressure system over the South Atlantic is very crucial in determining the patterns of westerly moisture influx from the Atlantic Ocean into the Congo Basin. The boundary of this air mass with southeasterly

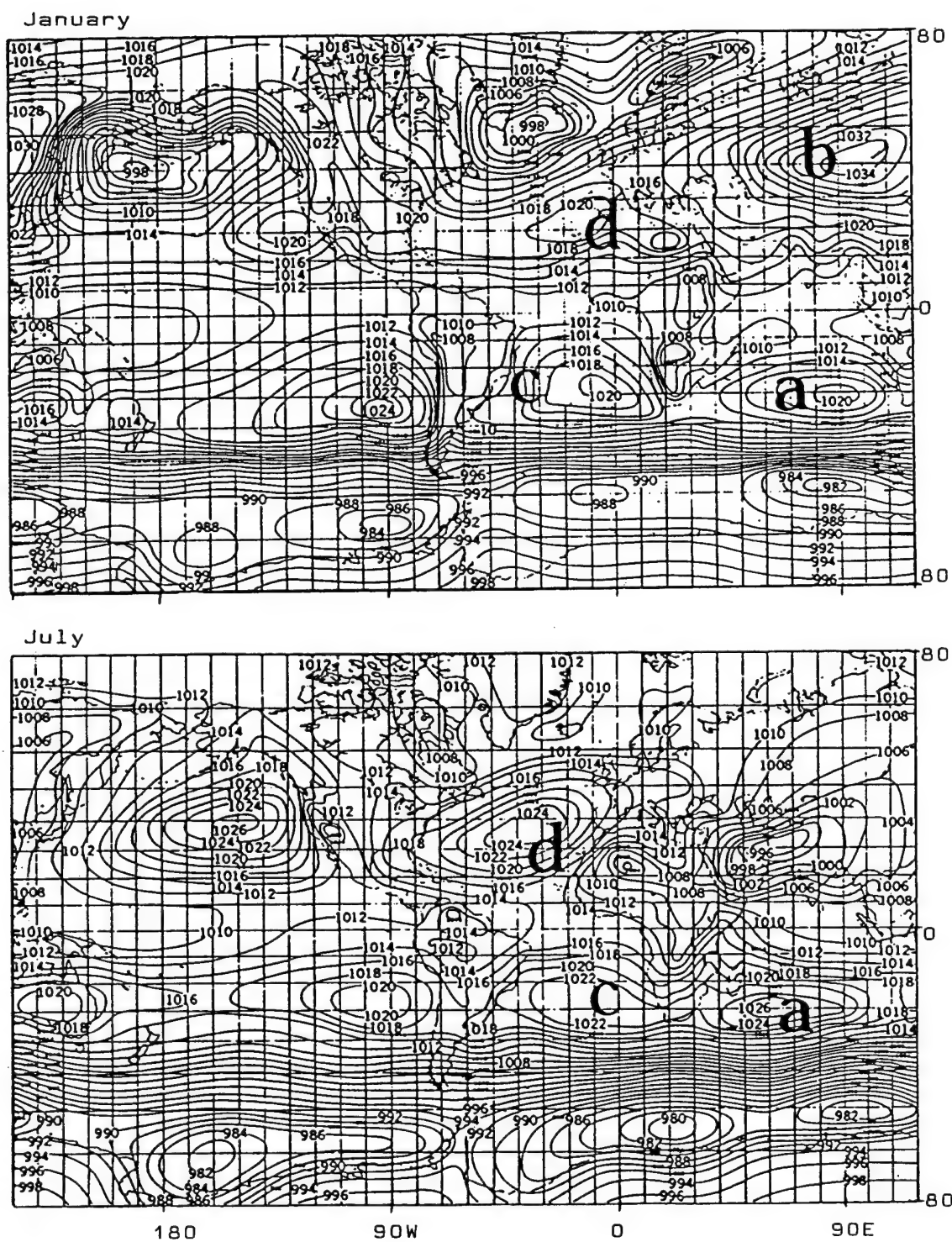


Fig. 12. Sea level pressure patterns for January and July. The high pressure cells surrounding Africa are indicated by: (a) Mascarene, (b) Arabian, (c) Saint Helena, and (d) Azores (adapted from Grotjahn, 1993).

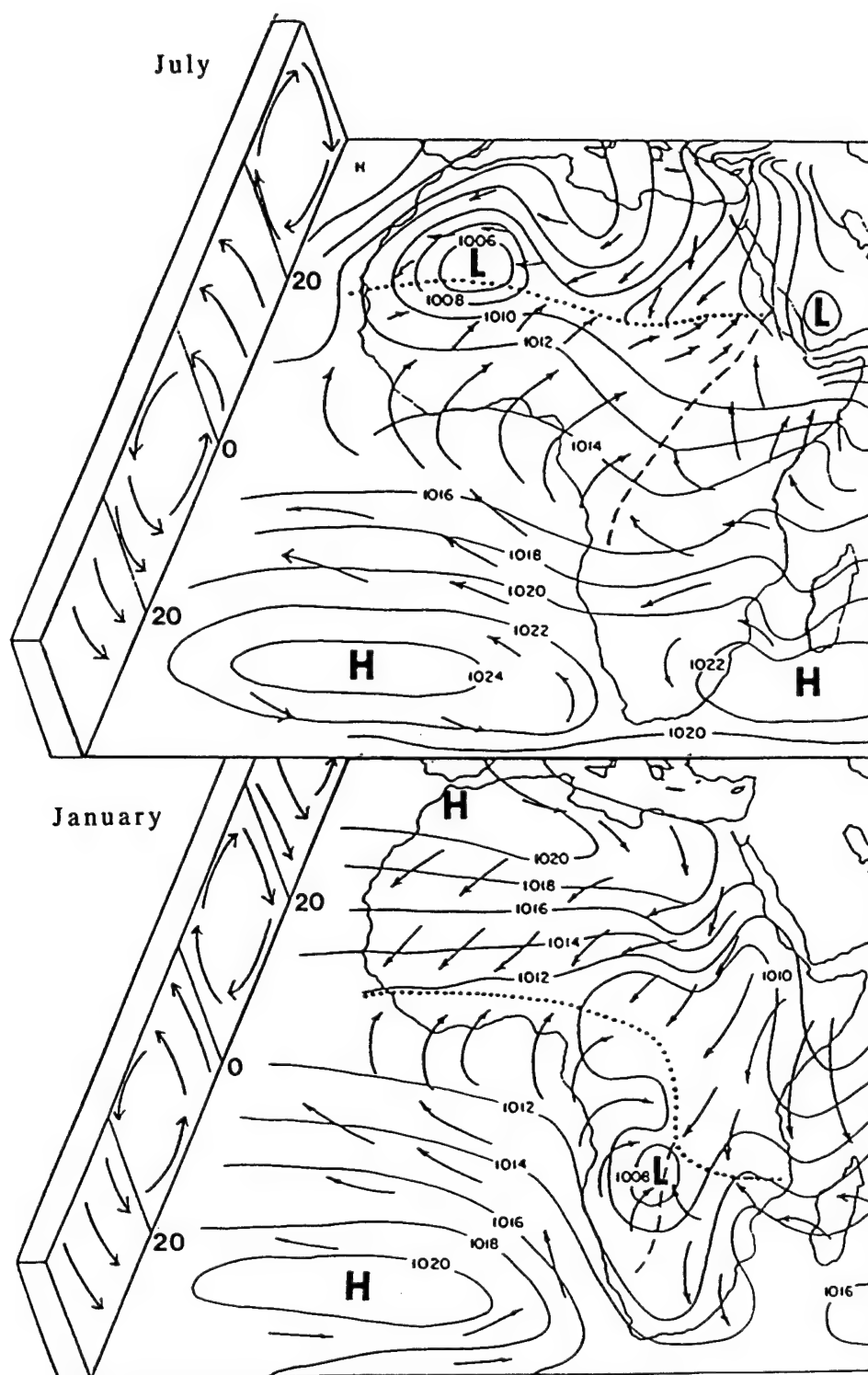


Fig. 13. General patterns of wind, pressure, and convergence over Africa (adapted from Nicholson et al., 1986a). Dotted lines indicate the ITCZ while dashed lines are secondary convergence zones.

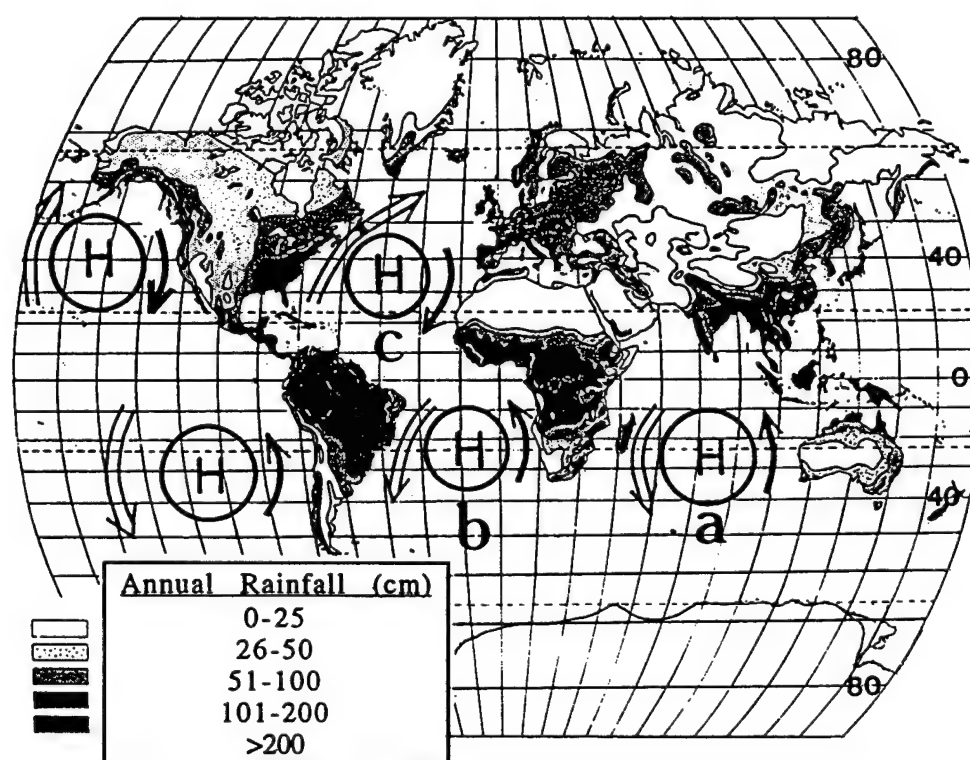


Fig. 14. Schematic of the subtropical highs, associated ocean currents, and mean annual precipitation amounts. Solid arrows indicate cold currents and blank arrows indicate warm currents. The high pressure cells surrounding Africa are indicated by: (a) Mascarene, (b) Saint Helena, and (c) Azores (adapted from Critchfield, 1983).

trades from the Indian Ocean is responsible for producing a third rainy season in the far western parts of the area and may be responsible for "early" starts to the expected ITCZ-associated rainy season. The cyclonic nature of this high pressure system is also responsible for the meridional orientation of the ITCZ over Africa during January. In addition, an intensification and eastward orientation of the Azores high pressure system may have negative impacts in the northern region of the research area by suppressing the northward progression of the ITCZ. However, little work has been done on the intensity and orientation changes of these anticyclones, especially in the Southern Hemisphere.

Figure 15 depicts the recorded tropical cyclone tracks over a 15-year period for both the northwestern and southwestern Indian Oceans. There are very little direct influences of tropical cyclones over the northern sector of Eastern Africa since any approaching disturbances are deflected northward by the Somali Jet. However, the extreme southern part of the region is affected by occasional tropical cyclones with the greatest frequency during December and January (which also corresponds with the rainy season in this region). Therefore, it is doubtful if ITCZ-associated features can be distinguished from synoptic ones in the AR region.

There is little evidence of any easterly wave activity affecting the BR region. In fact, the most eastward formation of easterly waves occurs over the Sudd region of Southern Sudan before they begin their westward progression. Little documentation is found on easterly waves affecting the AR region, however, easterly waves are common in tropical cyclone regions such as the southwestern Indian Ocean. These influences make it difficult to distinguish between ITCZ-associated rainfall effects and those of easterly wave synoptic systems in the AR region.

Of the two major tropospheric jet streams affecting Eastern Africa, only the East African Low-Level Jet significantly alters the flow over the research area by deflecting any Indian Ocean synoptic features toward the Asian continent. Commonly known as the Somali Jet, for its

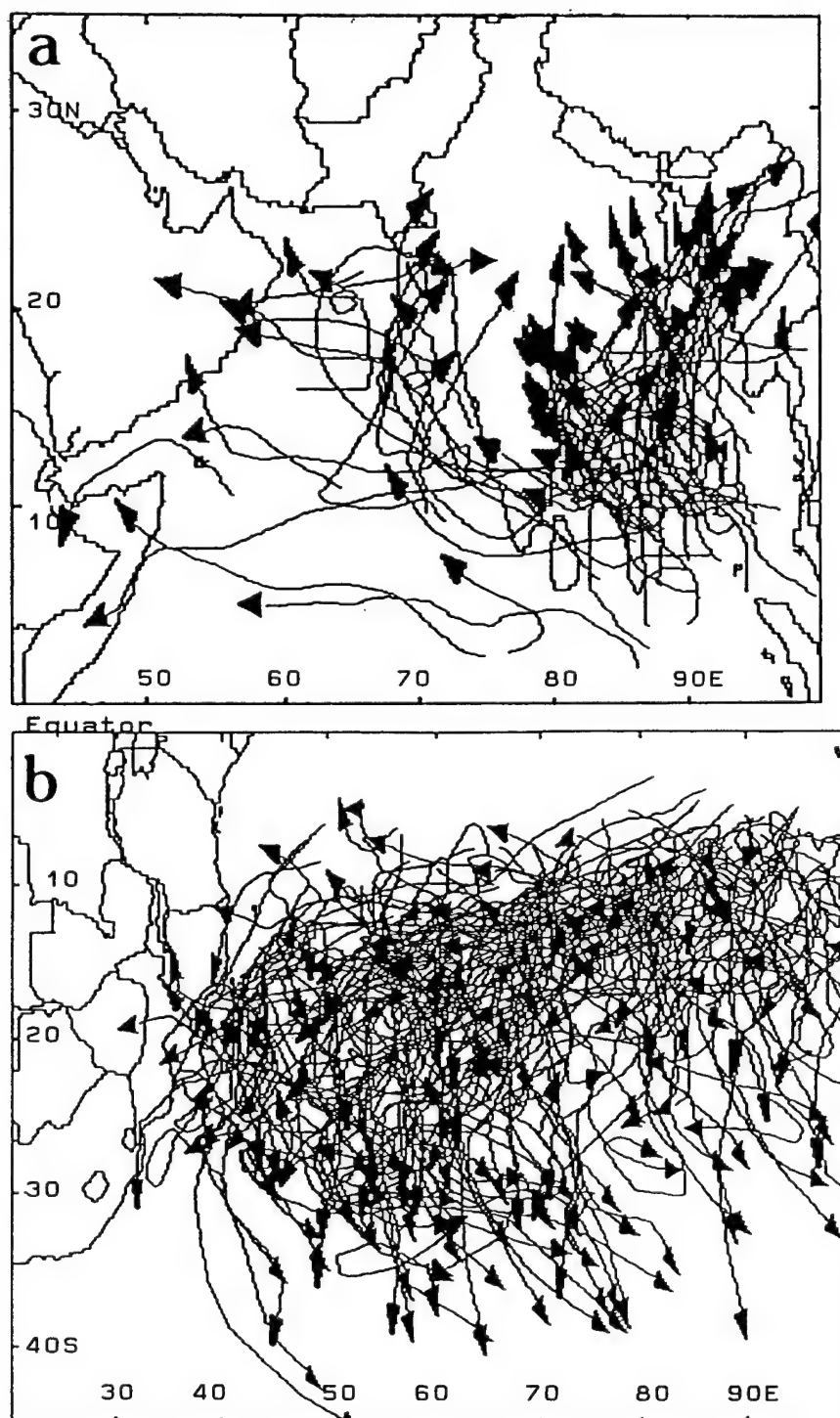


Fig. 15. Recorded tropical cyclone tracks over a 15 year period (1978-1992) for (a) the northwestern Indian Ocean and (b) the southwestern Indian Ocean (National Climatic Data Center, 1994).

position off the Somali coast, it is a dominant climatic feature in Eastern Africa. From April to late October it enters the NH between 4,000 to 7,000 feet near the Kenyan coast as flow from the Mascarene anticyclone is compressed into a high speed jet core along the eastern edge of Kenyan Highlands. Large scale forcing features cause the mean monthly jet core to oscillate northward from April to July (Fig. 16) and then back south between August and October. It has been suggested that studying the intensity of this jet (which feeds the Asian monsoon) may also lead to a prediction of the intensity of the Indian monsoons (Kazarian, 1977). Data unavailability is a primary limiting factor though. In any case, the presence of the Somali Jet inhibits any synoptic feature or significant moisture influx from the Indian Ocean from affecting the rainfall in the northern part of the research area since all such features cannot penetrate the jet and are deflected by it toward the Asian continent.

Extra-tropical weather systems are not major contributors to the region's climate but can affect it. Flohn (1965) documented cases in which Mediterranean Spring storms would effectively send relatively cool air up the Nile River Valley acting as a convective trigger for a shallow layer of moist westerly air intruding from the Congo Basin. Although these fronts are difficult to distinguish during the day due to daytime heating effects on both air masses, the result is that minor (early rainy season) rainfall peaks occurred in May in the BR region which hardly ever had any rainfall until the ITCZ arrived in July.

Due to the climatic influences and lack of observations previously discussed, the actual meridional cross-sectional shape of the ITCZ over Eastern Africa is little understood. Our view of the frontal structure is skewed by our knowledge of mid-latitude fronts and of the ITCZ fronts over the Pacific Ocean. However, the meridional structure over Eastern Africa is the procession of a shallow moist air-mass northward, following the ITCZ, and retreating southward when the ITCZ moves south.

Continental influences are effective on both sides of the equator and, consequently, the meridional shift of the ITCZ is much larger than elsewhere on the continent (Nieuwolt, 1977). In January, most of

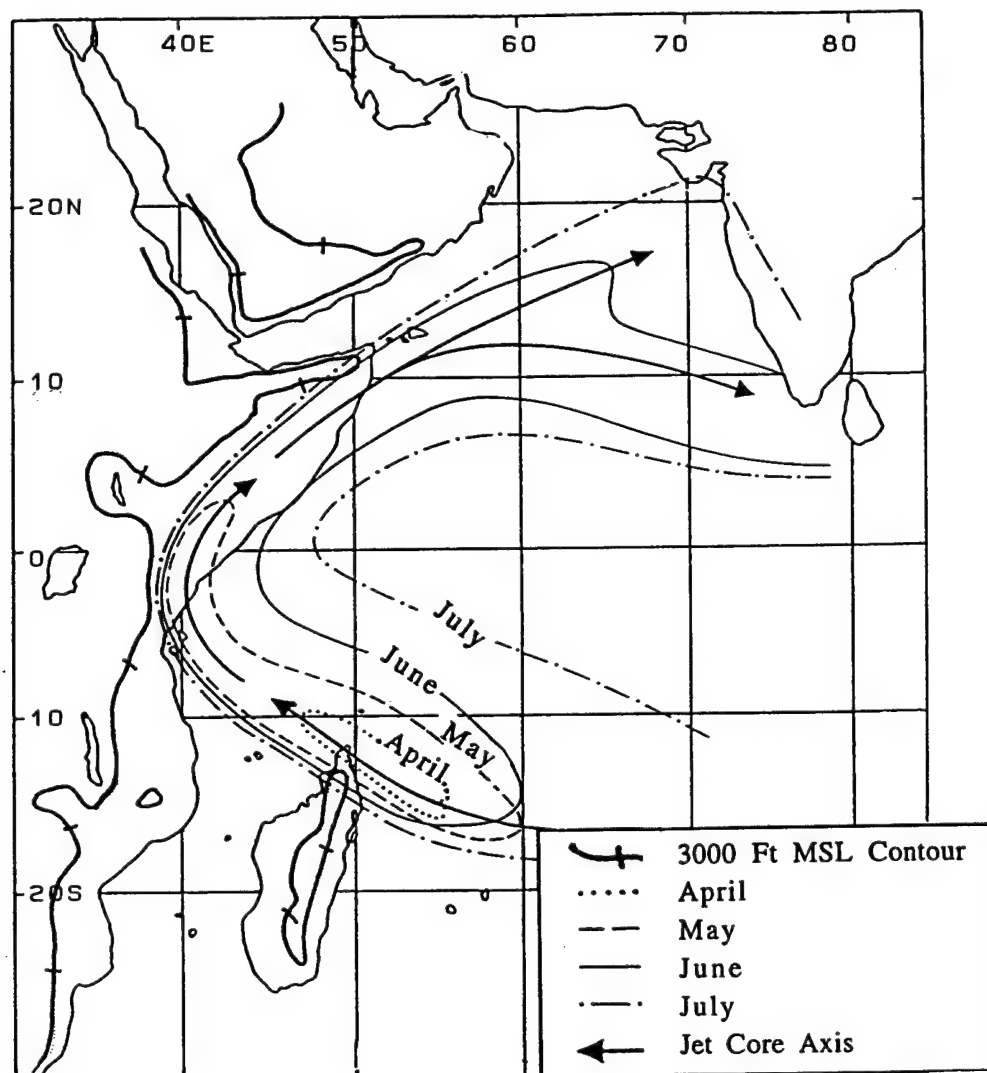


Fig. 16. Successive positions of the Somali Jet 20-knot isotach at 1km AGL between April and July (adapted from Findlater, 1971).

Eastern Africa is under the influence of northeasterly trades, which become northwesterly south of the equator (Fig. 13). These winds are largely of continental origin and widespread divergence prevails resulting in little rainfall from the air mass associated with them. The only regions with significant rainfall during this period are situated near the ITCZ. In July, when the ITCZ is at its most northward position, southeasterly trades prevail, yet, due to various climatic features discussed earlier, these winds bring little precipitation. The air-mass associated with them is partly of continental origin, coming from the high pressure area over South Africa. But even those air masses which come from the Indian Ocean are relatively dry since they have lost most of their moisture on the steep eastern mountain slopes of Madagascar and terrain features within Eastern Africa. Therefore, both monsoons are relatively dry, and the rainfall is concentrated during seasons associated with the passage of the ITCZ. The Eastern Africa monsoon region differs from the Asian monsoon region in several aspects. It is smaller in regard to the area covered and thickness of the layers, covers less latitudinal displacement, and involves no polar air mass. Figure 17 is thought to represent the meridional cross-sectional view of the ITCZ front as it progresses northward over Eastern Africa. Moisture is mostly supplied by the southwesterly trades and convection doesn't occur until the air mass is sufficiently deep enough to overcome the trade wind inversion.

The meridional view of the front as it moves southward with the ITCZ is somewhat less known but believed to start out at least with a retreat of the moist air mass of the southwesterly trades shown in Figure 17. As this air mass starts to move northward from the AR region, it is supplied with abundant moisture. However, as the ITCZ progresses into the NH, this moist air mass must reach a point whereby less moisture is behind it due to the terrain effects and low-level deflecting effect of the Somali Jet discussed earlier. If this air mass is cut off from its moisture source in the south, and little enters it from either the Congo Basin or the Indian Ocean, then it would seem likely that an element of continuity

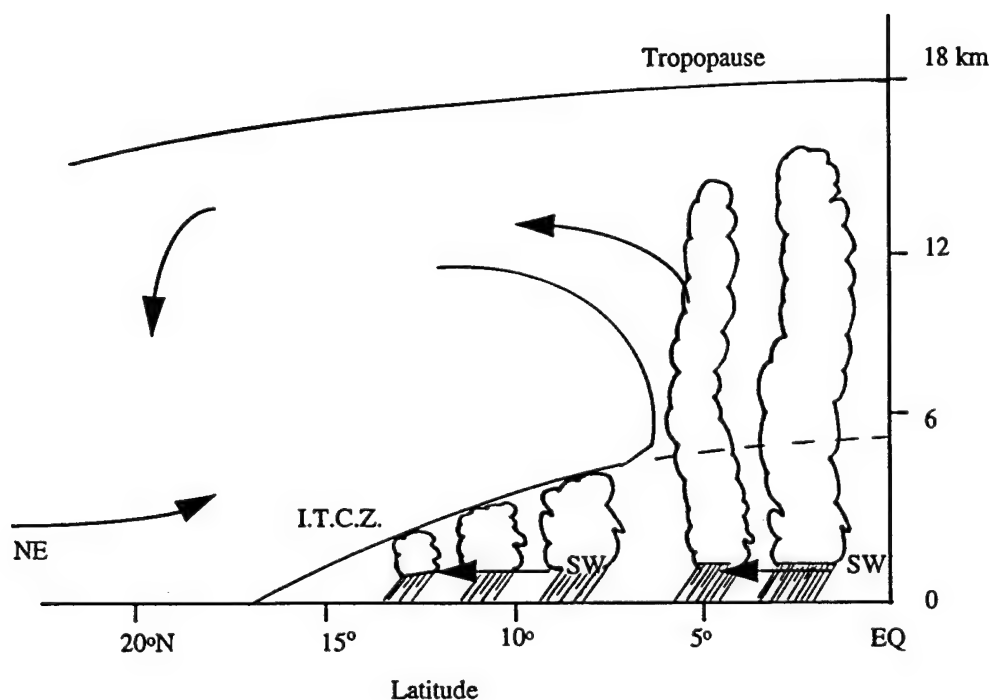


Fig. 17. Meridional cross-section of the troposphere (with a vertical exaggeration of 75 times) depicting air mass features associated with the ITCZ front as it moves northward into the BR region (adapted from Nieuwolt, 1977).

may exist to the moisture that it holds, and the rainfall that results from it.

Teleconnections

Teleconnections are defined as statistically (or empirically) determined couplings of large scale abnormalities of the atmospheric circulation, both in space and time (Fleer, 1981). They are further defined as relationships between temporal fluctuations of meteorological parameters at widely distant locations (Nicholson, 1986b). To the layperson, the concept of teleconnections is that something happened at a particular place on the globe, and as a consequence, something else happened elsewhere. In reality, teleconnections are nothing more than correlation analyses.

Nicholson (1986b) found evidence that over Africa, large scale teleconnections were indicated by an extreme coherence of rainfall anomalies between the tropical and extratropical regions of the continent. It was suggested that the coherence of these rainfall anomalies appeared to be continental in scale. The most consistent relationship found was the tendency for fluctuations of the same sign to occur in the subtropical latitudes of both hemispheres leading to a mirror dipole effect. In any case, the results seem to imply that causal factors within the tropical atmosphere persist over several seasons, however, these seasonal variations have not been explained.

Actually, there are a number of implied causes of rainfall anomalies which occur over Africa as well as many places around the globe. One of these, is the periodic anomalies in global circulation collectively known as ENSO events (Tadesse, 1994). There are no solid theories to account for any interannual variability of Eastern African rainfall as it relates to ENSO. However, its effects are widely studied and it is thought that if the Walker circulation cells are shifted eastward during an ENSO event, the convective cell over Africa also shifts eastward toward the coast (Webster and Chang, 1988). Some have theorized that the Short and Austral Rains would benefit from such a shift and observations from just a few ENSO years seems to imply the same, at least for the SR

region. However, no one has looked at the specific timing of individual ENSO events and how they relate to different seasonal rainfall patterns in Eastern Africa. In addition, there remains no universal single definition of ENSO (Trenberth, 1997) and, as a result, ENSO related scientific studies have used different years to describe various ENSO-type events. This makes it extremely difficult for follow-on researchers to compare results among such studies.

But ENSO is not the only teleconnection event that may affect Eastern African rainfall. During the SR season of 1961, most of Eastern Africa experienced unrivaled rainfall lasting 4-5 months (Kapala et al., 1994). Descriptions of this case have been provided by several authors (Flohn, 1983; Flohn, 1987; and Shahin, 1985), but it became clear that this event was part of a much larger anomaly after the publication of several Indian Ocean studies (Cadet and Diehl, 1984; Reverdin et al., 1986), which did not refer to any African rainfall observations. During the last four months of 1961, above normal SSTs and cloudiness were found in the Arabian Sea (60°-70°E) with negative anomalies around longitude 90°E. Recent rainfall records from the Indonesian Archipelago (Flohn, 1986) indicate a fairly intense drought period occurred which was not correlated with any ENSO anomaly in the Pacific and, over the Indian subcontinent, this event coincided with the rainiest high-sun monsoon in the last 150 years. It has been concluded that the essential features of this event occurred over the equatorial Indian Ocean with anomalously high SSTs in its western part and low SSTs in the eastern sector (Kapala et al. 1994); and that the uniqueness of the event was due to a reversal of the zonal (Walker) circulation across the Indian Ocean.

Another teleconnection event that may affect Eastern African rainfall is associated with the large radiational heating effect of the Tibetan Plateau and Asian continent as a whole during the NH summer. No other land mass heating effect on the planet draws the ITCZ more poleward, and, the extent to which it does must depend on the interannual variability of pressure over the region. The behavior of such a quasi-stationary planetary scale circulation is of considerable interest to meteorologists for a variety of reasons. One of which is that

it is strongly coupled with short term climate fluctuations at the surface, which we hope to predict (Klein, 1983).

Barnston and Livezey (1987) used orthogonally rotated principle component analysis (RPCA) of the NH 1-month mean 700 mb heights to identify and describe the seasonality and persistence of this major mode of interannual variability. A single-center Asian Summer Pattern (ASP) was found detailing the month-to-month changes in the dominant pressure patterns over southern Asia and northeastern Africa. The trouble with RPCA patterns though is that many question the actual physical meaning of the resulting index. It is easily explained in statistical terms but often lacks an associated physical meaning. For the ASP it is, in physical terms, a measure of the strength of the 700 mb pressure pattern over the area. Over high terrain features such as the Tibetan Plateau, this is actually a measure of surface pressure anomalies.

Since decreased pressure over the Asian continent in the summer is the causal factor for the monsoons and poleward shift of the ITCZ, a low ASP index would indicate lower pressures and a high ASP index would indicate higher pressures over southern Asia and northeastern Africa. Using this reasoning, a lower ASP would tend to pull the ITCZ more poleward over the region while a higher ASP would tend to indicate the ITCZ may remain more equatorward.

Barnston and Livezey (1987) found the ASP is only prominent from June-August and monopole in nature, with anomalies of the same sign observed throughout all of southern Asia and northeastern Africa. The ITCZ's position while traversing the BR region should be affected the most by the ASP, since one would theorize that if the ITCZ were pulled more poleward, the layer of tropical moisture (due to the characteristics of the ITCZ front (Fig. 17), would deepen over the BR region thus allowing more potential for convective activity.

Sea Surface Temperature Effects

A number of recent studies assessing the causes of interannual rainfall variability in the region found empirical links with SSTs in

various ocean basins (Hastenrath et al., 1993; Rowell et al., 1994). An important finding has been that these seasonal rainfall-SST relationships are substantially stronger during the Short Rains but only near the coast. Using a GCM, Rowell et al. (1994) explored possible reasons for the differing characters of the LR and SR seasons and their respective relationships with SSTs using gridded rainfall. Negligible correlations were found between Pacific SSTs and the Long Rains, however, significant correlations were found with the Short Rains. Several authors have explained this noting a strong influence of the Southern Oscillation on atmospheric circulation over the Indian Ocean during the SR season (Hastenrath et al., 1993; Meehl, 1987), with a resultant directly onshore flow. This onshore flow would tend to enhance any convective activity associated with the coastal land/sea breeze circulation.

Over the Indian Ocean, large month-to-month fluctuations of rainfall-SST relationships were found which only reflect changes to the preferred direction of surface flow into Eastern Africa (Rowell et al., 1994). For example, during the Long Rains, Eastern Africa is influenced to some degree by southeasterly trades from the Indian Ocean. However, the results were not consistent from month-to-month, and this would also account for the lack of spatial coherence across the region during the Long Rains, especially since these studies did not selectively try to eliminate coastal climate influences. However, the steep topography of the eastern Madagascar coast and of the highlands within Eastern Africa, and, the diversionary influence of the Somali Jet on Indian Ocean synoptic systems, all tend to reduce trade wind moisture before it affects the region. Otherwise, Eastern Africa would have a much more maritime tropical climate than it does now (Nieuwolt, 1977). During the Short Rains, correlation patterns reveal that warm SSTs in the western Indian Ocean and cool water in the eastern Indian Ocean tend to produce wetter years in Eastern Africa with the positive correlations concentrated along the coast (Rowell et al., 1994). This supports the idea that there may exist a notable influence of SST variability on rainfall in the region but only selectively from month to month since it is

dependent on the direction of flow into the region and only significantly for coastal areas. Since data near the coast tend not to have annual rainfall distributions conforming to the position of the ITCZ, most are excluded from this analysis.

Problem: ENSO Events

Comparisons between the SOI and seasonal rainfall indices are simpler than with El Nino warm episodic events since we can compute the seasonal SOI mean from the monthly CPC indices within the same season as the rainfall data. However, there remains no universal single definition of ENSO (Trenberth, 1997), and some researchers have used different years to describe various ENSO related events to benefit the focus of their work. In addition, SST measurements are sampled by different methods and in different Pacific grid boxes. It is therefore clear in the current literature, that from the standpoint of quantifying an El Nino warm episode and related phenomena, that the definition is still evolving and each case study needs to recognize the complexity of the phenomena.

The ENSO term is widely used to describe certain cases of collaboration between the atmosphere and ocean in the equatorial Pacific. The El Nino portion of the term refers to oceanic events and the Southern Oscillation refers to atmospheric events. The most commonly known aspect of the term is the occurrence of an El Nino warm episode whose typical sequence of events follows.

The SOI is in a high/dry phase with high pressure over the eastern Pacific and lower pressure over the central or western Pacific. The easterly trades, as the lower component of the Pacific Walker Cell, are strong and this steady westward flow of air literally drags the warm surface waters to the west resulting in a "piling up" of a thick layer of warm surface water and a higher sea level in the western Pacific. Meanwhile, strong coastal upwelling of cold water and a lower sea level characterize the eastern Pacific. A mostly sub-surface equatorial ocean counter current exists which carries some of the warm water back eastward. Near the end of each year, this warm counter current forces a

weak, warm ocean current to flow southward along the coast of Ecuador and Peru. The event was termed "El Nino", which is Spanish for "the boy Christ-child", since, on average, the warm water usually appeared about Christmas.

However, in some years, a much larger and more extensive warming of the ocean occurs and today, the name "El Nino" is now, confusingly, applied primarily to these major episodes of oceanic warming even though the area covered by them and the physical processes that produce them differ greatly from the relatively weak phenomenon that originally bore the name (Lutgens and Tarbuck, 1986). Some researchers have used "little El Nino" to refer to the annual event and "big El Nino" to refer to the major episodes which occur sporadically. In these sporadic years, something unknown happens which causes the easterly trades to decrease or fail altogether (this is the atmospheric component of an ENSO event). The extensive pool of warm water over the central and western Pacific is then released and travels eastward across the Pacific taking approximately four months to reach the South American coast (this is the oceanic component of an ENSO event). If the water is sufficiently warm as it spreads along the South American coast, wide-spread changes occur to the region's climate and related ecosystem as the warm water pushes the cold upwelling Humboldt Current far away from the coast. In addition, the rising motion within the upward branch of the Pacific Walker Cell moves with the warm pool of water as it crosses the Pacific and results in large scale pressure changes over the region as the SOI transitions into a low/wet phase. This, in turn, affects pressure fields in all directions surrounding the region resulting in impacts to neighboring climatic regimes as well.

Although there is wide-spread speculation of worldwide impacts associated with these El Nino warm episodes, one must realize that Eastern Africa is at least one and a half oceanic basins removed from SST effects in the central and eastern Pacific, therefore, lag times just do not permit the feasibility of a strong direct relationship between them during the same season. However, the Southern Oscillation is more closely linked temporal-wise with events in Eastern Africa since large

scale pressure changes affecting the Walker Circulation over the Western Pacific and Indonesia may influence events over the Indian Ocean and Eastern Africa on shorter time scales. Therefore, while this research focuses on comparing Eastern African rainfall with phases of the SOI using the CPC operational indices, we cannot ignore El Nino warm episodes in the Pacific since previous researchers have found some links between these events and the intensity of the Short Rains in Eastern Africa.

Since the general temporal pattern of an El Nino warm episode is that it starts in the late NH summer or early fall and ends around January, the Short Rains should be the season most affected by such an event. However, as discussed previously, the Short Rains are more likely influenced by the Southern Oscillation component of the ENSO phenomena, and most probably due to increased on-shore flow from the Indian Ocean due to changes within the Walker Circulation.

Interannual Variability

No tropical region of forecast interest other than Eastern Africa spans the equator with such significant land mass in both hemispheres (Janowiak, 1988). The annual cycle of rainfall as it moves across the continent following the solar declination has been studied by many authors, such as Hutchinson et al. (1995), Kidson (1977), Nicholson (1981), and Hsu and Wallace (1976). Other studies have examined the interannual variability of African rainfall (Ogallo, 1979; Nicholson, 1986a). Dyer (1979) investigated relationships between rainfall along coastal South Africa with general circulation features, while Tyson (1984) and Tyson et al. (1975) studied rainfall variations over the southern half of the continent. But for many of these studies, the datasets upon which the results were obtained were relatively small or focused on small regions. Annual rainfall departures were also examined using continental scale analyses as a whole (Nicholson, 1986b). No studies selectively chose stations specifically to examine the variability due to ITCZ influences or to limit large scale signal contamination by coastal and synoptic influences of the regional

climate. Neither have they examined a specific region's rainfall based on preceding conditions in other regions recently traversed by the same ITCZ system. And, neither have they developed a rainfall time series among multiple regions which would account for a time sequence of ITCZ-associated rainfall as the ITCZ traverses its annual cycle.

Some studies of climate prediction (Penland and Magorian, 1993; El-Fandy et al., 1994), using purely statistical techniques, are unsatisfactory due to a lack of insight into the circulation mechanisms involved (Hastenrath, 1995). This study attempts to recognize the circulation mechanisms involved beforehand and selectively choose stations to meet the research criteria. The hope is to select stations exhibiting rainy seasons as a result of ITCZ influences with minimal contamination from local synoptic influences. Stations in the same region not exhibiting these features are not necessarily left out of consideration since the goal of local forecasters should be to examine any predictability of large scale features and apply local forecasting techniques to identify local features and their impacts on the local weather.

El Fandy et al. (1994) examined the predictability of Nile water discharge using rainfall in the source region of the Ethiopian Highlands. The evolution one year ahead is projected from information on the past behavior of the respective time series. Remarkably though, no use is made of other regional rainfall amounts a few months beforehand or any other possible teleconnection links (Bhatt 1989, Hastenrath et al. 1993). On purely statistical grounds, Farmer (1988) and Hutchinson (1992) demonstrated predictability of a small portion of the variance of the Short Rains from the Southern Oscillation Index. This has been documented by other authors as well but with little statistical significance or predictive confidence.

Solar Forcing Factors

While a persistent signal has not been defined, meteorological variables in the region are suspected to be influenced, at least to some degree, by solar parameters (Faure and Leroux, 1990). The region has

rainfall patterns of successive sequences of drought and inundation, each lasting several years. Many authors have observed the area as showing a strong quasi-biennial fluctuation of around 2.3 years while an 11.4-year signal was also seen in many records of extreme (positive and negative) river run-off. While the mechanisms are not completely understood, some models inferred that small changes in the general circulation due to changing solar parameters may enhance or diminish ITCZ influences.

When considering the effects of solar forcing on regional rainfall, one cannot argue that there is no effect since past major climatic fluctuations have proven otherwise. It is widely known that lake level fluctuations occurred in Eastern Africa and that the lakes were at their most recent highest during the early Holocene around 9000-8000 years before present (yBP) (Butzer et al., 1972; Street-Perrott and Grove, 1976) and their most recent lowest during the last glacial maximum (LGM) around 18000-21000 yBP (Crowley and North, 1991). The reason for the high lake levels during the early Holocene is thought to be the result of an intensification and possibly more poleward extent of the ITCZ (Nicholson and Flohn, 1980; Street-Perrott and Roberts, 1983). This conclusion is also seen in evidence from deep sea cores in that the intensification of the ITCZ caused stronger monsoonal trade winds and upwelling in the adjacent seas off the African coast (Prell and Van Campo, 1986). Street-Perrott and Grove (1976) initially analyzed fluctuations in African closed-basin lakes and determined they were more related to climate than erosion or anthropogenic effects. The lakes in Eastern Africa are ideal to study since many are indeed closed basins and only produce outflow at their highest levels.

The most plausible explanation for the increased strength of the ITCZ is that which is due to Milankovich forcing mechanisms (Kutzbach, 1983; Street-Perrott et al., 1990). Using a GCM and different orbital parameters of the planet, an intensified ITCZ was found to occur over both Africa and Eurasia during the summer months of 9000 yBP (Kutzbach, 1981). Even though the average annual solar radiation for 9000 yBP is close to our present value, it was most likely 7% greater than

present in July and 7% less than present in January in the NH. Variations of the orbital parameters of obliquity, eccentricity, and precession (Fig. 18) have been found to be very important as the cause of glacial-interglacial fluctuations of the past (Hays et al., 1976; Imbrie and Imbrie, 1980). While Street-Perrott and Grove (1976) indicated that increased tropical precipitation might have lagged orbital forcing by a few thousand years, Crowley and North (1991) indicated tropical heating due to solar insolation may be sensitive on both semi-annual and annual cycles.

In any case, the result of the increased insolation during the early Holocene is thought to have been that of an enhanced or more poleward extent of the ITCZ over Eastern Africa during the NH summer. The large heating effect of the Saharan Desert and Tibetan Plateau might have even possibly pulled the ITCZ so far northward that the Coriolis force turned the southeasterly trades into southwesterlies over Eastern Africa bringing in additional moisture from the Congo Basin.

Atmospheric Aerosol Factors

During the LGM, it appears that increased aerosols may have lowered tropical rainfall since the stability of the atmosphere would have been increased (Crowley and North, 1991). Concerning the ITCZ, increased aerosols may reduce insolation thereby leading to weaker monsoonal forcing, less precipitation along the ITCZ and, therefore, lower lake levels over extended periods such as the LGM. While little work has been done on the effects of aerosols during past climates, recent work has been done on the climatic effects of volcanism. A significant volcanic vertical eruption throws huge amounts of ash and debris into the stratosphere and thus reduces insolation. The most recent eruptions with known climatic responses are the eruption of Mount Tambora in 1815 and the smaller eruption of Mount Pinatubo in 1991 (Duncan, 1996). The eruption of Mount Tambora (deemed the largest since the LGM) has been linked to exceptionally cold temperatures for two years thereafter and the year 1816 is known as the year without a summer over New England and Canada (Duncan, 1996; Stommel and Stommel, 1981; Stothers,

1984; and Crowley and North, 1991). Sear et al. (1987) and Bradley (1988) studied volcanic eruptions over the most recent 100 years and found significant eruptions can cause reduced insolation for a period of about six months while larger eruptions may affect the climate longer. Therefore, the evidence indicates that both changes in insolation due to varying solar parameters and atmospheric aerosol effects do indeed influence the climate. This study attempts to determine if such influences are detectable in the precipitation record on small enough time scales to aid in seasonal forecasting efforts.

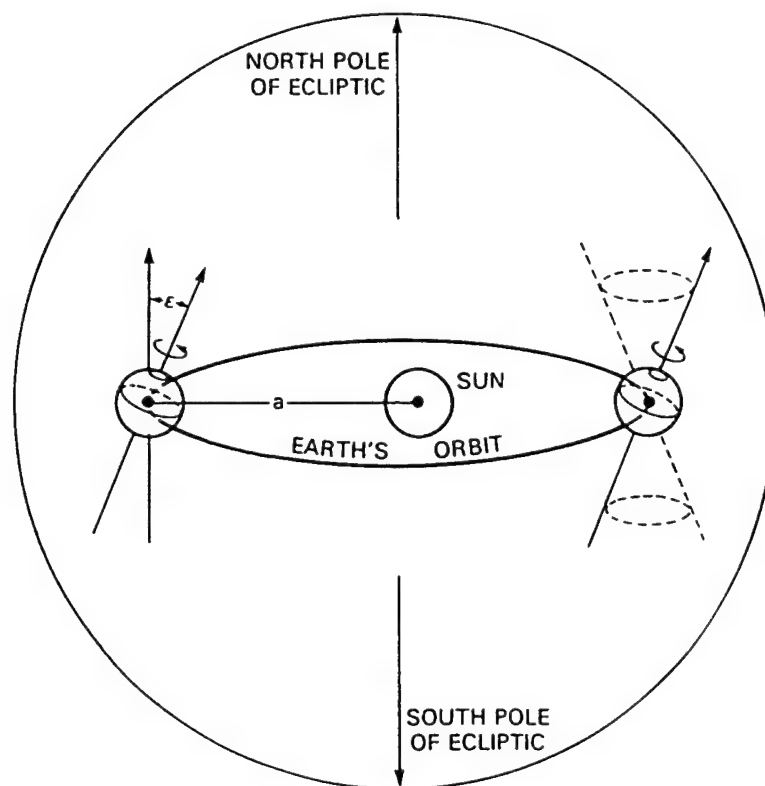


Fig. 18. Schematic diagram illustrating the effect of planetary forces on the earth's axis and orbit. These forces cause changes in the ellipticity of the orbit (eccentricity), the tilt of the rotational pole (obliquity), and the gyroscopic spin of the planet (precession).

CHAPTER III

DATA COLLECTION

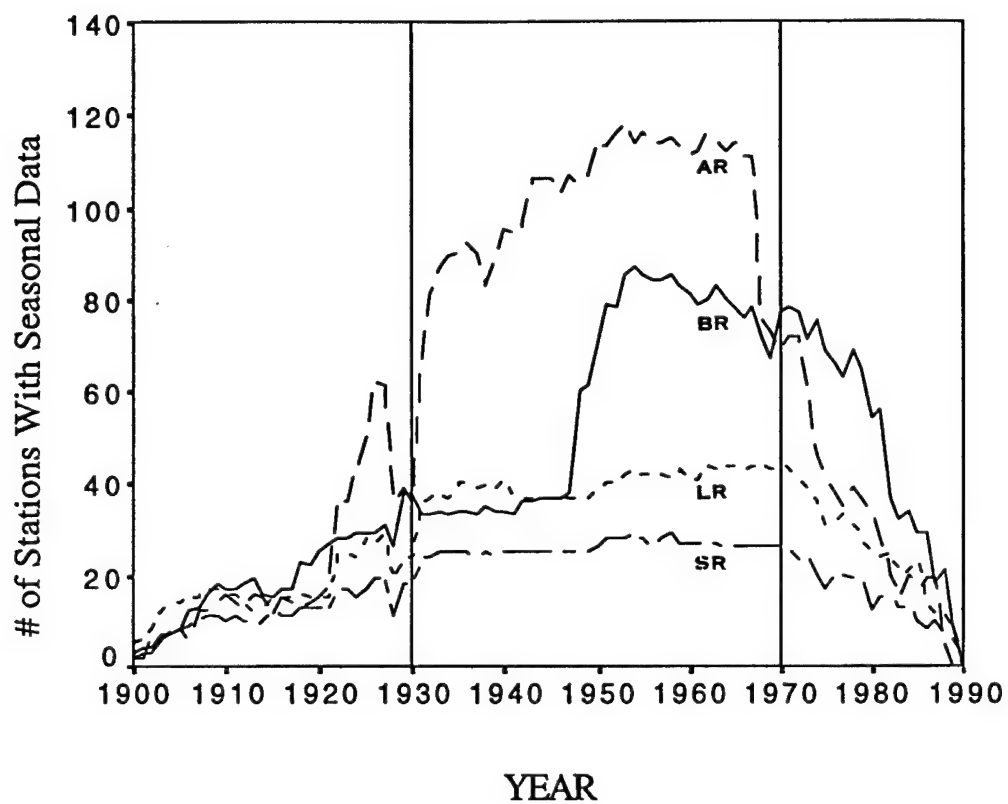
Rainfall Data

A thorough search of all available datasets was conducted to choose the one of highest research-quality. Precipitation data from the Global Historical Climatology Network (GHCN) project (Version 1) is used due to its high quality control. The dataset is substituted with additional observations from an ongoing historical data digitization effort at Texas A&M University which will be incorporated into future versions of the GHCN database. While other precipitation records were found for the region, they were notorious for missing data, poor (if any) quality control, short periods of record (POR), and having no WMO station numbers. To keep the dataset to the highest quality of standards, these observations are not used in the main analysis but were available for detailed synoptic analyses as required. Although 91 years of the GHCN data were available for analysis, a 41-year POR (1930-1970) was used for uniformity in the number of available observations (Fig. 19).

Radiational Forcing Data

Using solar insolation, atmospheric aerosol and greenhouse gas radiational forcing data as modeled by Stevens (1997), the rainfall data time series were compared with insolation forcing values to determine any detectable influences. Also analyzed were whether or not these same forcings affect the poleward extremity of the ITCZ's rainfall influence.

Stevens examined the records of solar cycle variability, stratospheric (mostly volcanic) aerosols, greenhouse gases, and tropospheric aerosols to estimate their radiational forcing effects on insolation by using an energy balance model (EBM). These effects (Fig. 20) are expressed in watts per square meter and may be combined through simple addition.



Rainfall Seasons

- Boreal Rains (BR)
- - - Long Rains (LR)
- - - Short Rains (SR)
- - - Austral Rains (AR)

Fig. 19. Number of locations within the research area with available monthly observations. The POR used is shown between the two vertical lines (1930-1970).

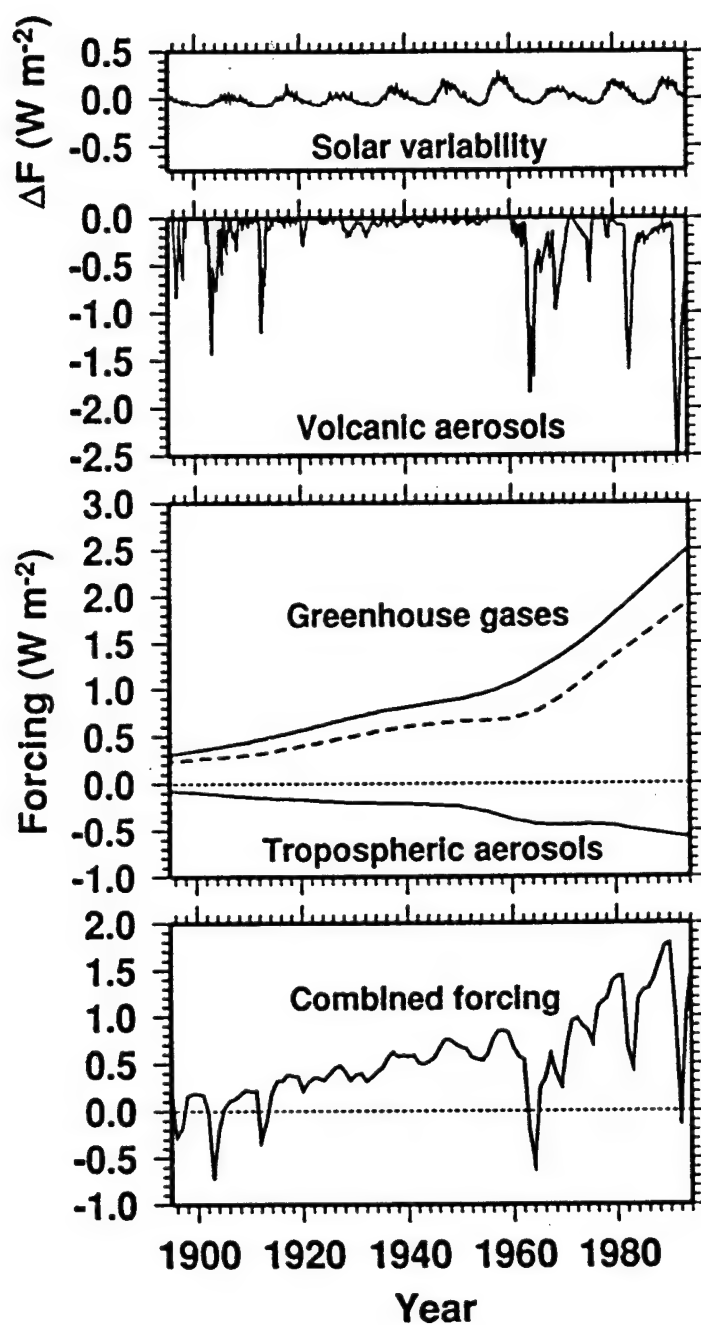


Fig. 20. Time series of the global means of climate forcings (by Stevens, 1997). The volcanic (stratospheric) aerosol forcing is a monthly mean, whereas the tropospheric aerosol, greenhouse gas, and combined forcings are annual means.

The effects due to tropospheric aerosols were not used since their measurement is extremely questionable over the African continent and little is known about their influence on the climate system.

Teleconnection Indices

Once significant results are found in a relationship, the next question asked is: Can they be improved upon? Two indices of physical climate teleconnections (or climatic events) were used to determine if the predictive relationships found could be strengthened during periods with anomalies of these climatic events. They are the SOI and the Asian Summer Pattern (ASP) index as used operationally by the U.S. Climate Prediction Center (CPC).

The SOI is simply a measure of the surface pressure at Tahiti minus the surface pressure at Darwin, Australia. While variations of the index are found, the most reliable is felt to be the SOI operational index at CPC despite a few missing years of early Tahiti data. CPC standardizes the monthly data (each monthly mean is divided by a long term mean) to remove any seasonality. It is an operational index, updated monthly, and is available via the internet for worldwide users. Therefore, when using the predictive guidelines of this research, users only need to reference the SOI values without having to know the process involved in their computation.

The CPC ASP index is used to evaluate forcing effects on the poleward progression of the ITCZ's rainfall influence over Eastern Africa. A low index, which indicates below normal pressure anomalies and a negative ASP phase, may tend to pull the ITCZ more poleward over the Asian continent and Eastern Africa. A high index, which indicates above normal pressure anomalies and a positive ASP phase, may indicate the ITCZ might remain more equatorward than its mean most poleward position (Fig. 6).

The ASP index is only statistically valid from June-August (Barnston and Livezey, 1987). Like the SOI, it is an operational index, updated monthly, and is available via the internet for worldwide users. Therefore, when using the predictive guidelines within this research,

users only need to reference the ASP values without having to know the process involved in their computation.

ENSO Events

Recent attempts to quantify the definition of an El Nino warm episode in terms of Pacific SST anomalies cannot cover the POR of this research due to the lack of adequate SST measurements during the period (Trenberth, 1997). Although they are qualitative and based on phenomena along the South American coast, the moderate to strong warm episodic (El Nino) years as identified by Rasmusson and Carpenter (1982) and Quinn et al. (1978) (Table 1) are considered reliable (Trenberth, 1997) and were used throughout this work.

Table 1. Warm episode (El Nino) years in the eastern equatorial Pacific as identified by (R), Rasmusson and Carpenter (1982); and (Q), Quinn et al. (1978).

Year	Source	Year	Source	Year	Source
1930	R	1941	Q	1957	R
1932	R	1951	R	1965	R
1939	Q	1953	R	1969	R

CHAPTER IV

PROCEDURES AND METHODS OF ANALYSIS

Determining Rainfall Seasonality

Ninety-one years of rainfall data (1900-1990) were extracted from the GHCN database for all stations within the research area (Fig. 2). The data from individual stations were first compared against data from other regional stations to investigate the seasonality of rainfall associated with the passage of the ITCZ. When examining the timing of seasonal rainfall in the equatorial region, nowhere is rainfall uniformity more evident than among the three stations located closely together in the metropolitan area of Nairobi, Kenya (Fig. 21). The dominating seasonal influences of both the Long and Short Rains are very evident as well as other features such as terrain influences. For example, the higher the elevation of each station in Figure 21, the higher is its monthly average rainfall. Another important timing aspect concerning rainfall uniformity throughout the region is that correlation coefficients (Pearson), which were computed between these three stations, are higher during seasons when ITCZ-forcing is present versus seasons when it is not (Fig. 22).

This same rainfall climatic pattern emerges when a broader view of the equatorial region is examined. Figure 23 depicts monthly average rainfall for stations located throughout northeastern Kenya and western Somalia, and again, there is a dominating seasonal influence of ITCZ-associated rainfall. Geographical influences are also evident in Figure 23 since some stations are influenced earlier than others by the ITCZ as it progresses north and south. And, even though several stations are separated by several degrees of latitude, the monthly seasonality of ITCZ-associated rainfall is fairly consistent on a temporal scale for all stations throughout the region. Most probably, this is attributed to the

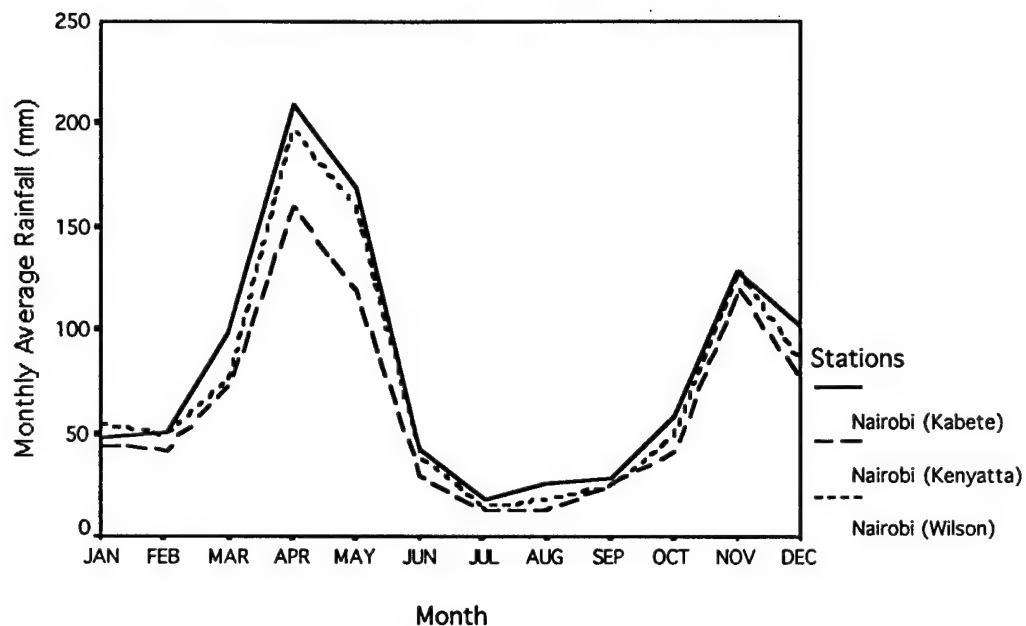


Fig. 21. Comparison of annual seasonal rainfall patterns for three stations located within Nairobi, Kenya.

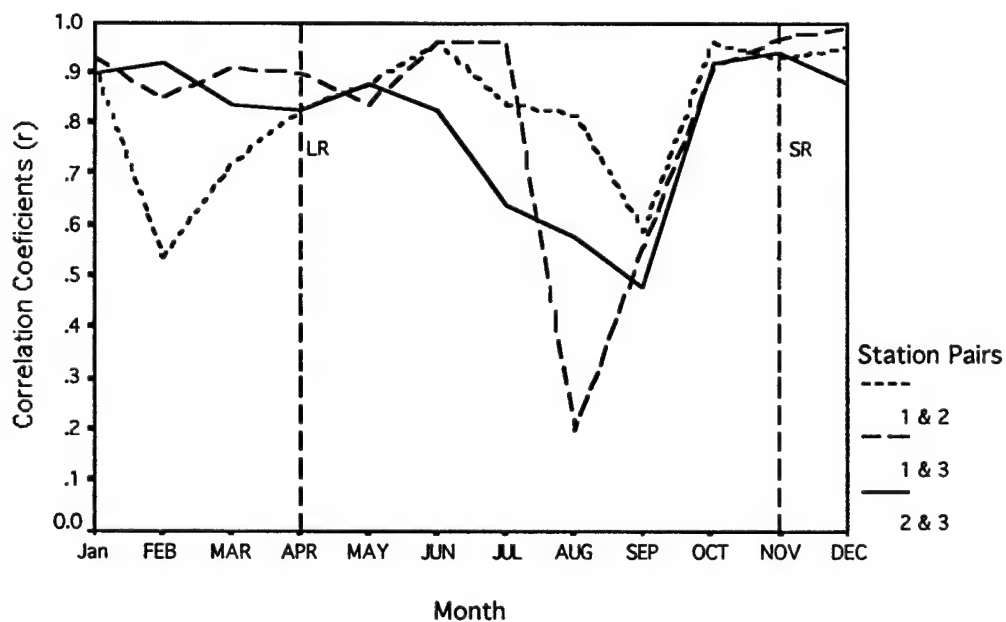


Fig. 22. Correlation coefficients between data from stations within the Nairobi, Kenya area (1-Kabete, 2-Kenyatta, 3-Wilson).

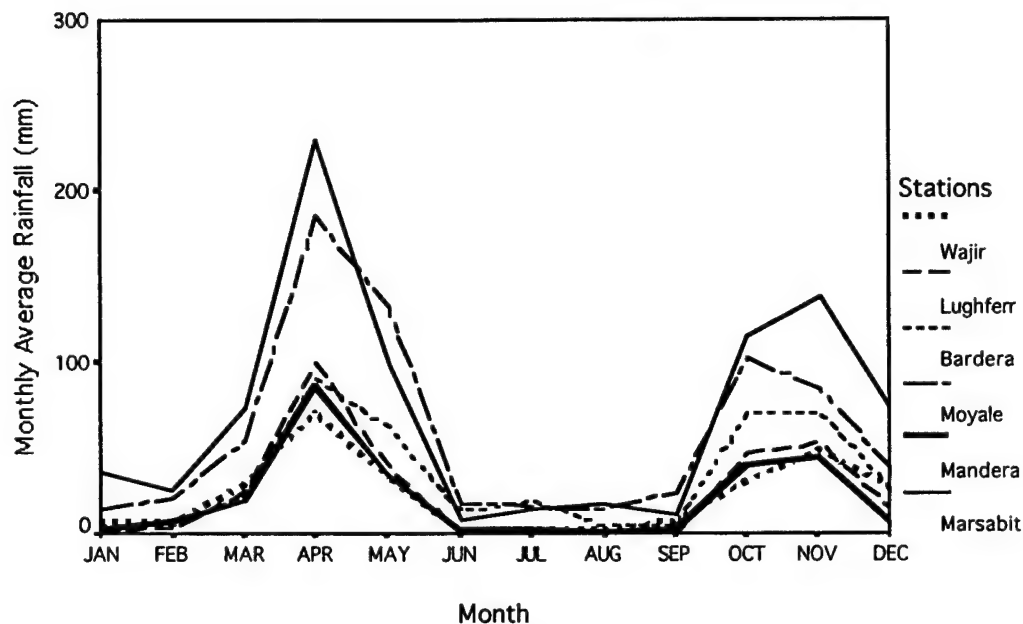


Fig. 23. Comparison of annual seasonal rainfall patterns for stations in northeastern Kenya and western Somalia.

speed at which the solar declination (which forces the ITCZ) travels across the region (roughly 15 miles/day or 450 miles/month).

Another finding was that data from coastal stations tend to experience a lag effect over data from inland stations in the eastern part of the region since during the LR season, the ITCZ passes to the north but, behind it, the flow (especially for coastal stations) is still onshore bringing additional moisture. The opposite situation occurs during the SR season since, after the ITCZ passes to the south, the flow tends to be offshore (Fig. 24). This phenomenon alone probably accounts for why the Short Rains are indeed shorter than the Long Rains and of a lesser intensity.

The spatial uniformity of rainfall within the region cannot be examined using rainfall totals due to a large variation of rainfall amounts between stations. A more appropriate method is to compare the percent of its average rainfall which each station receives. Therefore,

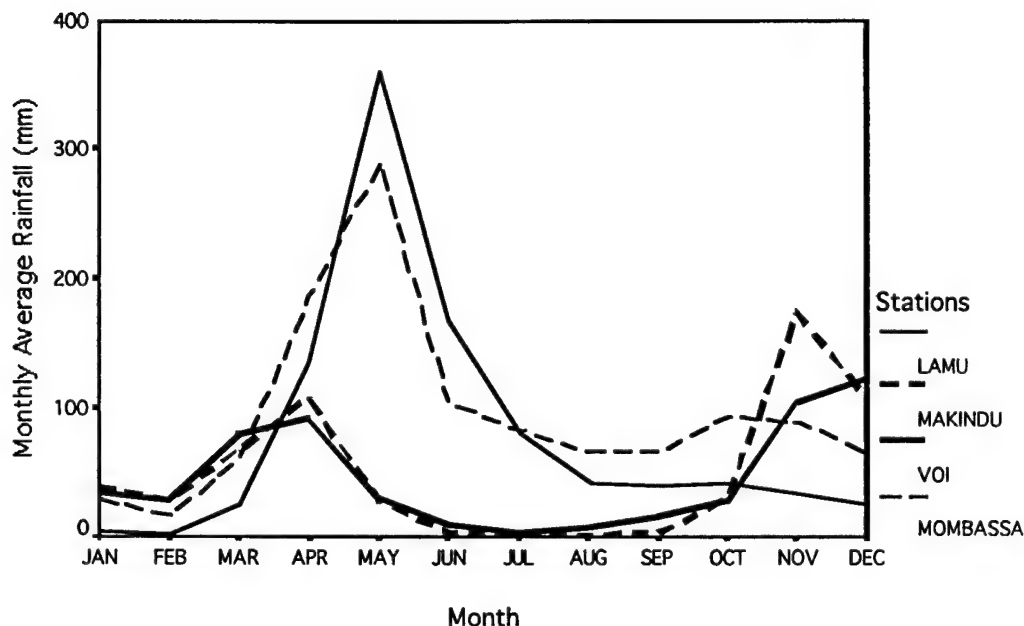


Fig. 24. Comparison of annual seasonal rainfall patterns for two inland stations (dark lines) and two coastal stations (light lines) in Kenya.

for each station, long term monthly means were calculated and the percent of average rainfall was then computed for each month by dividing by that month's long term mean. Using the percent of average rainfall is a valid means of comparing monthly or seasonal rainfall amounts and, performing such linear transformations on the data does not change the results of correlation analyses or many other statistical procedures.

To examine spatial uniformity, sixteen stations were chosen throughout the region of northeastern Kenya and western Somalia. The three driest as well as the three wettest years for each station (during the LR) were extracted and compared using the percent of average rainfall received. Despite difficulty due to coastal stations having a higher degree of variability than stations inland or at higher elevations, when the data were divided into categories of percent of average rainfall during these extreme years, the same climatic rainfall

signal (extremely dry or wet conditions), was seen throughout the region. Therefore, rainfall uniformity, associated with the passage of the ITCZ on both spatial and temporal scales, seems to exist on a regional scale throughout Eastern Africa.

The Development of Rainfall Seasons

Monthly rainfall patterns for all stations were next visualized and examined to begin the development of seasonal rainfall indices which are representative of regional rainfall amounts. The concept of a "rainy season" was developed by determining that if a station had a monthly average greater than (1/12th) of its annual average during any month, then that month was deemed a "rainy month." Two or more such months in succession were deemed to compose a "rainy season." The months were then viewed in tabular format to visualize the seasonal patterns and to selectively determine which stations do not fit the expected patterns of ITCZ-associated rainfall. Table 2 displays a sample tabular pattern from one of the tables for stations in the equatorial region (with an (X) depicting a "rainy month").

The influences of ITCZ-associated rainfall in this region come from both the Long Rains which occur from around March through May and the Short Rains which occur around October through November. While most stations near the equator do indeed fit the expected pattern of ITCZ-associated rainfall, the ones designated with a (P) do not (in the "Code" column of Table 2). Most of these were determined to be influenced by either coastal, terrain, or other local synoptic influences which a local forecaster would have to account for when using the predictive guidelines established in this research. Therefore, these stations were deleted from further analysis.

Tables 3 and 4 are the same as Table 2 except they represent samples from the northern and southern extremes of the research area. Most of the stations that were deleted from the northern portion had extremely low annual rainfall totals (desert locations) thus making their monthly patterns unreliable. But as one surveys the columns of monthly data within Table 3, a reliable pattern emerges away from the extremes since

Table 2. A visualization of seasonal rainfall patterns for stations near the equator. An (O) indicates average monthly rainfall is less than 1/12th of the annual average for that month and (X) indicates that it is equal to or above the annual average. A (P) in the Code column indicates that the station was deleted from the analysis due to a non-conforming rainfall pattern.

Lat	Lon	Station	Country	Month												Code
				1	2	3	4	5	6	7	8	9	10	11	12	
1.02	35.00	Kitale	Kenya	O	O	O	X	X	X	X	X	X	O	O	O	P
1.00	32.90	Namasagali	Uganda	O	O	X	X	X	O	O	X	X	X	X	O	
0.70	37.00	Fort Hall	Kenya	O	O	X	X	X	O	O	O	O	X	X	O	
0.68	34.17	Tororo	Uganda	O	O	X	X	X	O	O	O	O	X	O	O	
0.60	30.30	Fort Portal	Uganda	O	O	X	X	X	O	O	O	X	X	X	O	
0.53	35.28	Eldoret	Kenya	O	O	O	X	X	X	X	X	X	O	O	O	P
0.32	32.62	Kampala	Uganda	O	O	X	X	X	O	O	O	O	X	X	O	
0.08	37.65	Meru	Kenya	O	O	X	X	X	O	O	O	O	X	X	X	
0.00	32.40	Entebbe	Uganda	O	O	X	X	X	O	O	O	O	O	X	O	
-0.10	34.75	Kisumu	Kenya	O	O	X	X	X	O	O	O	O	O	X	O	
-0.37	35.35	Kericho	Kenya	O	O	X	X	X	O	O	X	O	O	O	O	P
-0.40	31.40	Kibanda	Uganda	O	O	X	X	X	O	O	O	O	X	X	X	
-0.40	36.30	Naivasha	Kenya	O	O	O	X	X	O	O	X	O	O	X	O	P
-0.47	39.63	Garissa	Kenya	O	O	X	X	O	O	O	O	O	O	X	X	
-0.50	37.45	Embu	Kenya	O	O	X	X	X	O	O	O	O	X	X	O	
-0.62	30.65	Mbarara	Uganda	O	O	X	X	X	O	O	O	X	X	X	O	
-0.67	34.78	Kisii	Kenya	O	O	X	X	X	O	O	X	X	O	X	O	P
-1.13	35.83	Narok	Kenya	X	X	X	X	X	O	O	O	O	O	O	X	P
-1.30	36.80	Nairobi (Kab)	Kenya	O	O	X	X	X	O	O	O	O	O	X	X	
-1.30	38.00	Kitui	Kenya	O	O	X	X	O	O	O	O	O	O	X	X	

most stations, do indeed, conform to the expected pattern of ITCZ-associated seasonal rainfall.

When the number of rainy months was totaled for each station, an interesting feature presented itself when the northern and southern extremes of the research area were compared. In the north, the rainy seasons of each station tend to be shorter since the northeasterly trades are dry and tend to originate over the Arabian Peninsula. The southeasterly trades, on the other hand, have already traveled a long distance over land by the time the ITCZ reaches its most northern position. But in the south, the trades tend to have trajectories more over the Indian Ocean in both directions which continuously bring moisture

Table 3. Same as Table 2 except that it represents the most northern extreme of stations in the research area.

Lat	Lon	Station	Country	Month												Code
				1	2	3	4	5	6	7	8	9	10	11	12	
22.22	36.65	Halaib	Sudan	0	0	0	0	0	0	0	0	0	X	X	X	P
21.82	31.48	Wadi Halfa	Sudan	0	0	0	0	X	0	X	X	0	X	0	0	P
19.53	33.32	Abu Hamed	Sudan	0	0	0	0	0	0	X	X	0	0	0	0	
19.17	30.48	Dongola	Sudan	0	0	0	0	0	0	X	X	0	0	0	0	
19.10	37.33	Suakin	Sudan	X	0	0	0	0	0	0	0	0	X	X	X	P
19.00	36.80	Gebeit	Sudan	0	0	0	0	X	0	X	X	X	0	0	0	P
18.90	36.80	Gebeit Town	Sudan	0	0	0	0	0	0	X	X	X	0	0	0	
18.55	31.85	Karima	Sudan	0	0	0	0	0	0	X	X	X	0	0	0	
18.43	37.73	Tokar	Sudan	X	0	0	0	0	0	0	0	0	0	X	X	P
18.30	36.40	Haiya	Sudan	0	0	0	0	0	0	X	X	X	0	0	0	
18.23	38.18	Aqiq	Sudan	X	X	0	0	0	0	0	0	0	0	X	X	P
16.90	36.00	Ungwatiri	Sudan	0	0	0	0	0	0	X	X	X	0	0	0	
15.90	33.80	Abu Deleiq	Sudan	0	0	0	0	0	0	X	X	X	0	0	0	
15.83	36.15	Aroma	Sudan	0	0	0	0	0	0	X	X	X	0	0	0	
15.80	38.50	Keren	Ethiopia	0	0	0	0	0	X	X	X	X	0	0	0	
15.62	39.45	Massawa	Ethiopia	X	X	0	0	0	0	0	0	0	X	X	X	P
15.60	32.50	Shambat	Sudan	0	0	0	0	0	0	X	X	X	0	0	0	
15.60	32.55	Khartoum	Sudan	0	0	0	0	0	0	X	X	X	0	0	0	
15.60	37.90	Agordat	Ethiopia	0	0	0	0	0	X	X	X	X	0	0	0	
15.20	32.50	Jebel Aulia	Sudan	0	0	0	0	0	0	X	X	X	0	0	0	
15.20	32.90	El Masid	Sudan	0	0	0	0	0	0	X	X	X	0	0	0	
15.20	32.90	La'Ota	Sudan	0	0	0	0	0	0	X	X	X	0	0	0	
15.17	38.55	Asmara	Ethiopia	0	0	0	0	0	0	X	X	0	0	0	0	
15.10	32.80	Sudeira	Sudan	0	0	0	0	0	0	X	X	X	0	0	0	
15.00	33.10	Kamlin	Sudan	0	0	0	0	0	0	X	X	X	0	0	0	
14.90	32.70	Abu Quta	Sudan	0	0	0	0	0	0	X	X	X	0	0	0	
14.90	32.70	Kemeir	Sudan	0	0	0	0	0	0	X	X	X	0	0	0	
14.90	33.00	Dubeiba	Sudan	0	0	0	0	0	0	X	X	X	0	0	0	
14.90	33.10	M.C.K. 169	Sudan	0	0	0	0	0	0	X	X	X	0	0	0	
14.80	32.30	El Geteina	Sudan	0	0	0	0	0	0	X	X	X	0	0	0	
14.80	32.80	Abdel Magid	Sudan	0	0	0	0	0	0	X	X	X	0	0	0	
14.70	32.90	Kassawi	Sudan	0	0	0	0	0	0	X	X	X	0	0	0	
14.70	33.20	Qurashi	Sudan	0	0	0	0	0	0	X	X	X	0	0	0	
14.70	33.30	Rufa'a	Sudan	0	0	0	0	0	0	X	X	X	0	0	0	
14.60	32.20	Fatisa	Sudan	0	0	0	0	0	0	X	X	X	0	0	0	
14.60	33.00	Tabat	Sudan	0	0	0	0	0	0	X	X	X	0	0	0	
14.60	33.10	Tabat K55	Sudan	0	0	0	0	0	X	X	X	X	0	0	0	
14.60	33.10	Umm 'Udam	Sudan	0	0	0	0	0	X	X	X	X	0	0	0	
14.60	33.10	Wad Hussein	Sudan	0	0	0	0	0	X	X	X	X	0	0	0	
14.60	33.30	Wad Bilal	Sudan	0	0	0	0	0	X	X	X	X	0	0	0	
14.50	32.10	Wad Nimr	Sudan	0	0	0	0	0	0	X	X	X	0	0	0	
14.50	33.10	Futeis	Sudan	0	0	0	0	0	0	X	X	X	0	0	0	
14.40	33.30	Tuleih	Sudan	0	0	0	0	0	X	X	X	X	0	0	0	

Table 4. Same as Table 2 except that it represents the most southern extreme of stations in the research area.

Lat	Lon	Station	Country	Month												Code
				1	2	3	4	5	6	7	8	9	10	11	12	
-18.40	35.00	Inhaminga	Mozambique	X	X	X	O	O	O	O	O	O	O	X	X	
-18.50	36.40	Chinde	Mozambique	X	X	X	O	O	O	O	O	O	O	O	X	
-18.60	34.00	Vila Paiva	Mozambique	X	X	X	O	O	O	O	O	O	O	X	X	
-19.10	33.40	Vila Pery	Mozambique	X	X	X	O	O	O	O	O	O	O	X	X	
-19.12	33.47	Chimoio	Mozambique	X	X	X	O	O	O	O	O	O	O	X	X	
-19.20	34.20	Vila Machado	Mozambique	X	X	X	O	O	O	O	O	O	O	X	X	
-19.80	34.90	Beira	Mozambique	X	X	X	O	O	O	O	O	O	O	O	X	
-20.60	35.00	Nova Mamb.	Mozambique	X	X	X	O	O	O	O	O	O	O	X	X	
-22.00	34.10	Mabote	Mozambique	X	X	X	O	O	O	O	O	O	O	X	X	
-22.00	35.32	Vilanculos	Mozambique	X	X	X	O	O	O	O	O	O	O	O	X	
-22.30	31.20	Pafuri (RSA)	Mozambique	X	X	X	O	O	O	O	O	O	O	X	X	
-22.40	31.30	Pafuri	Mozambique	X	X	X	O	O	O	O	O	O	O	X	X	
-23.30	35.40	Massinga	Mozambique	X	X	X	O	O	O	O	O	O	O	O	X	

into the region. Although the steep eastern slopes of Madagascar tend to limit the effect, the AR region has relatively flat terrain on its eastern side, thus allowing the trades to fully penetrate the region.

Several additional criteria were used to selectively delete stations from further analysis whose data may reflect the influence of terrain or local synoptic factors more than ITCZ-associated rainfall. Any station whose data showed the expected ITCZ-associated rainfall pattern was kept while others, that may not offer an accurate representation of regional rainfall amounts, were deleted. Roughly 10-15% of stations in the BR and AR regions and 15-20% of the stations in the LR and SR regions were deleted.

First deleted were any stations with average annual rainfall totals less than 150 mm since these amounts may only derive from a few storms each year. Out of 13 stations deleted for this purpose, 12 were the most northern stations in the BR region (located in the desert) and all were north of the Ethiopian Highlands, which is the critical catchment area for the Blue Nile River.

Secondly, several stations were deleted for having less than 10 years (120 months) of data. Although any amount of data is helpful for determining representative regional rainfall amounts, stations with less than 10 years of data were deemed unreliable and most had periods of missing monthly data which prevented the computation of seasonal totals anyway.

Thirdly, station elevations were examined since one might argue that rainfall in high terrain locations may not represent the regional rainfall amounts as a whole. Since half of the stations in the GHCN database did not list station elevation data, elevations were also obtained from the Digital Terrain Elevation Data database developed by the Defense Mapping Agency (United States Air Force Environmental Technical Applications Center, 1992) which has a 100 meter horizontal grid resolution. However, after evaluating the data and station elevations, it became evident that even data from stations over 2,000 meters in elevation, depicted the same "rainy season" climate signal as stations in lower elevations within the same region. In addition, stations located in high terrain areas had a tendency to be located in very critical water resource catchment areas such as the Ethiopian Highlands which have a limited number of reporting stations to begin with. And, since the research was examining the percent of average rainfall instead of rainfall amounts, these stations were critical for the purpose of developing regional indices representative of regional rainfall amounts.

To develop seasonal indices, monthly data from the remaining stations were then totaled for each season to create rainy season totals for each year. In computing the seasonal data, all of the months in any one season had to have data in order for that season to be non-missing. In areas affected by both the Long and Short Rains, a rainy season total was calculated for each season although some stations only experience a LR season. And finally, due to the wide variation in rainfall amounts among stations, a linear transformation was performed on the data by dividing the seasonal rainfall totals for each station by the long-term

seasonal mean of that station to compute a seasonal percent of average rainfall for each season.

Creating Geographical Regions

The stations were then geographically separated into four main zones as shown in Figure 3. Buffer zones were established between the regions since, within these transition zones, the rainfall data from one station might exhibit a rainy season pattern indicative of the Long and Short Rains one year while exhibiting one indicative of the Austral Rains the next year.

Since no stations were found exhibiting a distinct LR or SR pattern more than 5° latitude from the equator, the central area was bounded by 5°S-5°N latitude. In the BR region, since no stations north of 16°N latitude exhibited the expected ITCZ-induced rainfall pattern (or received any annual rainfall at all), the region was bounded on the north by 16°N latitude and on the south by 8°N latitude leaving a 3°-wide buffer zone between the LR/SR and BR regions. Figure 25a displays yearly rainfall totals for a sample station located within the BR region using a 15-year POR (1930-1944) and, a distinct Boreal Rains seasonal rainfall pattern is identified. In Figure 25b, the yearly rainfall totals for a station located in the LR/SR region are displayed and, the distinct Long Rains and Short Rains seasonal rainfall patterns are easily identified. On the other hand, Figure 26 displays the yearly rainfall totals for a station located in the northern buffer zone (5°N-8°N) using the same POR. As can be seen, rainfall is difficult to categorize in this zone since the different seasonal patterns (except for the AR) are evident in different years. Therefore, too many factors are involved to identify any distinct spatial or temporal rainfall patterns within the buffer zones and it is left up to the local forecaster to produce seasonal guidelines for these regions.

For the AR region, stations exhibiting the expected ITCZ-associated rainfall pattern extend far to the south of 23.5°S latitude (the southern boundary of the research area). However, the AR seasonal rainfall pattern is also indicative of activity from transient synoptic weather

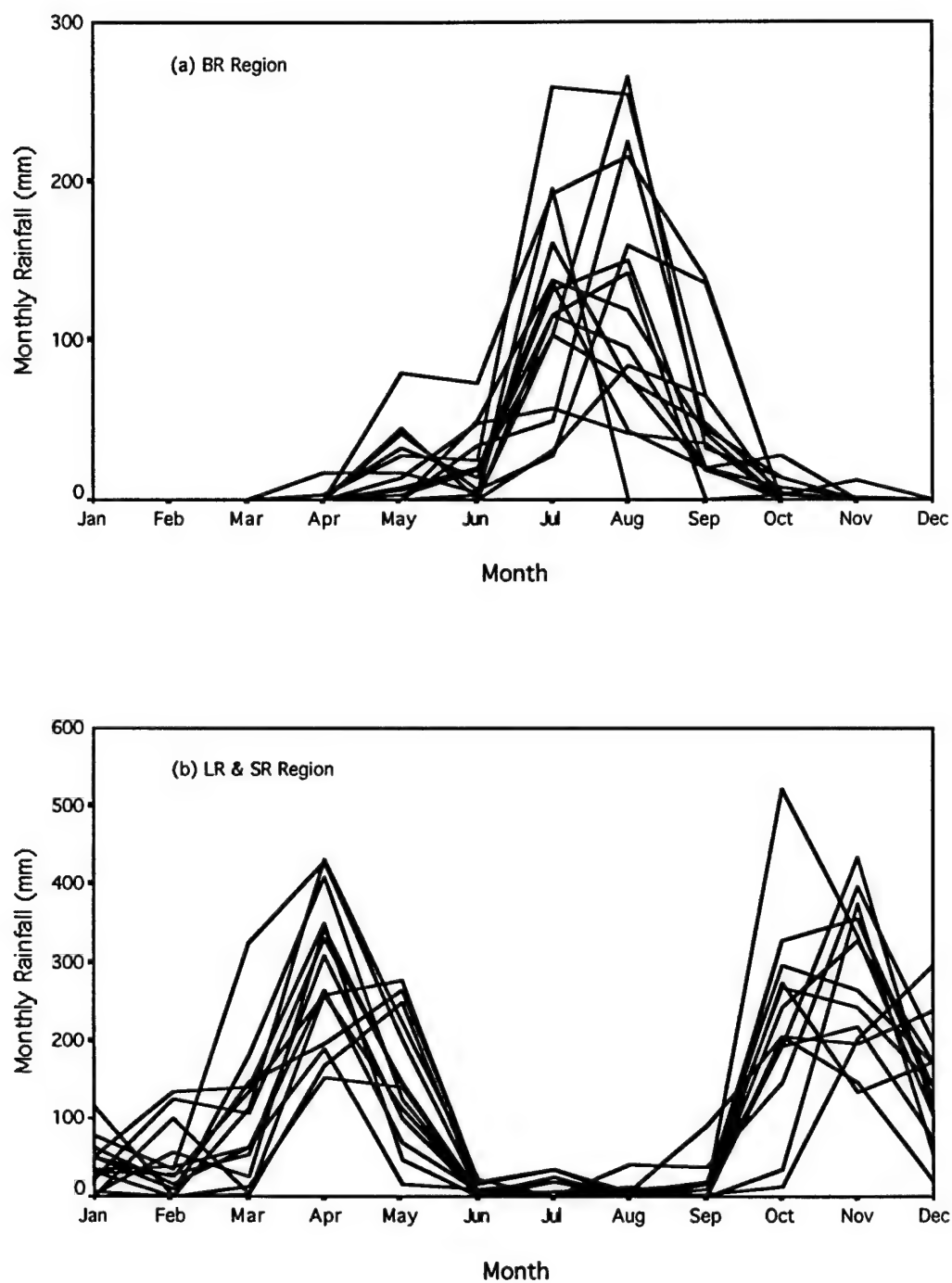


Fig. 25. Comparison of yearly rainfall patterns for (a) a BR station (Agordat, Ethiopia) and (b) a LR/SR station (Fort Hall, Kenya).

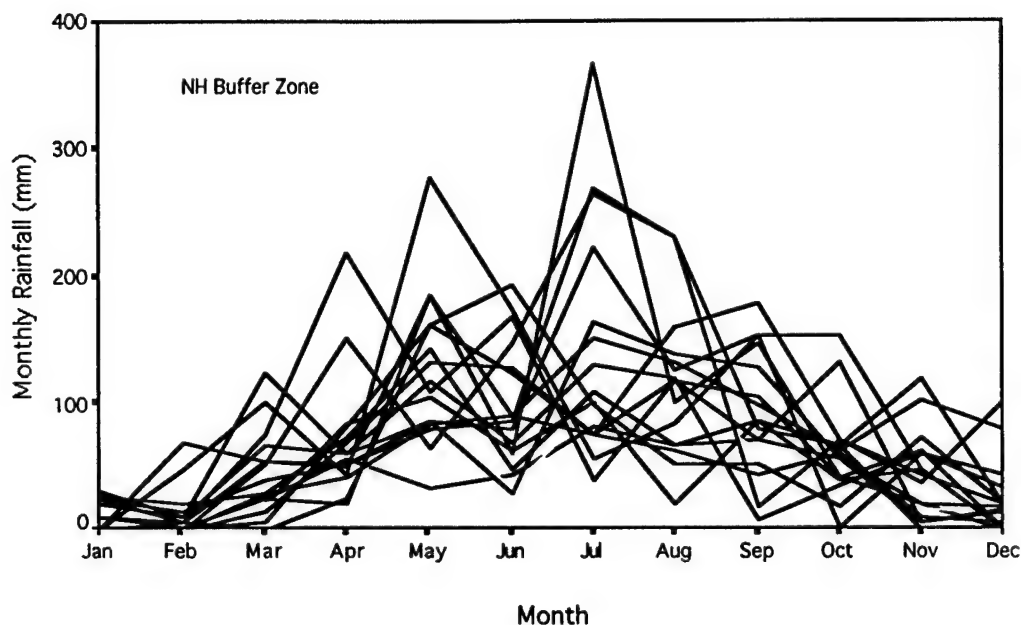


Fig. 26. Comparison of yearly rainfall patterns for a NH buffer zone station (Piber Post, Sudan).

systems off the eastern coast of the African continent. These systems follow a storm track which exists as a result of flow around the western side of the Mascarene high pressure cell and, on occasion, tropical cyclone activity is also present in this area southward of around 10°S . These systems combine to complicate the climate of the AR region making any predictive analyses of ITCZ-associated rainfall difficult. In other words, in any geographically defined region, representative of the Austral Rains season, rainfall activity is not only due to ITCZ-associated mechanisms but also from these transient synoptic weather systems as well. So, to be consistent with the area defined for the BR region and to limit these outside synoptic influences, the AR region was defined, consistent with the BR region, as bounded by $8\text{--}16^{\circ}\text{S}$ latitude which left a 3° latitude wide buffer zone between the LR/SR and AR regions.

After the elimination processes discussed in the previous section and the separation of the area into these four distinct geographical rainfall regions (Fig. 3), data for 174 locations were available for further analyses. Of these, 37 were located in the LR region, 71 in the BR region, 27 in the SR region, and 66 in the AR region. The 27 stations in the SR region are also included in the 37 stations within the LR region. Half of the 10 stations which were not included in both did not meet the criterion for a two month rainy season (they had 1 month only) or they were located on or very near the coast and are subject to coastal climate influences. Therefore, a total of 201 seasonal totals were available for further analyses each year (assuming no missing data). Figures 27-30 depict station locations and terrain features within the defined LR, BR, SR, and AR regions; respectively. Each station was identified with a unique number and a complete listing of all stations along with their locations within each region are found in Appendix A.

Cornu Criterion Normality Test

There are two very important concepts involved with statistics in climatology. First, statistical techniques are only tools and they may suggest, but cannot prove, a cause and effect relationship. Second, they usually require that certain conditions are met by the data before any tests are considered valid (Griffiths, 1990). But, whether or not any statistical tests are performed using the data is irrelevant to the fact that one must know the distribution of the data beforehand in order to determine if these conditions are met. These conditions may determine any limitations toward the use of the data.

With this in mind, the data from stations within each region were examined to determine whether or not they met the criteria for assuming that they may derive from a near normal distribution. Rainfall data are usually not normally distributed and previous studies have faltered by assuming normality when it may not have existed. Existing tests for normality are difficult to use though since they are difficult to interpret and not suitable for small samples.

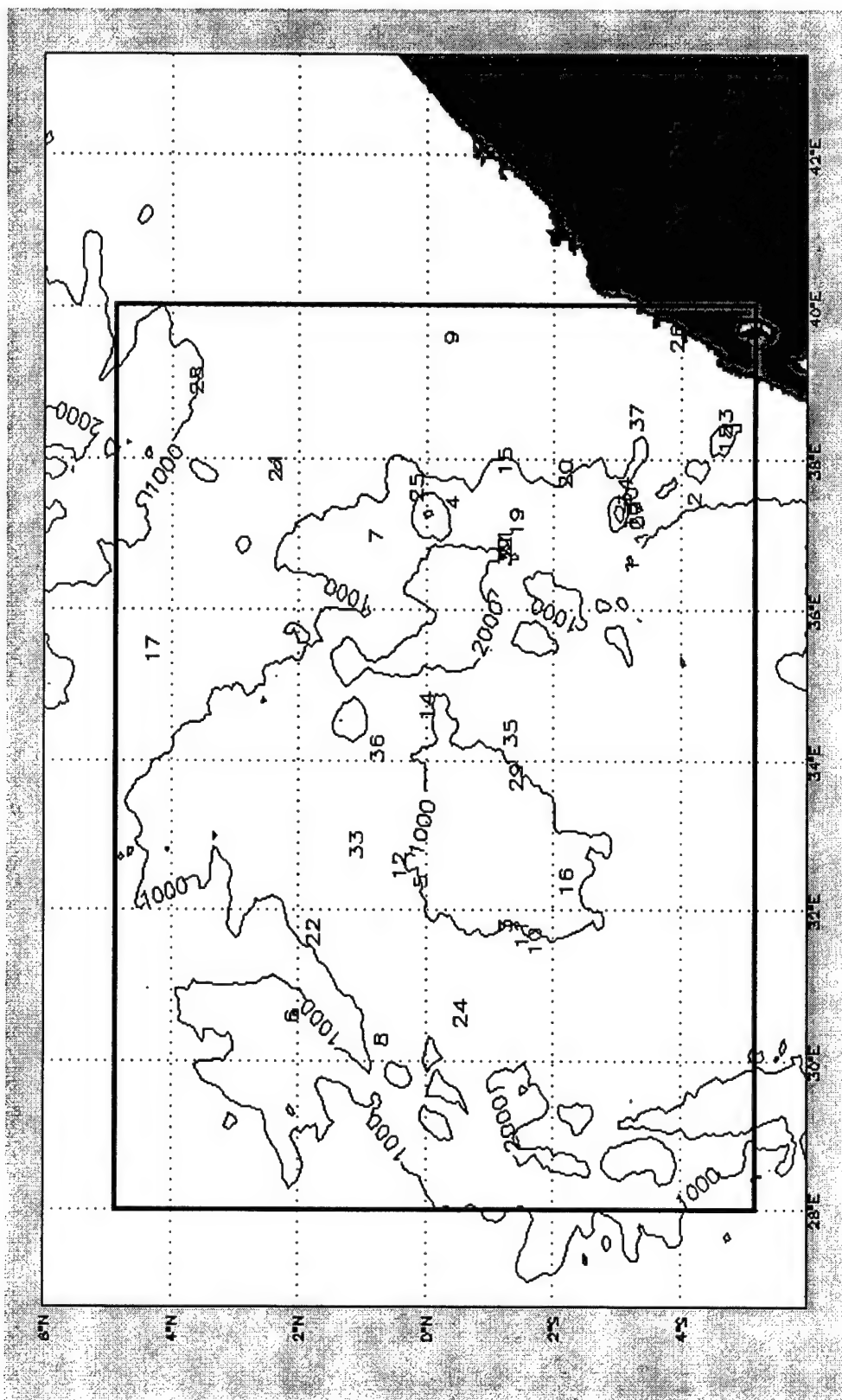


Fig. 27. Graph of the Long Rains (LR) region (enclosed in box). Stations are identified by number and listed in Appendix A. Terrain is contoured in 1,000 meter increments.

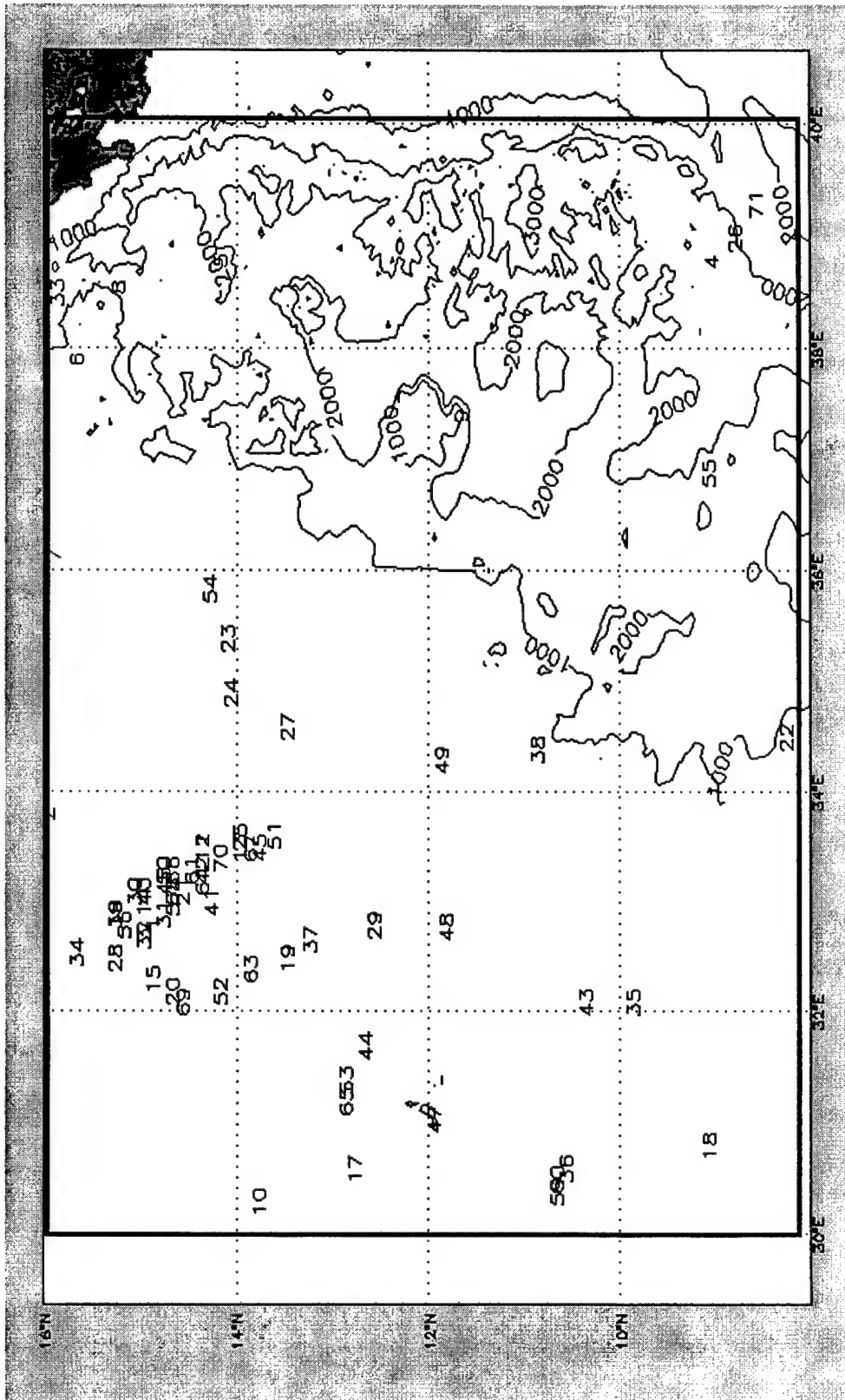


Fig. 28. Same as Figure 27 except for Boreal Rains (BR) region.

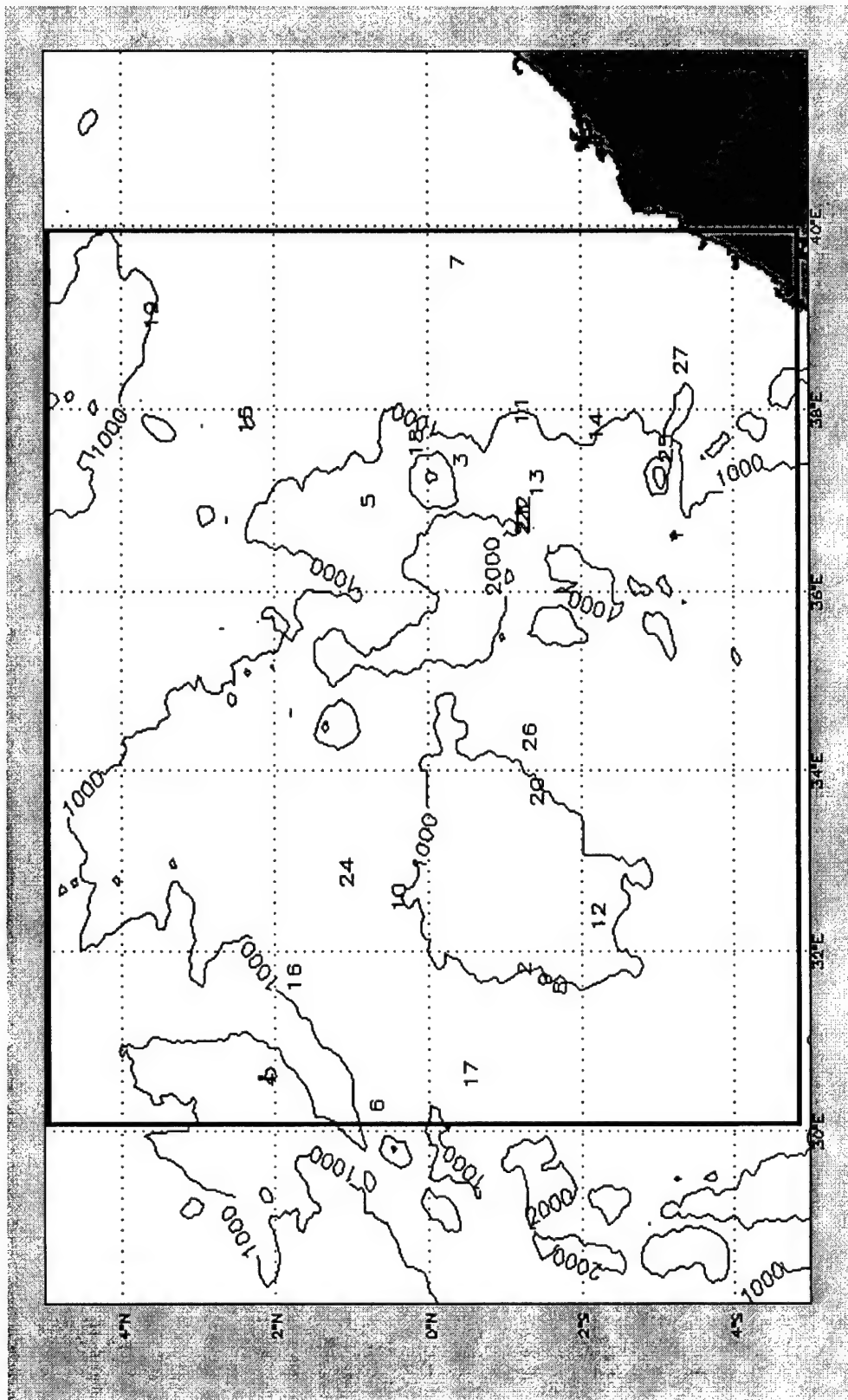


Fig. 29. Same as Figure 27 except for Short Rains (SR) region.

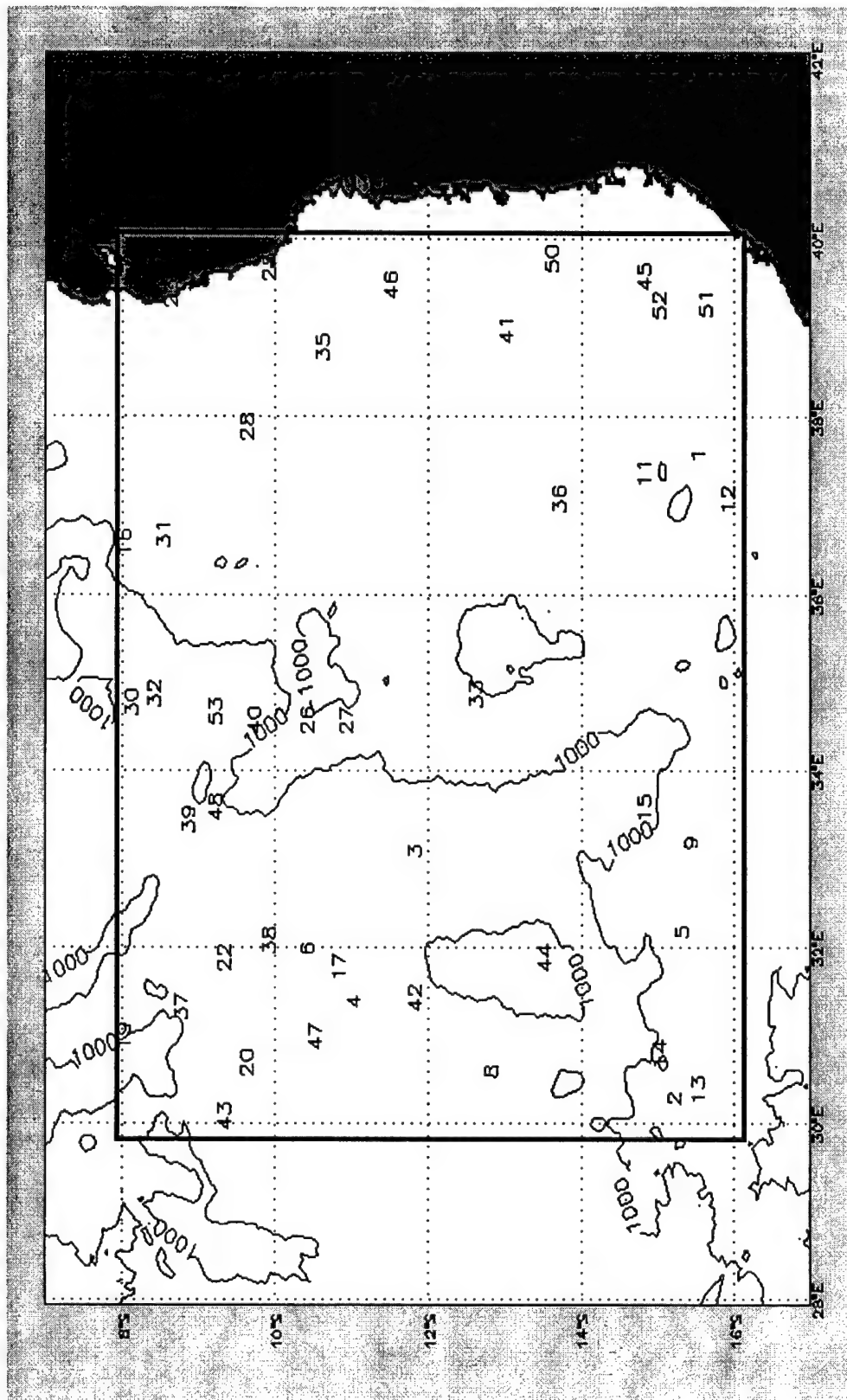


Fig. 30. Same as Figure 27 except for Austral Rains (AR) region.

This work uses the Cornu Criterion as a test for normality since it is suitable for small sample sizes (Geary, 1935; Brooks and Carruthers, 1953). The Cornu Criterion is based on the premise that within a purely normal distribution, the relationship between the mean deviation and the standard deviation is:

$$|e|/s = ((2/\pi)^{**1/2}) \approx 0.80$$

where (e) is the mean deviation of the data (or the average data difference from the overall average, irrespective of sign) and (s) is the standard deviation. However, due to the very complex computations involved, Geary only computed values for selected sample sizes (every 5) and used them to only graph the probability limits instead of listing them in tabular form also. As a result, this test was forgotten in the computer age since statistical computer programs require exact values for all sample sizes and these were missing from Geary's work. However, by using what values Geary did compute, and linear interpretation techniques between them, the Cornu Criterion was revitalized in this research to compute the lower and upper probability limits for each sample size shown in Figure 31. These limits are also listed in tabular form in Appendix B.

When using Figure 31, if the computed Cornu value for a particular sample falls outside the 1% limit lines, then there is only a 1% chance that the distribution is near normal. If the value falls outside the 5% limit lines, then there is only a 5% chance that the distribution is near normal. However, if the value falls within the limit lines, it does not guarantee that the distribution is normal since there is the opposite chance that it is not. One must always remember, that in actuality, nothing is perfectly normally distributed.

Data from individual stations within each region were examined for normality using the Cornu test with the results listed in Table 5. The first row (X) in Table 5 lists the percent of stations within each region whose observations failed the Cornu Criterion at both the 1 and 5% probability levels. For the 37 stations in the LR region, one would expect a 5% failure rate at the 5% level; however, a 19% failure rate was computed. The SR region had the largest failure rate with over 50%

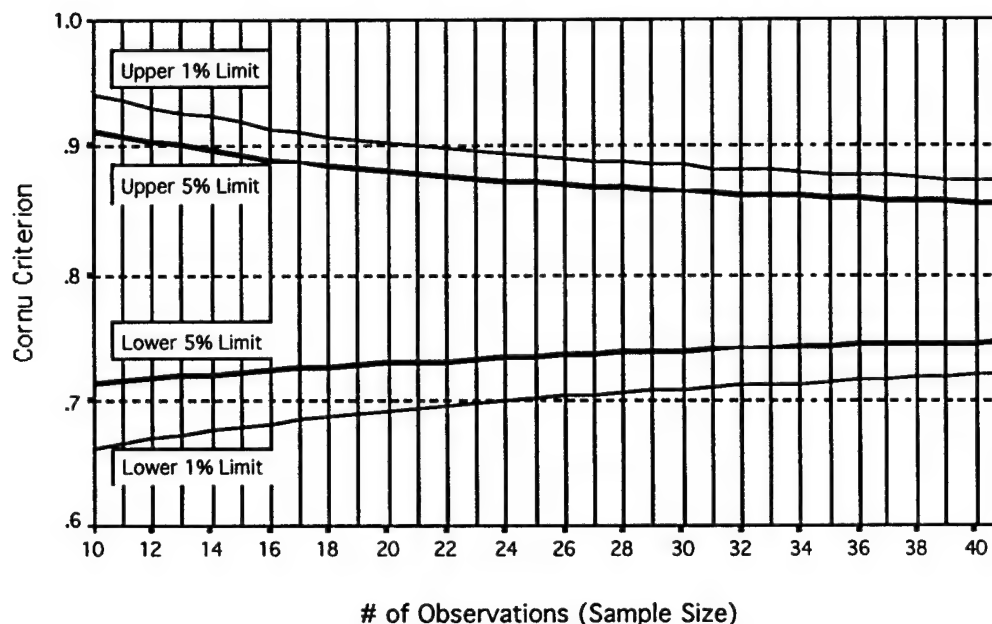


Fig. 31. Cornu Criterion probability levels for $n=10$ through $n=41$.

Table 5. The percent of stations within each region whose observations failed the Cornu Criterion at the 5 and 1% probability levels. (X) represents the data with no transformations and $\text{LOG}(X+6)$ represents the best linear transformation of the data.

Transformation	5% Level					1% Level				
	LR	BR	SR	AR	Average	LR	BR	SR	AR	Average
X	19	13	52	18	25	8	8	37	9	16
$\text{LOG}(X+6)$	16	8	15	26	16	14	3	4	15	9

failing at the 5% level. It was determined that most of these failures were stations located on the shores of Lake Victoria or in the highlands near Mount Kenya.

So by using the Cornu Criterion, it can be concluded that the failure rate within each region is unacceptable and prohibits us from assuming the data come from a near normal distribution. However, sometimes, linear transformations may be used on data to change its distribution to

one which may be more nearly normal. To examine this, a model was developed to compute all known linear transformations of the data and each one was tested using the Cornu Criterion. The linear transformation of $\text{LOG}(X+6)$, where (X) is the seasonal percent of average, was found to minimize the failure rates (on average) among all four regions (Table 5). However, even with these improved results, the failure rate was still unacceptable for using any assumption of normality.

The Creation of Regional Indices

Descriptive statistics on the rainfall data must be used with caution since the assumption of normality is not valid for the data from all the stations within each region. However, the assumption of normality is not required when simply averaging the seasonal percent of average rainfall amounts within each region for each year. Doing so creates regional means representative of an areal average for each region.

After computing these regional means, they themselves were tested for normality using the Cornu Criterion. While the data for the LR, BR, and AR regions passed at both the 5 and 1% levels, the data for the SR region did not. However, when four outlier years in the SR data (1951, 1961, 1963, and 1968), whose yearly means lay the farthest from the overall mean, were removed from the analysis, the SR data did pass the normality test. While 1951, 1963, and 1968 were determined to be years in which ENSO related events occurred, 1961 was not, but is theorized to be associated with a rare sequence of events that are discussed further in a later section.

In order to compare the data between the four separate regions (which is the same as comparing data between the four rainfall seasons), the regional mean's data were manipulated by a linear transformation into differences from their overall mean in terms of standard deviations from that mean. In doing so, regional indices were created which also represent the mean percent of average rainfall received within a region for a particular rainfall season. For example,

Table 6. Regional means and indices for the LR region.

Year	Regional Mean	POR Mean	POR STD	Difference From Mean	Difference in STD
1930	133.00	101.43	21.14	31.57	1.49
1931	110.03	101.43	21.14	8.60	0.41
1932	110.37	101.43	21.14	8.94	0.42
1933	55.84	101.43	21.14	-45.59	-2.16
1934	86.37	101.43	21.14	-15.06	-0.71
1935	87.88	101.43	21.14	-13.56	-0.64
1936	115.25	101.43	21.14	13.82	0.65
1937	131.00	101.43	21.14	29.57	1.40
1938	92.78	101.43	21.14	-8.65	-0.41
1939	98.29	101.43	21.14	-3.14	-0.15
1940	128.38	101.43	21.14	26.94	1.27
1941	105.40	101.43	21.14	3.97	0.19
1942	130.10	101.43	21.14	28.67	1.36
1943	88.37	101.43	21.14	-13.06	-0.62
1944	103.23	101.43	21.14	1.80	0.09
1945	73.27	101.43	21.14	-28.16	-1.33
1946	82.00	101.43	21.14	-19.43	-0.92
1947	136.40	101.43	21.14	34.97	1.65
1948	92.17	101.43	21.14	-9.26	-0.44
1949	69.90	101.43	21.14	-31.53	-1.49
1950	113.00	101.43	21.14	11.57	0.55
1951	136.67	101.43	21.14	35.24	1.67
1952	95.59	101.43	21.14	-5.84	-0.28
1953	80.68	101.43	21.14	-20.75	-0.98
1954	103.34	101.43	21.14	1.91	0.09
1955	77.44	101.43	21.14	-23.99	-1.13
1956	75.41	101.43	21.14	-26.02	-1.23
1957	107.97	101.43	21.14	6.54	0.31
1958	94.33	101.43	21.14	-7.10	-0.34
1959	90.06	101.43	21.14	-11.37	-0.54
1960	110.24	101.43	21.14	8.81	0.42
1961	85.48	101.43	21.14	-15.95	-0.75
1962	93.97	101.43	21.14	-7.46	-0.35
1963	119.51	101.43	21.14	18.08	0.86
1964	100.74	101.43	21.14	-0.69	-0.03
1965	73.94	101.43	21.14	-27.49	-1.30
1966	112.18	101.43	21.14	10.75	0.51
1967	121.76	101.43	21.14	20.33	0.96
1968	145.38	101.43	21.14	43.95	2.08
1969	78.79	101.43	21.14	-22.64	-1.07
1970	112.03	101.43	21.14	10.60	0.50

Table 6 lists the LR regional means, the overall mean and standard deviation, the difference from the overall mean, and that difference expressed in terms of standard deviations from the mean (which is just the difference divided by the standard deviation). From here on in this work, the terms regional means and regional indices are used interchangeably and both give an indication of the average percent of average rainfall received over each region during each season. In addition, the data are used in the form of their differences from the overall mean in terms of standard deviations from that mean. And, this form of the data is simply a linear transformation of the original regional means (average of the seasonal percent of average rainfall amounts among all stations within each region). This form is necessary since the means and standard deviations are different for each region.

Even though these regional indices were computed by only performing a linear transformation on the regional mean's data, they were again tested for normality using the Cornu Criterion. Figures 32-35 display the histograms of the regional indices for each region and, as one would expect, the data passed the Cornu Criterion for normality for all regions except the SR. However, when the four outlier years were removed from the analysis, the SR data passed. Figure 36 displays the histogram of the SR regional indices with the data from four outlier years removed (this series of data passed the normality test) and, Figure 37 displays the histogram of the SR regional indices with only the data from 1961 removed. Although the SR data still failed the Cornu Criterion when only the 1961 data were removed, the histogram depicting this distribution (Fig. 37) shows a remarkable improvement towards normality when compared to the distribution (Fig. 34) which includes the 1961 datum.

Time Series Analysis of the Regional Indices

A time series is defined as a set of observations obtained by measuring a single variable regularly over a period of time. In this work, the period of time is the POR (1930-1970) and the single variables are the regional indices (or regional means if one prefers) for each

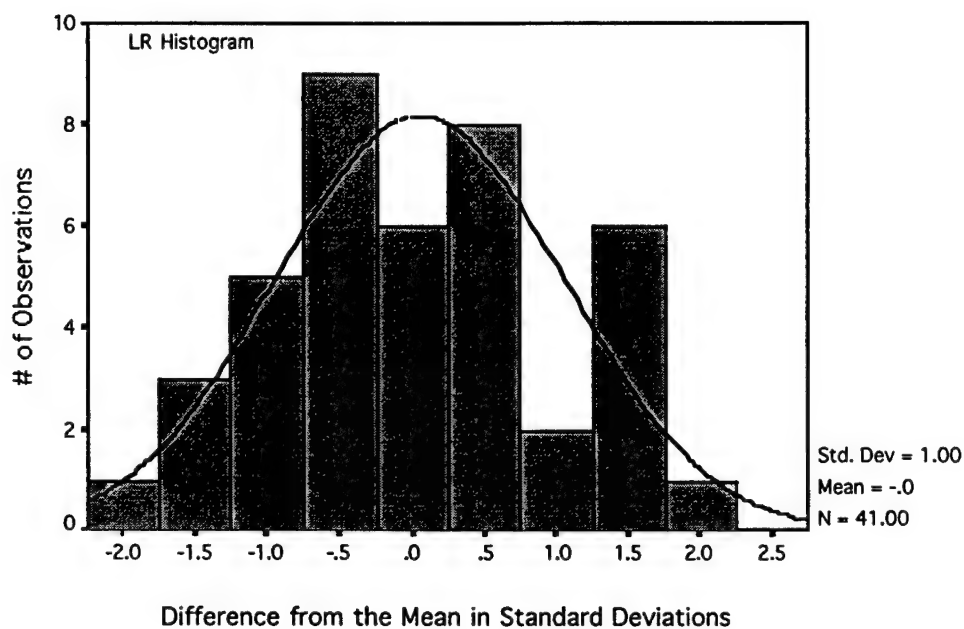


Fig. 32. Histogram of the LR regional indices expressed in terms of standard deviations from the mean. A normal curve is fitted to the data.

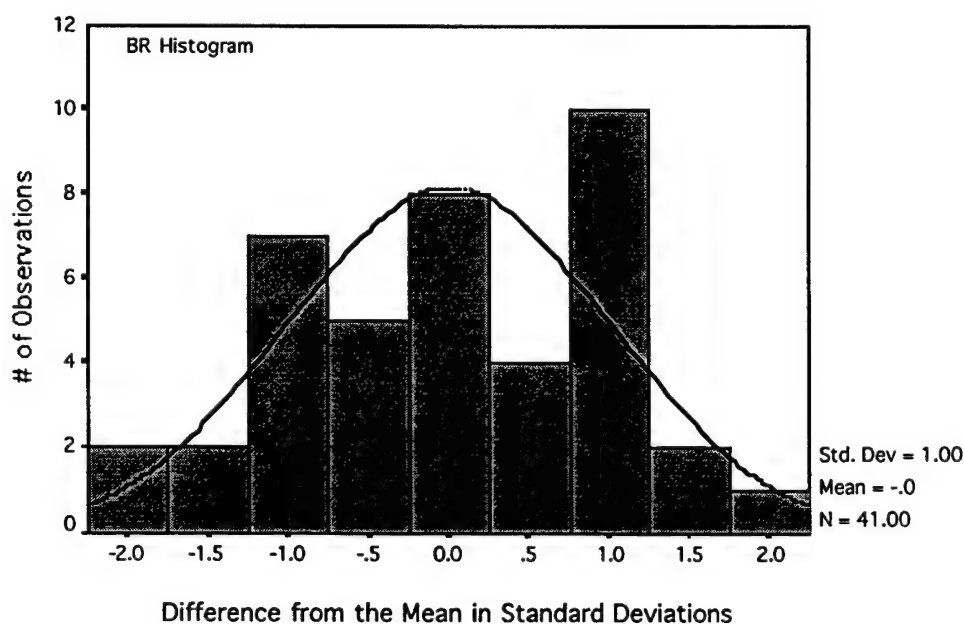


Fig. 33. Same as Figure 32 except for the BR region.

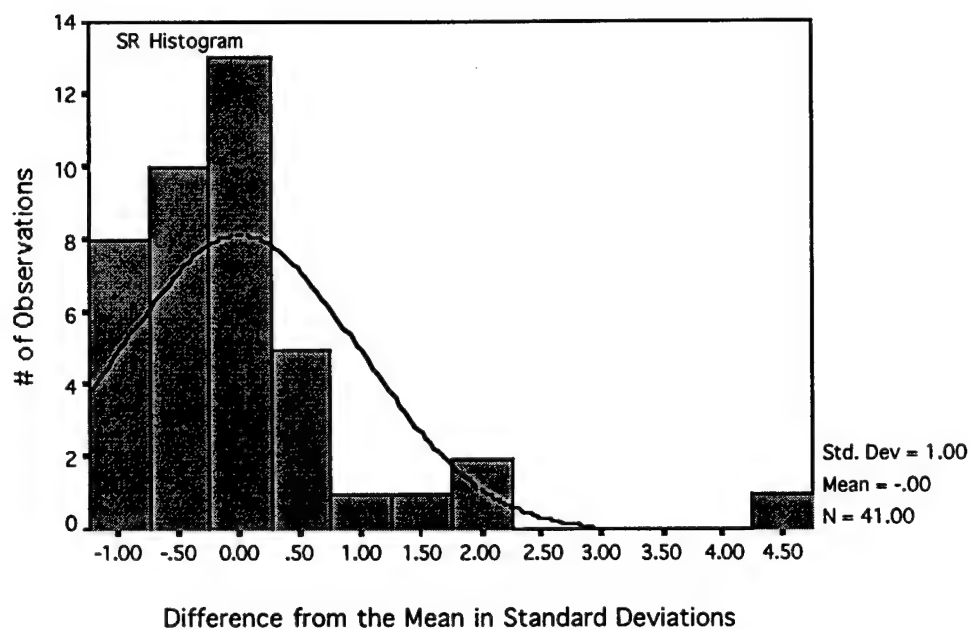


Fig. 34. Same as Figure 32 except for the SR region.

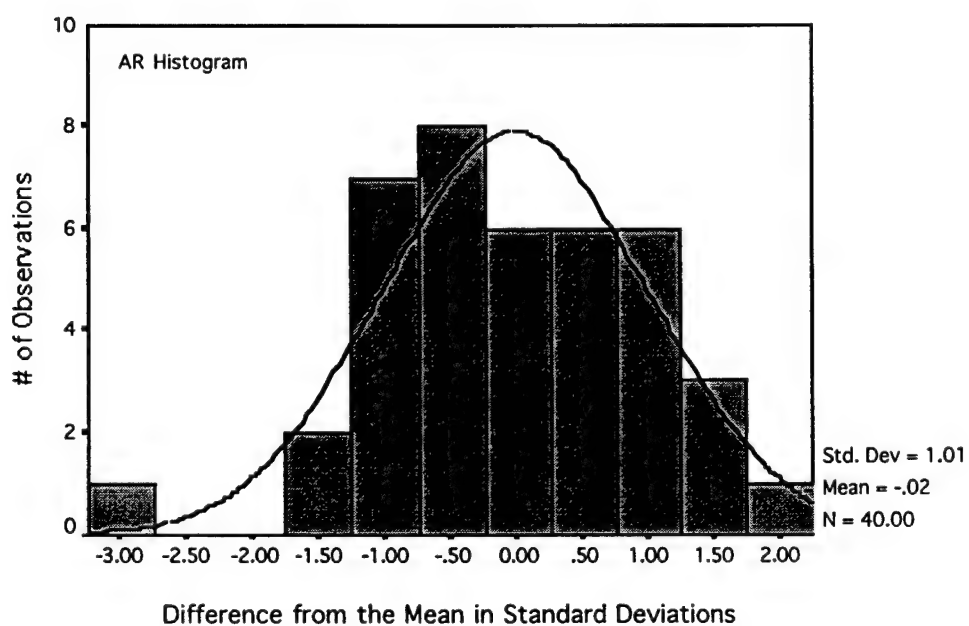


Fig. 35. Same as Figure 32 except for the AR region.

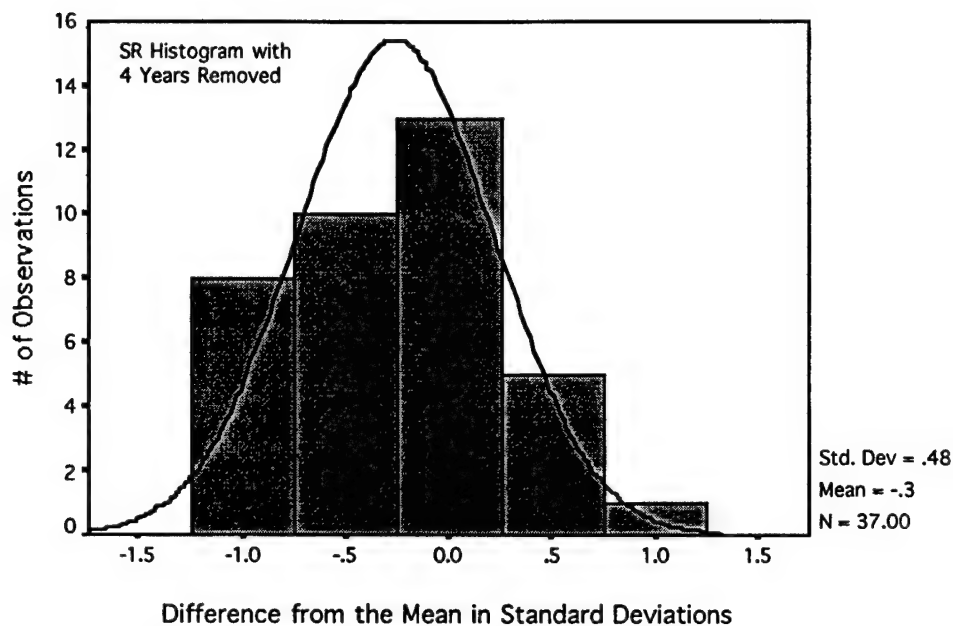


Fig. 36. Histogram of the SR regional indices expressed in terms of standard deviations from the mean with the outlier years (1951, 1961, 1963, and 1968) removed. A normal curve is fitted to the data.

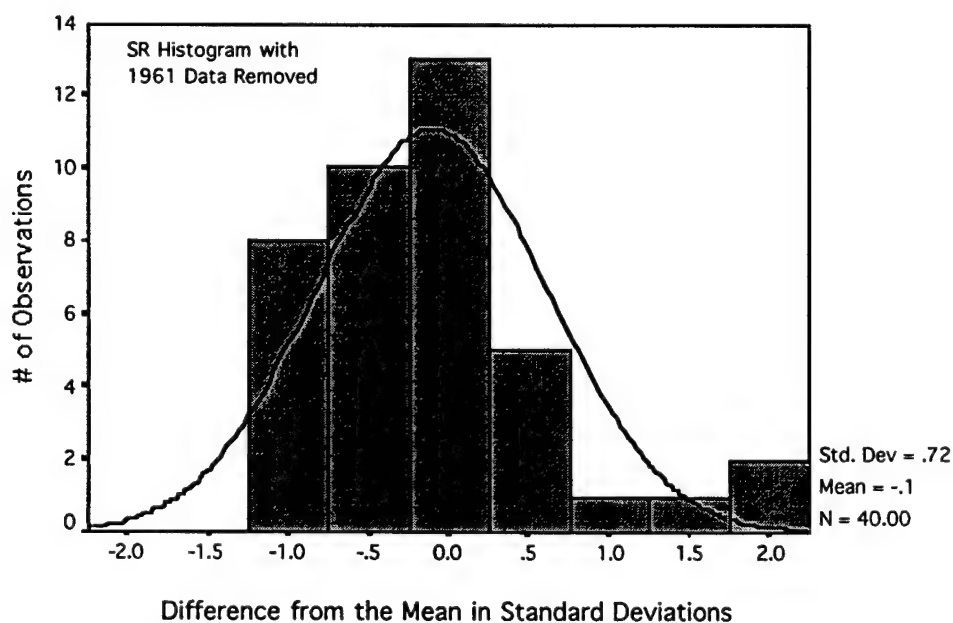


Fig. 37. Same as Figure 36 except only data from the year 1961 is removed.

year. Figures 38-41 show the time series for the four regional indices. The analysis of a time series is useful in explaining a variable's past behavior so that one can attempt to forecast future values. Therefore, time series analysis was used in this work to analyze the ability to make seasonal rainfall forecasts successfully based on any patterns found in the analysis of the regional indices. Another reason for analyzing these time series data was to evaluate any effects that some events may have if they are found to intervene or change the normal behavior of the time series (such as the SR data for 1961).

First evaluated was whether or not any significant trends were evident in the rainfall data time series using the regional indices. Simple linear regression was performed independently on each of the four time series. No significant trends were detected for any region (or season). However, since the t-test used in the regression analysis is not a valid statistical test for a non-normal distribution, the results for the SR series were questionable. So, to evaluate the SR series further, the four years (1951, 1961, 1963, and 1968) were removed from the analysis (as shown in Figure 36) thus enabling the SR data to pass the normality test. Then, simple linear regression was again performed on the data, however, the results only strengthened the original conclusion that no significant trend was evident in the SR rainfall record over the POR of this research.

When viewing the regional time series in Figures 38-41, the cyclical patterns of the data seem to imply that some form of periodicity may exist. To examine this further, spectral analysis was performed on each time series. In most time series analyses, adjacent data values are often highly correlated. To examine the strength of the relationship among the values at different lags (years), autocorrelation coefficients were computed and graphed as an autocorrelation plot for each region (Fig. 42). Each bar in the figure corresponds to a particular lag and the 95% confidence limits of the autocorrelations around zero are also shown. If the observed autocorrelation falls within the confidence limits, then not enough evidence exists to reject the null hypothesis that

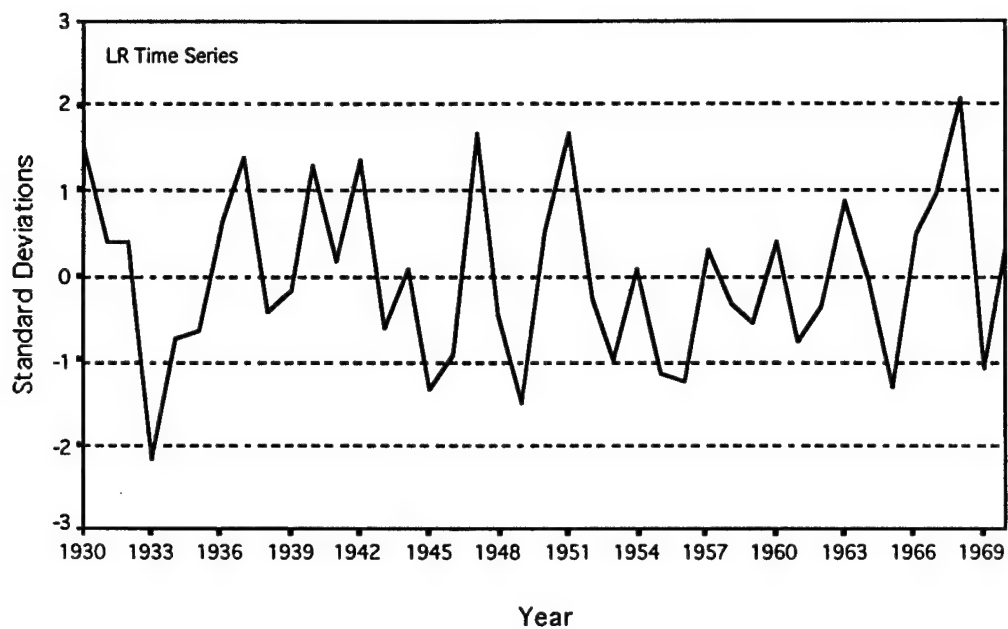


Fig. 38. Time series record of LR rainfall in terms of standard deviations from the mean.

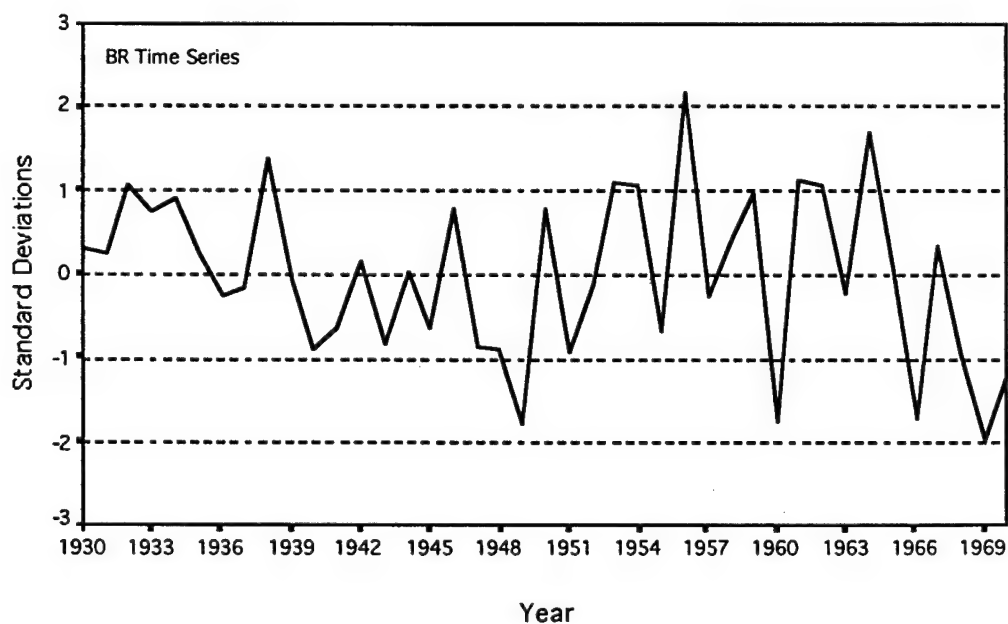


Fig. 39. Time series record of BR rainfall in terms of standard deviations from the mean.

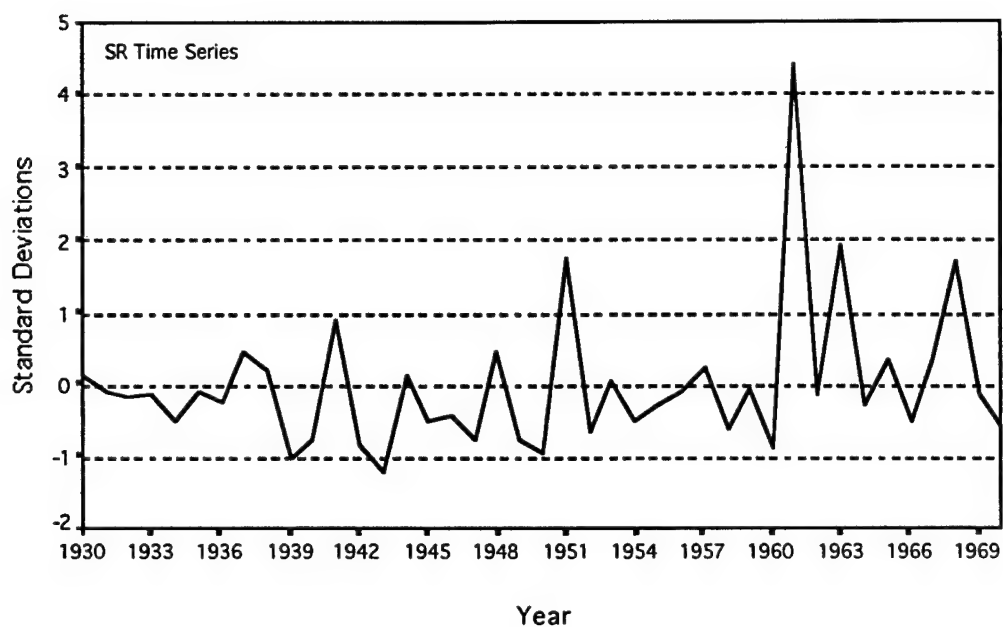


Fig. 40. Time series record of SR rainfall in terms of standard deviations from the mean.

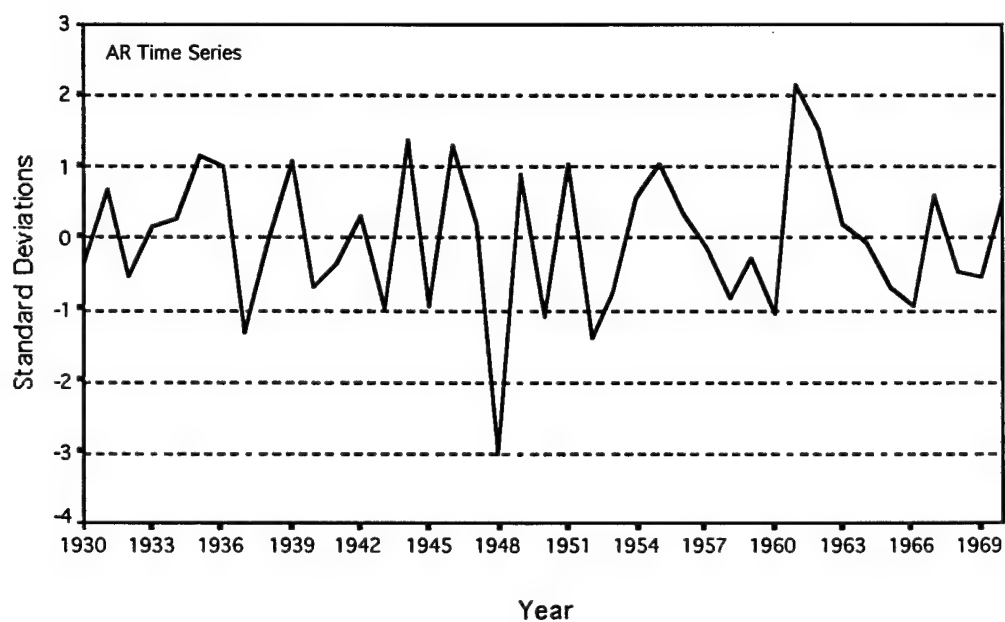


Fig. 41. Time series record of AR rainfall in terms of standard deviations from the mean.

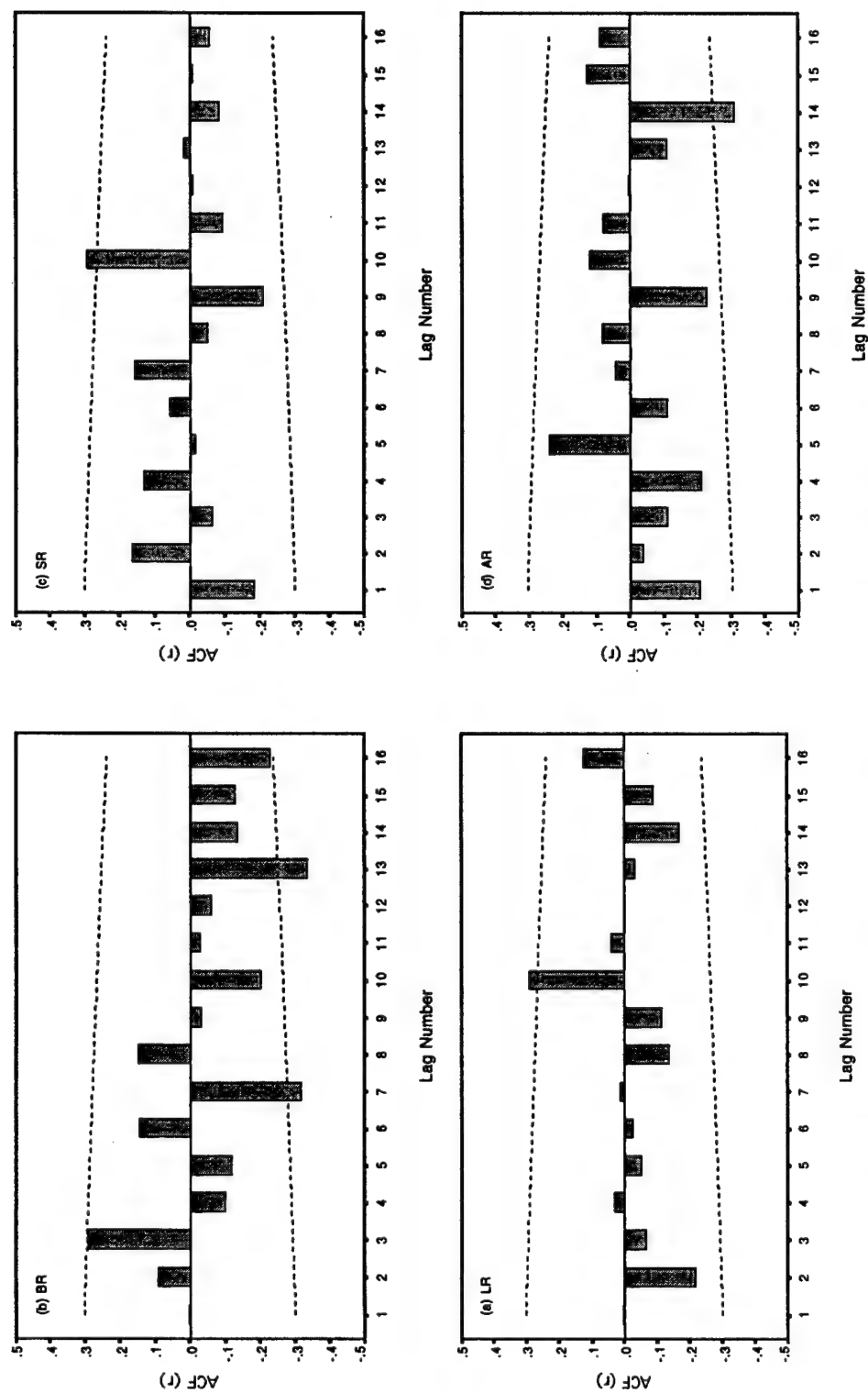


Fig. 42. Autocorrelation coefficients (r) at different lags for each of the four regions.
The dashed lines represent the 95% confidence limits.

the true value might be zero. The results seems to indicate the LR and SR regions experience a significant positive autocorrelation at a lag of 10 years (which may be associated with the solar cycle). The BR region shows significant negative autocorrelation at the 7 and 13 year lag points while the AR region shows the same at the 14 year lag point. No physical reasoning is known for these but since the research POR is only 41 years in length, the autocorrelation found at the 13-14 year lag points is based on very few comparisons and is, therefore questionable for such a short time series.

Spectral Analysis of the Regional Indices

Next, the regional indices were evaluated using spectral analysis. Spectral analysis is concerned with periodic rhythms within the data and is used to find various kinds of periodic behavior within a time series. Spectral analysis of a time series yields a description of that series in terms of the cycles of different frequency or period that generate the series. This is portrayed in a graph called a periodogram which shows an estimate of the amount of variance of the series accounted for by the cycles of each frequency. Since both the frequency and period of the data are reciprocals of one another, this work uses the period for ease of understanding. However, while the periodogram is a useful tool for analyzing data, it is strictly a mathematical tool which breaks the time series down into sine and cosine curves. No theories or reasoning about any physical processes that may underlay the series are involved. Consequently, spectral methods are not worth doing for only a small amount of data and at least 50 data points are recommended for such an analysis.

Since each set of regional indices is only composed of 41 data points, any results from spectral analyses should be used with caution. However, since previous researchers have found periodicity within East Africa rainfall data on the same time scales as the QBO and ENSO events, we were compelled to produce both periodograms and spectral density graphs (which are just smoothed periodograms) to determine if any dominant periods were evident. All of regional time series showed

several peaks in the time frame that ENSO events are thought to occur (3-6 years). However, they were different for each region and there is no distinct period known between occurrences of ENSO-related events. Some interesting features that were found included distinct signals in the SR and AR data corresponding to about the same time scale as the QBO phenomenon. Another distinct signal was found in the BR region with a period of around 10 years (which may be associated with effects from the solar cycle). The BR rainfall is thought to be the most affected by solar forcing changes since insolation amounts over northeastern Africa and Asia, are thought to determine how far or to what degree the ITCZ is pulled northward each year during the BR season.

Time Series Analysis of the ITCZ-associated Rainfall Data

A time series of ITCZ-associated rainfall data was created by combining the regional indices for all four rainfall regions (or seasons) in sequential order through the POR. As stated earlier, a time series is defined as a set of observations obtained by measuring a single variable regularly over a period of time. Therefore, in the time series just created, the set of observations was the combined set of rainfall indices for all four regions, the single variables are the individual regional rainfall indices, and the period of time is the POR in sequential order by season. For example, the time series starts with the data: LR (1930), BR (1930), SR (1930), AR (1930-31), LR (1931), BR (1931), and so on; which creates a time series of rainfall data associated with the ITCZ as it traverses north and south over Eastern Africa (Fig. 43). In essence, this time series represents ITCZ-associated rainfall and is referred to as the ITCZ rainfall data from here on in this research.

Figure 44 shows the histogram of the ITCZ rainfall data and, as one can clearly see, there are two outliers within the 164 data points. They are the 1961 SR heavy rain season (over four standard deviations above the SR mean) and the 1948 AR drought season (near three standard deviations below the AR mean). With all years and seasons included, the data passed the Cornu Criterion for normality at the 5 and 1% levels along with the Kolmogorov-Smirnov test for normality; however, the

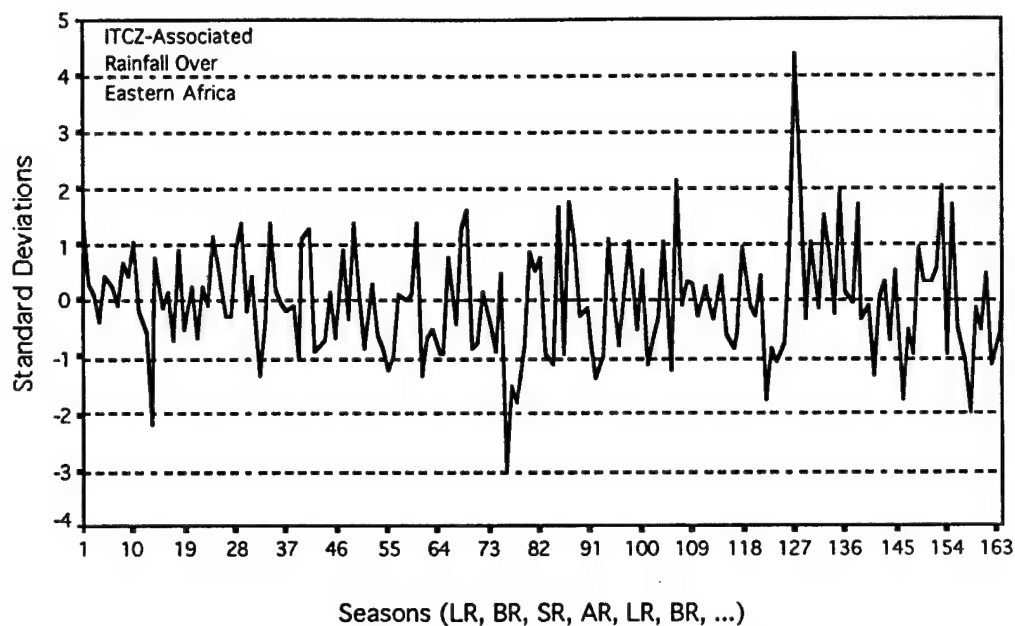


Fig. 43. Times series of ITCZ-associated rainfall which includes all four seasons. The seasons are in sequential order starting with the Long Rains in 1930 and ending with the Austral Rains in 1970.

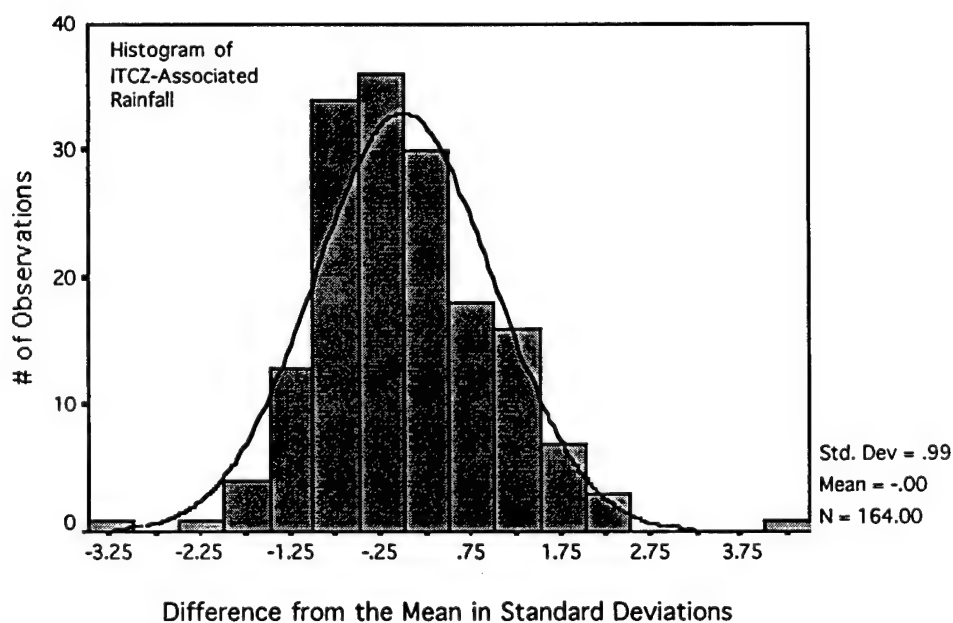


Fig. 44. Histogram of ITCZ-associated rainfall data expressed in terms of standard deviations from the mean. A normal curve is fitted to the data.

data failed the skewness and kurtosis tests for normality. After the datum for the 1961 SR season was removed from the analysis, the remaining data passed all four tests for normality.

The 1961 SR season was such an extreme anomaly that its inclusion when computing the SR regional indices (see Fig. 34) adjusted the SR regional mean by four percentage points and greatly exaggerated the standard deviation as well (see Table 7). The 1961 SR index datum exceeded four standard deviations above the SR mean (see Fig. 43). However, when the index was recompiled with the event's influence on the SR mean and standard deviation removed from the analysis, the 1961 SR season was shown to be over six standard deviations above the mean which is a practical impossibility by chance alone in a normal distribution of 41 data points. In contrast, the other outlier in Figure 43 (the 1948 AR drought event) was only three standard deviations below the mean which can easily occur by chance alone in a sample of 41 points from a normal distribution. Using this justification, the 1961 SR season datum was deleted from further analyses. This study suspects the 1961 event was associated with a rare sequence of events across the Pacific and Indian Oceans occurring over a time span of three years. Since these events did not directly relate to the objectives of this study, this theory of the causal factors for the anomaly is presented separately in Appendix C.

Table 7. Descriptive Statistics of the SR Regional Indices.

1961 Datum	Mean	Std. Dev.	Minimum	Maximum	N
Included	99.7	36.0	57.0	258.1	41
Excluded	95.7	25.8	57.0	169.7	40

The deletion of the 1961 SR datum also helped the analysis meet one of the objectives of this study which was to analyze the data using minimal statistical assumptions (we can now assume normality of the data if

required to do so). However, by deleting the 1961 SR datum, one must also delete any influences it had on remaining data. To accomplish this, the regional indices for the SR region were recompiled using the mean and standard deviation of the SR data in Table 7 which were computed with the 1961 datum excluded. These new seasonal rainfall indices that compose the new ITCZ-associated rainfall data time series are listed in Table 8 and were used to plot the time series shown in Figure 45.

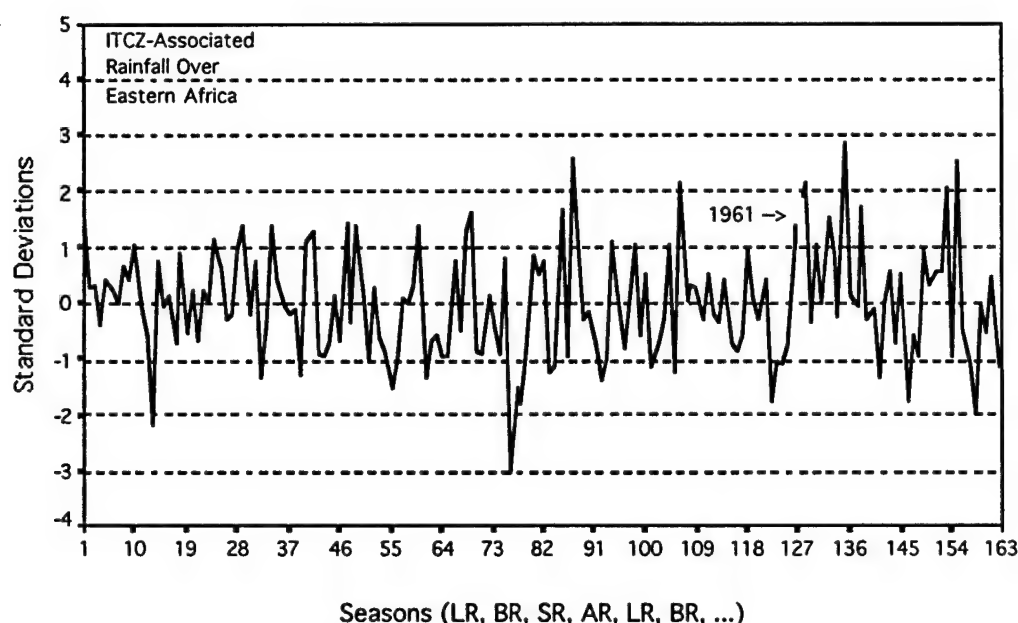


Fig. 45. Same as in Figure 43 except with the 1961 SR datum and its influence on the remaining SR indices removed.

Next evaluated was whether or not any significant trends were evident in the ITCZ-associated rainfall data over the POR. Simple linear regression was performed on the time series and no significant trend was found. However, most of the seasonality of the data was removed previously by transforming the regional indices into standard deviations from their mean. Yet, one could also argue that the data are still seasonalized since the means between regions of the transformed values are slightly different from each other. To account for this, the

Table 8. Seasonal rainfall indices (for ITCZ-associated rainfall) for each rainfall season over Eastern Africa.

Year	Rainfall Season			
	AR	LR	BR	SR
1930	.	1.49	0.31	0.32
1931	-0.36	0.41	0.25	0.04
1932	0.68	0.42	1.07	-0.06
1933	-0.54	-2.16	0.76	-0.04
1934	0.15	-0.71	0.90	-0.51
1935	0.27	-0.64	0.23	0.01
1936	1.15	0.65	-0.25	-0.19
1937	0.98	1.40	-0.15	0.77
1938	-1.31	-0.41	1.38	0.44
1939	-0.04	-0.15	-0.08	-1.27
1940	1.08	1.27	-0.88	-0.92
1941	-0.70	0.19	-0.65	1.43
1942	-0.34	1.36	0.16	-0.99
1943	0.31	-0.62	-0.82	-1.50
1944	-0.98	0.09	0.03	0.33
1945	1.40	-1.33	-0.63	-0.54
1946	-0.93	-0.92	0.79	-0.45
1947	1.28	1.65	-0.87	-0.90
1948	0.19	-0.44	-0.90	0.81
1949	-3.01	-1.49	-1.77	-0.93
1950	0.88	0.55	0.78	-1.18
1951	-1.11	1.67	-0.92	2.60
1952	1.04	-0.28	-0.13	-0.74
1953	-1.38	-0.98	1.10	0.25
1954	-0.77	0.09	1.06	-0.54
1955	0.55	-1.13	-0.66	-0.27
1956	1.03	-1.23	2.17	0.05
1957	0.34	0.31	-0.26	0.51
1958	-0.16	-0.34	0.43	-0.70
1959	-0.84	-0.54	0.97	0.09
1960	-0.27	0.42	-1.74	-1.05
1961	-1.06	-0.75	1.14	.
1962	2.15	-0.35	1.06	-0.01
1963	1.52	0.86	-0.21	2.86
1964	0.19	-0.03	1.69	-0.26
1965	-0.06	-1.30	0.06	0.62
1966	-0.71	0.51	-1.73	-0.54
1967	-0.93	0.96	0.33	0.62
1968	0.61	2.08	-0.95	2.52
1969	-0.45	-1.07	-1.96	-0.02
1970	-0.53	0.50	-1.13	-0.69

data were further deseasonalized (normalized by the overall mean of all regions combined) and simple linear regression was performed again. The new series also showed no significant trends and very little difference was observed between the seasonalized and deseasonalized values. Since, this was also observed in the results of correlation analyses performed later on, the deseasonalized data were deemed unnecessary and not used any further.

Therefore, the final result was that no significant trend was observed in the ITCZ-associated rainfall data over the POR. However, one item of interest is that the six values greater than two standard deviations above the mean in Figure 45 were all located in latter half of the POR. This may lend support to recent theories that the intensity of rainfall events may be increasing in some areas, along with global warming.

Spectral Analysis of the ITCZ-associated Rainfall Data

Spectral analysis was performed on the ITCZ rainfall data to determine any periodicity within the data. Since the ITCZ rainfall data had 163 data points (41 years with 4 seasons each except 1961), the results of any spectral analysis should be statistically valid. Autocorrelation coefficients were computed and graphed as an autocorrelation plot in Figure 46. However, since only one lag was determined to be only slightly significantly different from zero (at lag 11 with a period of 2.75 years), it was suspected that the data may be close to being just random noise. A data set with random noise (sometimes called white noise spectra) has no memory and no prediction capability within it. In other words, the most probable or best prediction for the future of the series is probably the average of what has happened in the past. A periodogram and spectral density graph could not be computed to confirm the white noise since the series now contains a missing datum for the 1961 season. However, a periodogram and spectral density analysis just present the same information that is already contained in the autocorrelation plot.

In most applications of time series analysis, if data are determined to be white noise, then there is little reason to examine them further.

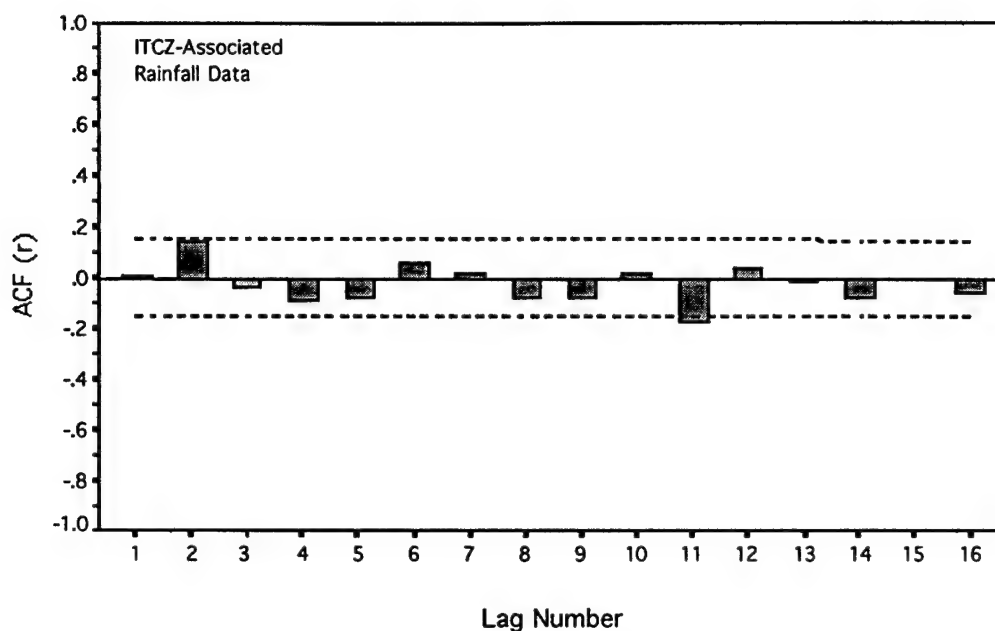


Fig. 46. Autocorrelation coefficients (r) at different lags for the ITCZ-associated rainfall data. The dashed lines represent the 95% confidence limits and the only significant relationship found occurred at lag 11 (a period of 2.75 years since each lag is one season in length).

However, a first-difference transformation was performed on the ITCZ-associated rainfall data to create a new time series which consisted of the differences between the regional indices in sequential order through the POR. Figure 47 shows this new time series and the values used to create it are listed in Table 9. The histogram of this new time series is shown in Figure 48. Its data passed the four tests for normality previously discussed.

To explore the possibility of periodicity within the data, a spectral analysis was performed. Autocorrelation coefficients were computed and graphed as an autocorrelation plot (Fig. 49) and, as a result, an unexpected discovery was made. The differences in this new time series were highly negatively correlated ($r=-0.55$) with the previous differences. In physical terms, this indicates the change between

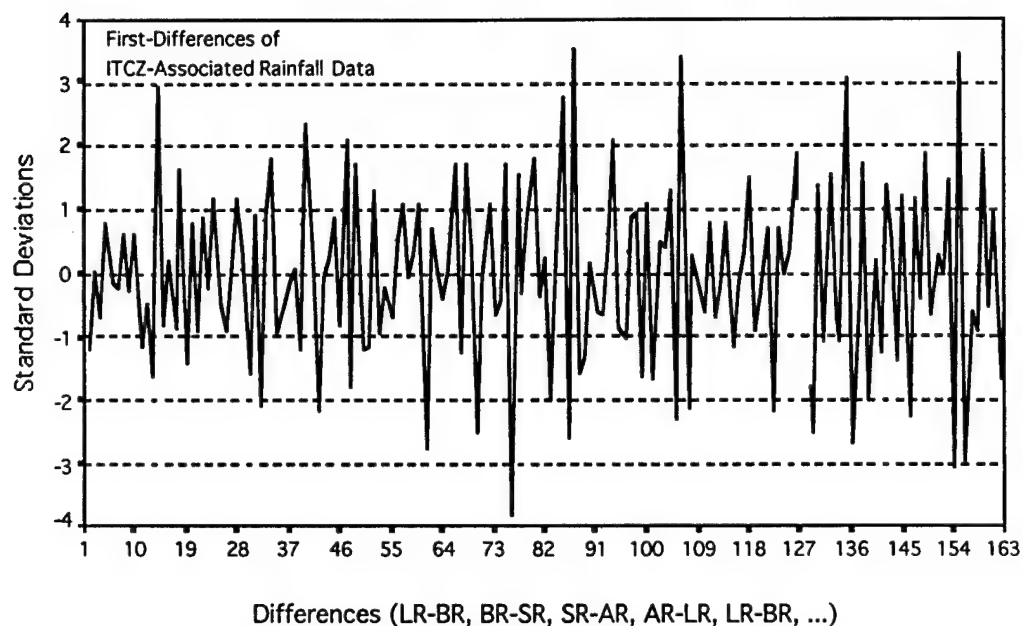


Fig. 47. Times series of the first-difference transformation of the ITCZ-associated rainfall data. The changes are in sequential order starting with the LR-BR data in 1930 and ending with the SR-AR data in 1970.

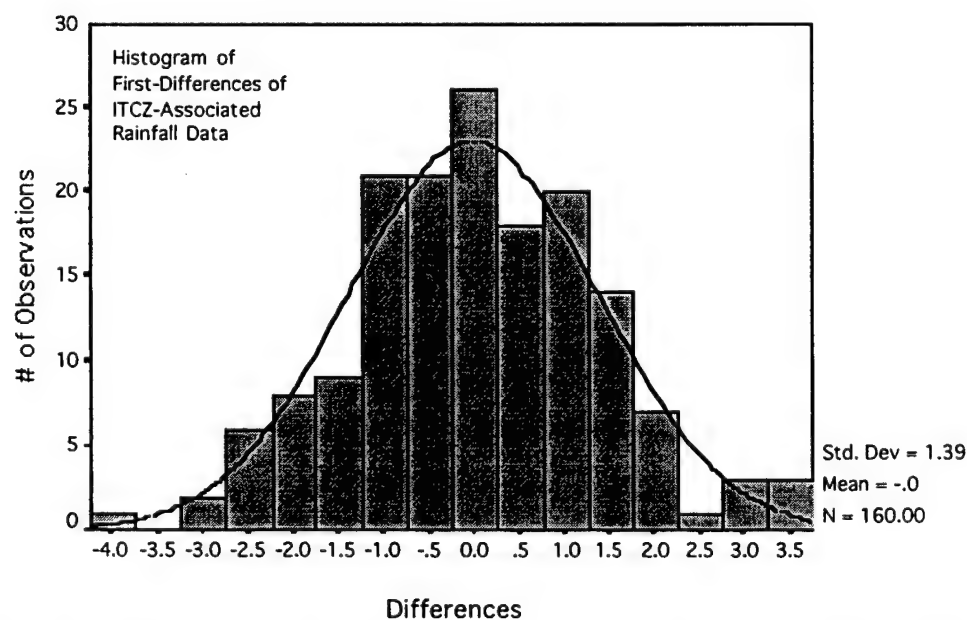


Fig. 48. Histogram of the first-difference transformation of the ITCZ-associated rainfall data. A normal curve is fitted to the data.

Table 9. Changes between rainfall indices (for ITCZ-associated rainfall).
 These values created the time series shown in Figure 47.

Year	Changes Between Regional Rainfall Indices			
	AR→LR	LR→BR	BR→SR	SR→AR
1930	.	-1.18	0.01	-0.68
1931	0.77	-0.16	-0.21	0.64
1932	-0.26	0.65	-1.13	-0.48
1933	-1.62	2.92	-0.80	0.19
1934	-0.86	1.61	-1.41	0.78
1935	-0.91	0.87	-0.22	1.14
1936	-0.50	-0.90	0.06	1.17
1937	0.42	-1.55	0.92	-2.08
1938	0.90	1.79	-0.94	-0.48
1939	-0.11	0.07	-1.19	2.35
1940	0.19	-2.15	-0.04	0.22
1941	0.89	-0.84	2.08	-1.77
1942	1.70	-1.20	-1.15	1.30
1943	-0.93	-0.20	-0.68	0.52
1944	1.07	-0.06	0.30	1.07
1945	-2.73	0.70	0.09	-0.39
1946	0.01	1.71	-1.24	1.73
1947	0.37	-2.52	-0.03	1.09
1948	-0.63	-0.46	1.71	-3.82
1949	1.52	-0.28	0.84	1.81
1950	-0.33	0.23	-1.96	0.07
1951	2.78	-2.59	3.52	-1.56
1952	-1.32	0.15	-0.61	-0.64
1953	0.40	2.08	-0.85	-1.02
1954	0.86	0.97	-1.60	1.09
1955	-1.68	0.47	0.39	1.30
1956	-2.26	3.40	-2.12	0.29
1957	-0.03	-0.57	0.77	-0.67
1958	-0.18	0.77	-1.13	-0.14
1959	0.30	1.51	-0.88	-0.36
1960	0.69	-2.16	0.69	-0.01
1961	0.31	1.89	.	.
1962	-2.50	1.41	-1.07	1.53
1963	-0.66	-1.07	3.07	-2.67
1964	-0.22	1.72	-1.95	0.20
1965	-1.24	1.36	0.56	-1.33
1966	1.22	-2.24	1.19	-0.39
1967	1.89	-0.63	0.29	-0.01
1968	1.47	-3.03	3.47	-2.97
1969	-0.62	-0.89	1.94	-0.51
1970	1.03	-1.63	0.44	

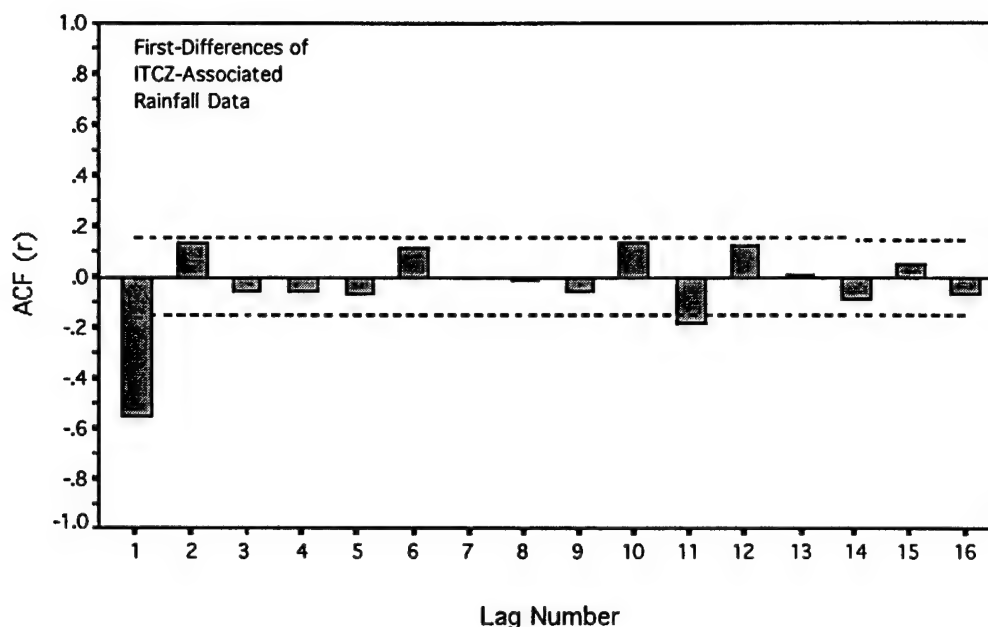


Fig. 49. Autocorrelation coefficients (r) at different lags for the first-difference transformation of the ITCZ-associated rainfall data. The dashed lines represent the 95% confidence limits.

example), is highly negatively correlated with the previous change (the LR to the BR). Therefore, once the indices are known in a given year for the first two regions, the change between them (LR→BR) can then be used to predict the second change (BR→SR). Since the BR rainfall datum would be already known, this effectively produces a seasonal forecast for the SR rainfall datum (or average rainfall over the SR region) during the Short Rains.

The first-difference transformation of a random number time series would also be highly correlated at lag one. However, the correlation would not be as significant as the one found or vary as greatly among sets of changes and, no physical reasoning would consistently relate to the results. This discovery could also have been made without even creating the ITCZ-associated rainfall data time series or a first-difference transformation of it. Therefore, this discovery is deemed to be very significant for seasonal rainfall forecasting purposes.

CHAPTER V

FORECAST METHODOLOGY

Methodology Reasoning

As discovered in the previous chapter, the change (or first-difference transformation of the time series) between rainfall indices for two regions in any given year is highly correlated with the previous change. Therefore, knowing the indices for the first two regions leads to a prediction of the index for the third region. In physical terms, this suggests that by examining the difference between rainfall amounts over two regions as they are traversed sequentially by the ITCZ a forecast can therefore be made for the next region traversed. It is important to note, however, that the time series differences referred to are not mathematical differences but rather the positive or negative change between two consecutive regional indices. Therefore, in the remainder of this work, they are referred to as time series (TS) changes between regional indices.

As the ITCZ traverses Eastern Africa southward into the Southern Hemisphere synoptic features advect plenty of moisture into the air mass which resides over the region. However, as this shallow air mass moves northward following the seasonal displacement of the ITCZ, little moisture is advected into it from the east due to the blocking effects of the low-level Somali Jet and the strong surface pressure differential between the Asian continent and Indian Ocean. Little moisture is advected into the air mass from the west due to the blocking effect of continental terrain features and the strong surface pressure differential between West Africa (the Sahel) and the Saint Helena high pressure cell in the South Atlantic. In addition, virtually no moisture is advected into Eastern Africa from the north due to the lack of an adequate moisture source in northeastern Africa. Therefore, it is suggested by this work that a large percentage of the moisture

associated with this air mass is advected into it as the ITCZ traverses southward into the Southern Hemisphere. The evidence presented in this research suggests that a continuity to the moisture content of this air mass might exist as it traverses northward and back south again following the seasonal displacement of the ITCZ. In other words, the air mass is not resupplied with moisture on a large scale until the ITCZ nears its southern extremities.

The moist air mass shown in Figure 17 while the ITCZ is positioned in the NH cannot extend far southward over the AR region. The upward vertical motion is mostly confined in a narrow band near the ITCZ with large scale subsidence to the north and south of it. This large scale subsidence keeps the moisture in a shallow layer below the trade wind inversion. If this were not the case, Figure 7 would show continuous heavy rainfall amounts during July extending from the Ethiopian Highlands southward into the SH. Therefore, a modified version of Figure 17 is proposed in Figure 50 which depicts a theorized meridional cross-section of the troposphere as the ITCZ is positioned over the BR region. As the ITCZ begins its southward progression, this air mass is thought to retreat to the south ahead of the ITCZ, at least while the ITCZ is in the NH.

In practical terms to the layman, this evidence suggests that if rainfall is greater than normal over the LR and BR regions, little moisture may be left for rainfall over the SR region. In addition, while a strong relationship ($r=-0.55$) was found while examining all of the sets of changes together, it was also found that this relationship could be improved upon when examining the sets of changes separately and, during certain years associated with known teleconnections or atmospheric phenomena.

Before developing a prediction methodology though, an attempt was made to adjust the size of the AR region and buffer zones in between the regions both to maximize the relationships found and, to further reduce any coastal and synoptic influences in the SH portion of the research area. But, as an example, when the AR region was reduced in size to 8-12°S latitude, the observations, as a whole in this smaller region, were

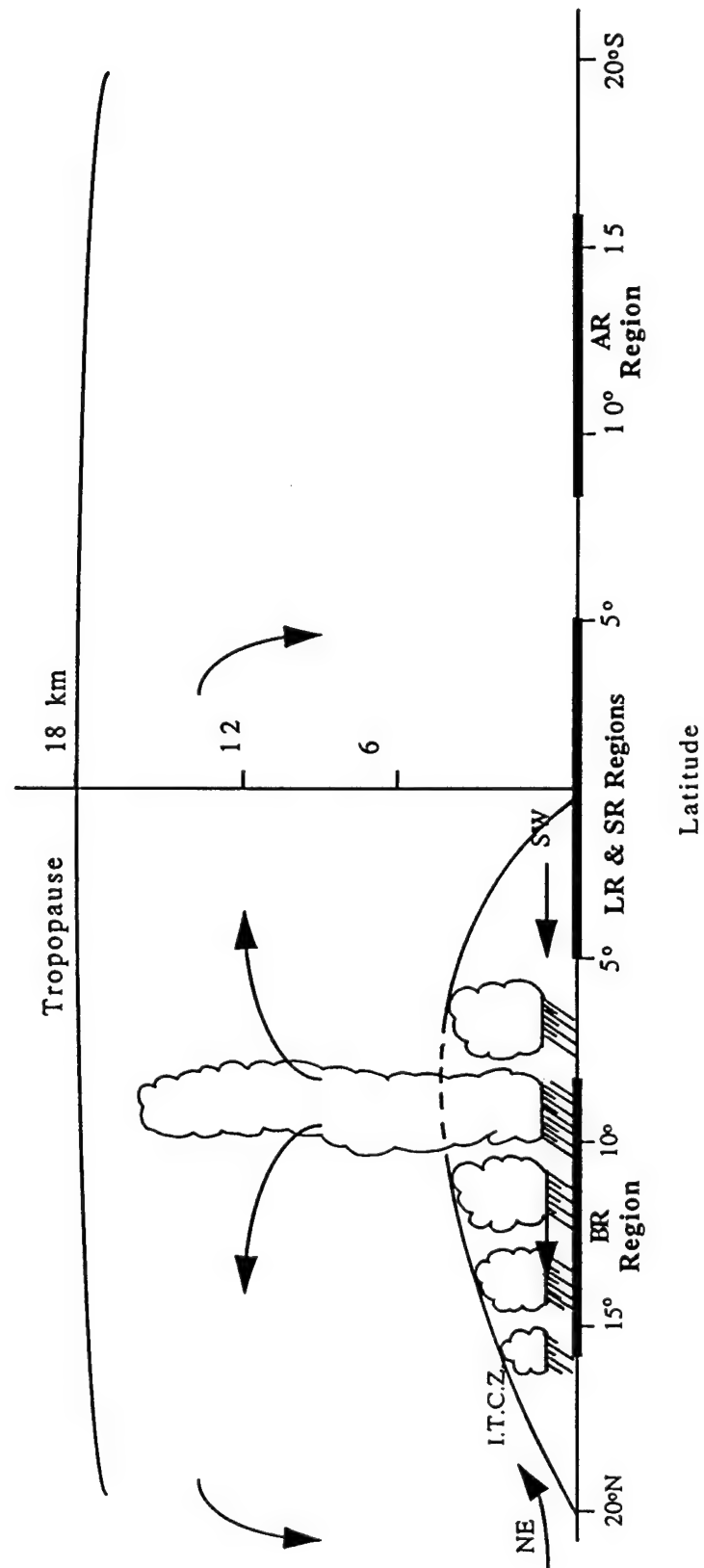


Fig. 50. Proposed meridional cross-section of the troposphere (with a vertical exaggeration of 75 times) depicting air mass features associated with the ITCZ as it resides over the BR region.

more closely correlated with the observations in the SR region. Therefore, this increased positive correlation between the observations decreased the negative correlation of the changes between the regions. This result only solidified the need for the buffer zones between the regions. Therefore, while the exact areas defined may well be manipulated to maximize any relationships found, it was not a direct objective of this research to do so.

Methodology Development

To examine the relationships between each set of changes, scatter graphs were plotted in Figure 51 for each set. Correlation coefficients were then computed and listed in Table 10 along with their probability levels and the total amount of variance (r^2) associated with the relationships. Simple linear regression was then performed between each set and a line of best fit was overlaid onto each graph in Figure 51. In addition, the number of occurrences in each quadrant of the graph (with the quadrants separated by zero) were counted and listed in each graph's corners.

Table 10. Results of correlation analyses between sets of changes including all years of data.

Set of Changes	Correlation (r)	N	Probability Level	Variance Associated With
AR→LR vs LR→BR	-0.55	40	0.000	30%
LR→BR vs BR→SR	-0.68	40	0.000	47%
BR→SR vs SR→AR	-0.63	39	0.000	39%
SR→AR vs AR→LR	-0.34	39	0.035	11%

Several predictive methods may be used with this information for the purpose of producing seasonal rainfall climate forecasts. Users of such forecasts need to utilize the information to reduce their risks in potentially "poor" years and to maximize their gains in potentially

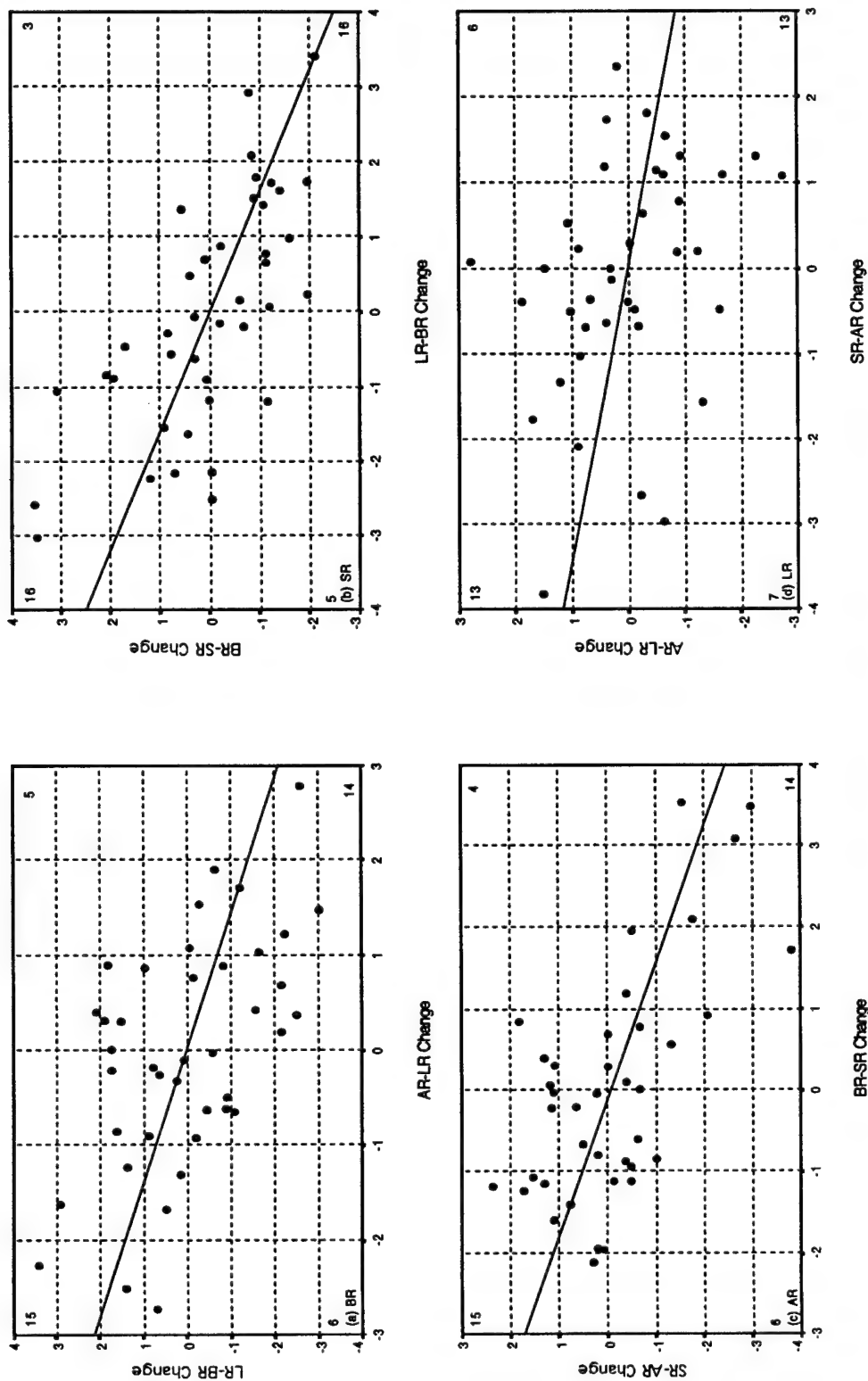


Fig. 51. Using all years with data, scatter graphs with linear regression lines are shown for predicting the seasonal rainfall of the (a) BR, (b) SR, (c) AR, and (d) LR rainy seasons. The numbers in each corner represent occurrences in that quadrant.

“good” years. Therefore, the method of forecasting chosen by the user depends to a large extent on the amount of risk that they are willing to assume for the possibility of receiving an incorrect forecast.

First, one simple method of climate forecasting using these data would be to use the regression lines of best fit shown in Figure 51. This method assumes a significant linear relationship between the sets of changes and that the line of best fit can be used to summarize the relationship. The equation for the predictive relationship would be:

$$\text{predicted second change} = B_0 + B_1 \times (\text{first change}); \quad (5.1)$$

where B_1 and B_0 are the slope and intercept of the regression line, respectively. These variables (for the data in Figure 51) are listed in Table 11 along with the probability level of the (F) statistic used in the analysis of variance and, the R-Square value which ranges from zero to one and represents the goodness of fit of the regression line. Since the two indices used to compute the first change are known, the formula for a prediction of the third region's index would be:

$$(\text{3rd region's index}) = (\text{2nd region's index}) - (\text{second change}). \quad (5.2)$$

However, since the relationship is not a perfect linear one, the use of this method forces users to assume more risk than many of them can afford to take.

Table 11. Coefficients of regression analyses for use in seasonal rainfall climate forecasts using all years of data.

Change Being Predicted	Equation Variables B_1	Variables B_0	Significance Level	R Square
LR→BR	-0.706	0.014	0.000	0.30
BR→SR	-0.626	0.002	0.000	0.47
SR→AR	-0.597	0.079	0.000	0.39
AR→LR	-0.290	0.018	0.035	0.11

Secondly, users who are unable to assume such a large risk may, as an alternative, benefit from a predictive outlook type of forecast such as the forecasting of rainfall trends during an upcoming rainy season. However, along with such a predictive outlook type of forecast, users also want an estimate for the chances of the forecast being correct or incorrect. With such information, they can then balance the forecast with any risks they are willing to assume, if indeed, the forecast turns out to be incorrect.

In Figure 51a, the observation counts for each quadrant are listed in each corner. Regression analyses of these data suggested that a trend exists which indicates that when the AR→LR change is negative, then the LR→BR change tends to be positive, and vice versa. The observation counts for each quadrant can therefore be used to compute the chance of being correct or incorrect while using such a method. Overall in Figure 51a (which is used to predict for the BR region), out of 40 occurrences, 29 of them (15+14) agree with the trend relationship found through regression analysis. In other words, one could state that there is a 72.5 percent chance $((15+14)/40)$ of producing a correct trend forecast and a 27.5 percent chance $((6+5)/40)$ of producing an incorrect trend forecast using this methodology alone.

The significance of this relationship can be tested by placing the number of occurrences into a 2x2 contingency table and by using the Chi-Squared (χ^2) statistic to test their level of significance. Table 12 lists the data for such a contingency table using the occurrences by quadrant in Figure 51a. The numbers in parentheses depict the frequencies of occurrence in each quadrant that should occur by chance alone, on average, if no relationship existed between the changes. In such a table, the degrees of freedom are computed by the formula $(m-1)(n-1)$ where m and n are the number of columns and rows, respectively. Using one degree of freedom, the occurrences by quadrant in each graph were tested using the χ^2 test for significance (Table 13). The results indicate the highest probability of a correct climate forecast using this method occurs when forecasting for the SR region.

A third method of climate forecasting is similar to the second method but provides a better indication of the chance for error. Since the two indices used to compute the first change are known, the information in Figure 51 and Table 13 may be used to more accurately indicate the probability of making a correct or incorrect forecast while predicting the trend of the next change. For example, using the frequencies of occurrence in Fig. 51a, if the AR→LR change is known to be positive, then there is a $(14/(14+5))=74\%$ chance that the LR→BR change will be negative and, the opposite $(5/(14+5))=26\%$ chance that it will be positive. If the AR→LR change is negative, then there is a $(15/(15+6))=71\%$ chance that the LR→BR change will be negative and, the opposite $(6/(15+6))=29\%$ chance that it will be positive. These probabilities are listed in Table 13 for each set of changes. The strongest relationship found when using this method was also for the prediction of the SR region with an 84% chance of producing a correct forecast. The

Table 12. Example of a 2x2 contingency table representing the number of occurrences by quadrant found in Fig. 51a. The numbers in parentheses list the expected frequencies by chance alone.

	AR<LR	AR>LR	Row Totals
LR>BR	15 (10)	5 (10)	20 (20)
LR<BR	<u>6 (10)</u>	<u>14 (10)</u>	<u>20 (20)</u>
Column Totals	21 (20)	19 (20)	40

Table 13. Significance of observation counts using the χ^2 test and the probabilities (P) of making a correct forecast using the trend method when the first change (or first two indices) is known.

Set of Changes	Region Being Predicted	χ^2 Level of Significance	P if 1st Change >0	P if 1st Change <0
AR→LR vs LR→BR	BR	1%	74%	71%
LR→BR vs BR→SR	SR	0.1%	84%	76%
BR→SR vs SR→AR	AR	1%	78%	71%
SR→AR vs AR→LR	LR	5%	68%	65%

weakest relationship was found when forecasting for the LR region, most probably, since the amount of moisture advected into the air mass during its transgression into the SH is unknown on a year-to-year basis.

Improvement of the Results

In many relationships among meteorological variables, there is a tendency for the relationship to strengthen toward the extremities of the data distributions. The data shown in Figure 51 were restricted to only those occurrences where the absolute value of the first change was greater than the probable error of the data distribution (or >0.675 standard deviations). Therefore, 50% of the observations in the distribution are within these limits and 50% are greater. The data for this new comparison were graphed in Figure 52 along with the regression lines of best fit overlaid on the graphs. In addition, Tables 14-17 list the same information that was provided earlier in Tables 10-13 except for only those data where the absolute value of the first change was greater than the probable error.

In Table 14, the correlations improved for all sets of changes. In Table 15, the R-Square value which represents the goodness of fit of the regression line improved for each change being predicted. And in Tables 16 and 17, the results show that improvements were made to most of the probabilities of getting a correct or incorrect forecast. All of the relationships passed the χ^2 test for significance. Overall, the relationships strengthened when the data were restricted to only when first change was greater than the probable error or, in other words, using only the lower and upper quartiles of the data distribution. Therefore, when this condition occurs, users are assured of a higher probability of receiving a correct forecast.

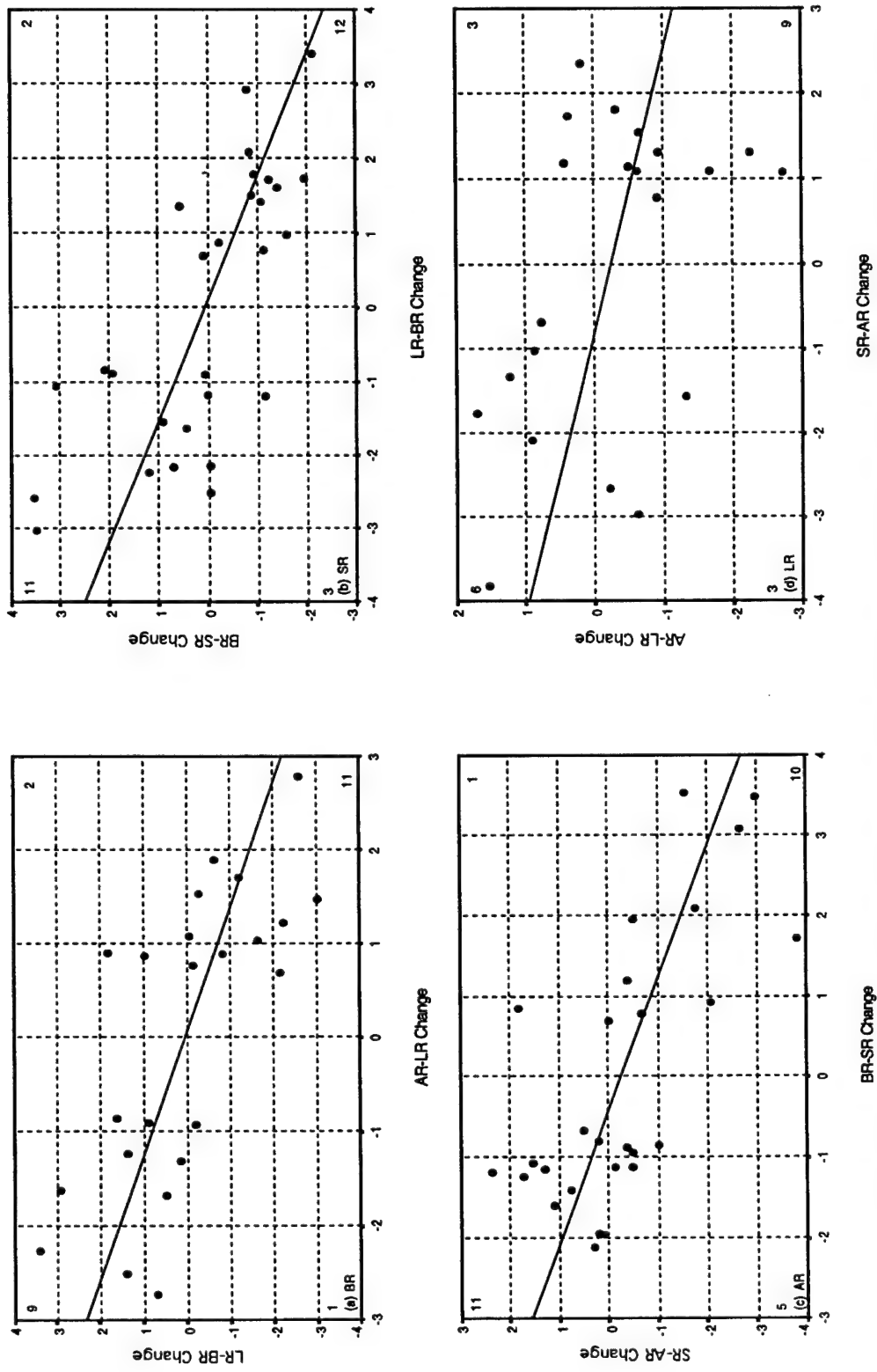


Fig. 52. Same as Figure 51 except using only years where the absolute value of the first change (horizontal axis) is greater than the probable error (0.675).

Table 14. Same as Table 10 except only when the absolute value of the first change was greater than the probable error (0.675).

Set of Changes	Correlation (r)	N	Probability Level	Variance Associated With
AR→LR vs LR→BR	-0.71	23	0.000	50%
LR→BR vs BR→SR	-0.72	28	0.000	52%
BR→SR vs SR→AR	-0.69	27	0.000	48%
SR→AR vs AR→LR	-0.47	21	0.034	22%

Table 15. Same as Table 11 except only when the absolute value of the first change was greater than the probable error (0.675).

Change Being Predicted	Equation Variables B ₁	Variables B ₀	Significance Level	R Square
LR→BR	-0.758	0.050	0.000	0.51
BR→SR	-0.608	0.068	0.000	0.52
SR→AR	-0.607	-0.260	0.000	0.48
AR→LR	-0.301	-0.253	0.034	0.22

Table 16. Same as Table 12 except only when the absolute value of the first change was greater than the probable error (0.675).

	AR<LR	AR>LR	Row Totals
LR>BR	9 (5.75)	2 (5.75)	11 (11.5)
LR<BR	<u>1 (5.75)</u>	<u>11 (5.75)</u>	<u>12 (11.5)</u>
Column Totals	10 (11.5)	13 (11.5)	23

Table 17. Same as Table 13 except only when the absolute value of the first change was greater than the probable error (0.675).

Set of Changes	Region Being Predicted	χ^2 Level of Significance	P if 1st Change >0	P if 1st Change <0
AR→LR vs LR→BR	BR	<0.1%	90%	84%
LR→BR vs BR→SR	SR	<0.1%	79%	86%
BR→SR vs SR→AR	AR	<1%	69%	91%
SR→AR vs AR→LR	LR	<5%	67%	67%

Next, the data shown in Figure 51 were restricted even further to only those occurrences where the absolute value of the first change was greater than one standard deviation. The data for this new comparison were graphed in Figure 53 with the regression lines of best fit overlaid on the graphs. In addition, Tables 18-21 list the same information that was provided earlier in Tables 10-13 except for only those data where the absolute value of the first change was greater than one standard deviation.

In Table 18, the correlations improved for all sets of changes. In Table 19, the R-Square value which represents the goodness of fit of the regression line improved for each change being predicted. And, in Tables 20 and 21, the results show that improvements were made to most of the probabilities of getting a correct or incorrect forecast. Overall, the relationships strengthened even further than when all the data were included or when the data were restricted to the upper and lower quartiles of the data distribution. Therefore, when this condition occurs, users are further assured of a higher probability of receiving a correct forecast.

However, in this analysis, only one of the relationships (prediction of the SR region) could be tested using the χ^2 test since it requires the expected value in each quadrant to be five or more. It is clear though that these relationships are significant, at least when predicting for the BR, SR, and AR regions, since the trend toward improvement was also seen while examining the data greater than the probable error.

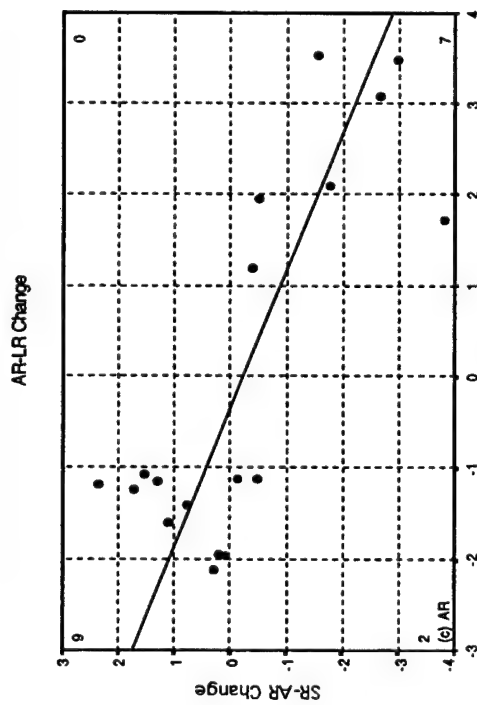
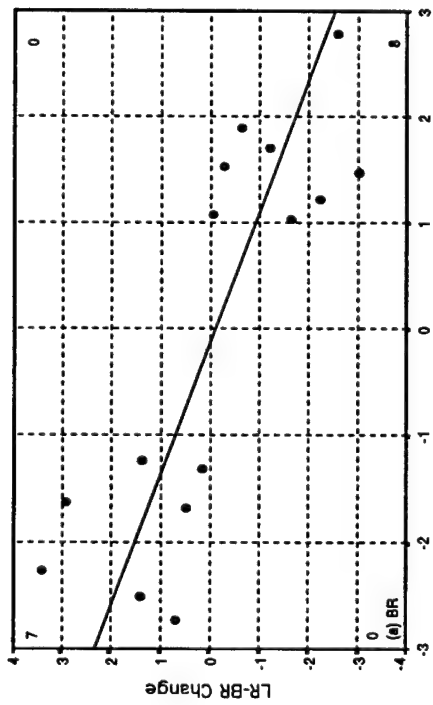
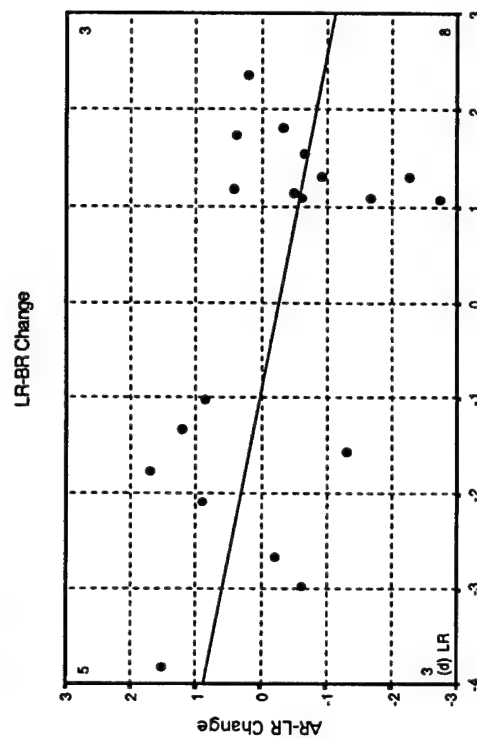
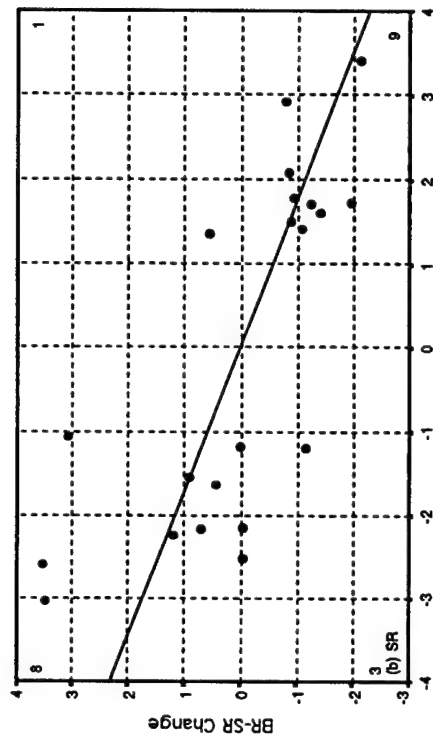


Fig. 53. Same as Figure 51 except using only years where the absolute value of the first change (horizontal axis) is greater than one standard deviation.

Table 18. Same as Table 10 except only when the absolute value of the first change was greater than one standard deviation.

Set of Changes	Correlation (r)	N	Probability Level	Variance Associated With
AR→LR vs LR→BR	-0.81	15	0.000	66%
LR→BR vs BR→SR	-0.73	21	0.000	53%
BR→SR vs SR→AR	-0.79	18	0.000	62%
SR→AR vs AR→LR	-0.45	19	0.051	21%

Table 19. Same as Table 11 except only when the absolute value of the first change was greater than one standard deviation.

Change Being Predicted	Equation Variables B_1	B_0	Significance Level	R Square
LR→BR	-0.809	-0.119	0.000	0.65
BR→SR	-0.575	0.016	0.000	0.53
SR→AR	-0.659	-0.238	0.000	0.62
AR→LR	-0.289	-0.272	0.051	0.21

Table 20. Same as Table 12 except only when the absolute value of the first change was greater than one standard deviation.

	AR<LR	AR>LR	Row Totals
LR>BR	7 (3.75)	0 (3.75)	7 (7.5)
LR<BR	<u>0 (3.75)</u>	<u>8 (3.75)</u>	<u>8 (7.5)</u>
Column Totals	7 (7.5)	8 (7.5)	15

Table 21. Same as Table 13 except only when the absolute value of the first change was greater than one standard deviation.

Set of Changes	Region Being Predicted	χ^2 Level of Significance	P if 1st Change >0	P if 1st Change <0
AR→LR vs LR→BR	BR	<0.1%	100%	100%
LR→BR vs BR→SR	SR		90%	73%
BR→SR vs SR→AR	AR		100%	82%
SR→AR vs AR→LR	LR		73%	63%

CHAPTER VI

FORECASTING TOOLS

The data provided in Tables 10-21 may be used to produce seasonal climate forecasts for an upcoming rainy season for each of the four regions. However, since most users are not applied climatologists by trade, they require guidelines to help them employ these methods. Three forecasting tools are provided which users can employ directly. All that is required to produce a seasonal climate forecast for the next region traversed by the ITCZ is the regional rainfall indices for the last two regions traversed by the same ITCZ system.

Regression Tool and Decision Flowchart

The first tool uses the regression lines of best fit shown in Figures 51-53. Figure 54 is a flowchart diagram which users can easily follow to produce a seasonal forecast. By knowing the first two regional indices which compose the first time series change, the second change and the next (3rd) region's index can therefore be predicted using Equations 5.1 and 5.2.

To illustrate the use of this regression flowchart tool (Fig. 54), two examples are provided, using actual data, to guide the user through the process of creating a seasonal rainfall forecast. The regional indices (from Table 8) and their time series changes (from Table 9), are listed again in Table 22 for the two specific periods. For example, the 1956 period begins with the AR season of December, 1955 through February, 1956 (listed in Table 22 as the AR season of 1956) and ends with the AR season of December, 1956 through February, 1957 (listed in Table 22 as the AR season of 1957). Figures 55 and 56, for the 1934 and 1956 data respectively, show the paths taken in the forecasting process through

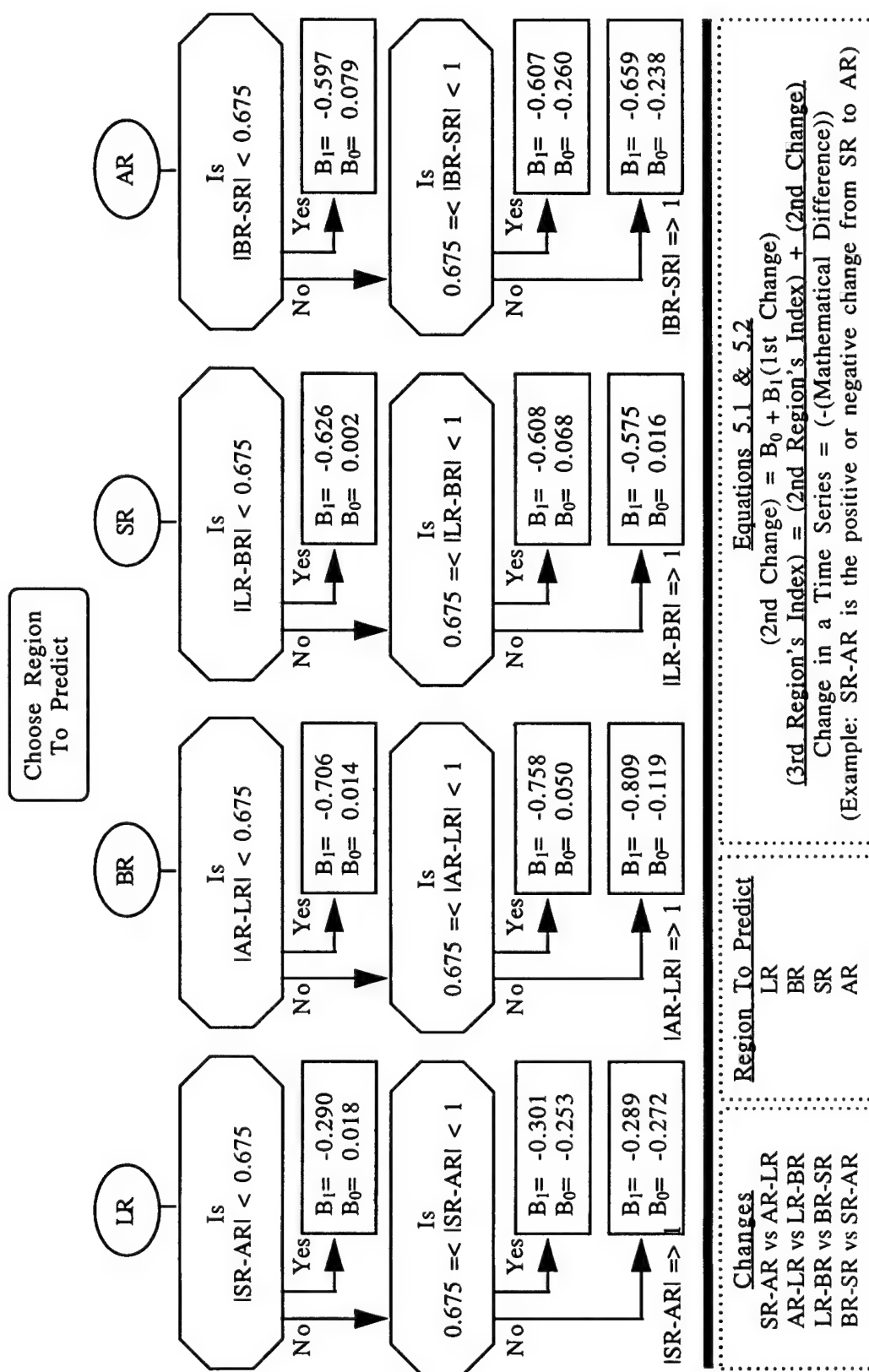


Fig. 54. Predictive flowchart tool for the regression forecasting method to predict the third region's seasonal rainfall index.

Table 22. Example seasonal rainfall indices and changes between them for the rainfall seasons of 1934 and 1956.

1934 Example				
Year	Seasonal Rainfall Indices			
	AR	LR	BR	SR
1933	.	.	.	-0.04
1934	0.15	-0.71	0.90	-0.51
1935	0.27	.	.	.
	Changes Between Indices			
	AR→LR	LR→BR	BR→SR	SR→AR
1933	.	.	.	0.19
1934	-0.86	1.61	-1.41	0.78
1956 Example				
Year	Seasonal Rainfall Indices			
	AR	LR	BR	SR
1955	.	.	.	-0.27
1956	1.03	-1.23	2.17	0.05
1957	0.34	.	.	.
	Changes Between Indices			
	AR→LR	LR→BR	BR→SR	SR→AR
1955	.	.	.	1.30
1956	-2.26	3.40	-2.12	0.29

Table 23. Results of the regression forecasting flowchart tool (Fig. 54) for the two example periods. The paths taken through the flowchart are shown in Figure 56 for the 1934 data and in Figure 57 for the 1956 data.

1934 Example						
Region To Predict	Predicted 1st Change	Predicted 2nd Change	Actual 2nd Change	2nd Region's Index	Predicted 3rd Region's Index	Actual 3rd Index
LR	0.19	-0.04	-0.86	0.15	0.11	-0.71
BR	-0.86	0.70	1.61	-0.71	-0.01	0.90
SR	1.61	-0.91	-1.41	0.90	-0.01	-0.51
AR	-1.41	0.69	0.78	-0.51	0.18	0.27
1956 Example						
Region To Predict	Predicted 1st Change	Predicted 2nd Change	Actual 2nd Change	2nd Region's Index	Predicted 3rd Index	Actual 3rd Index
LR	1.30	-0.65	-2.26	1.03	0.38	-1.23
BR	-2.26	1.71	3.40	-1.23	0.48	2.17
SR	3.40	-1.94	-2.12	2.17	0.23	0.05
AR	-2.12	1.16	0.29	0.05	1.21	0.34

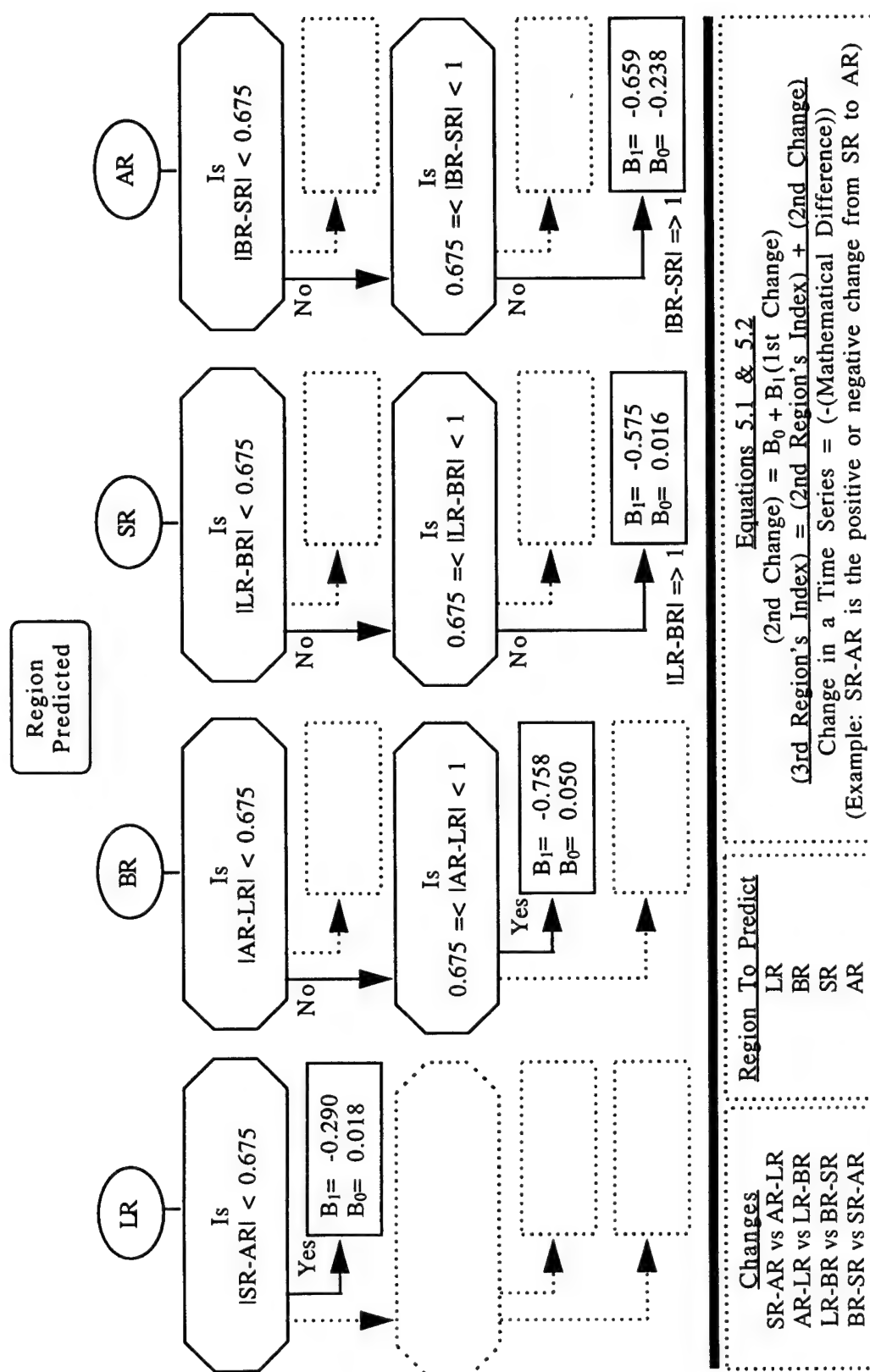


Fig. 55. Same as Figure 54 except showing the paths taken through the flowchart while producing the example forecasts listed in Table 24 for the year 1934. The dotted lines represent paths not taken.

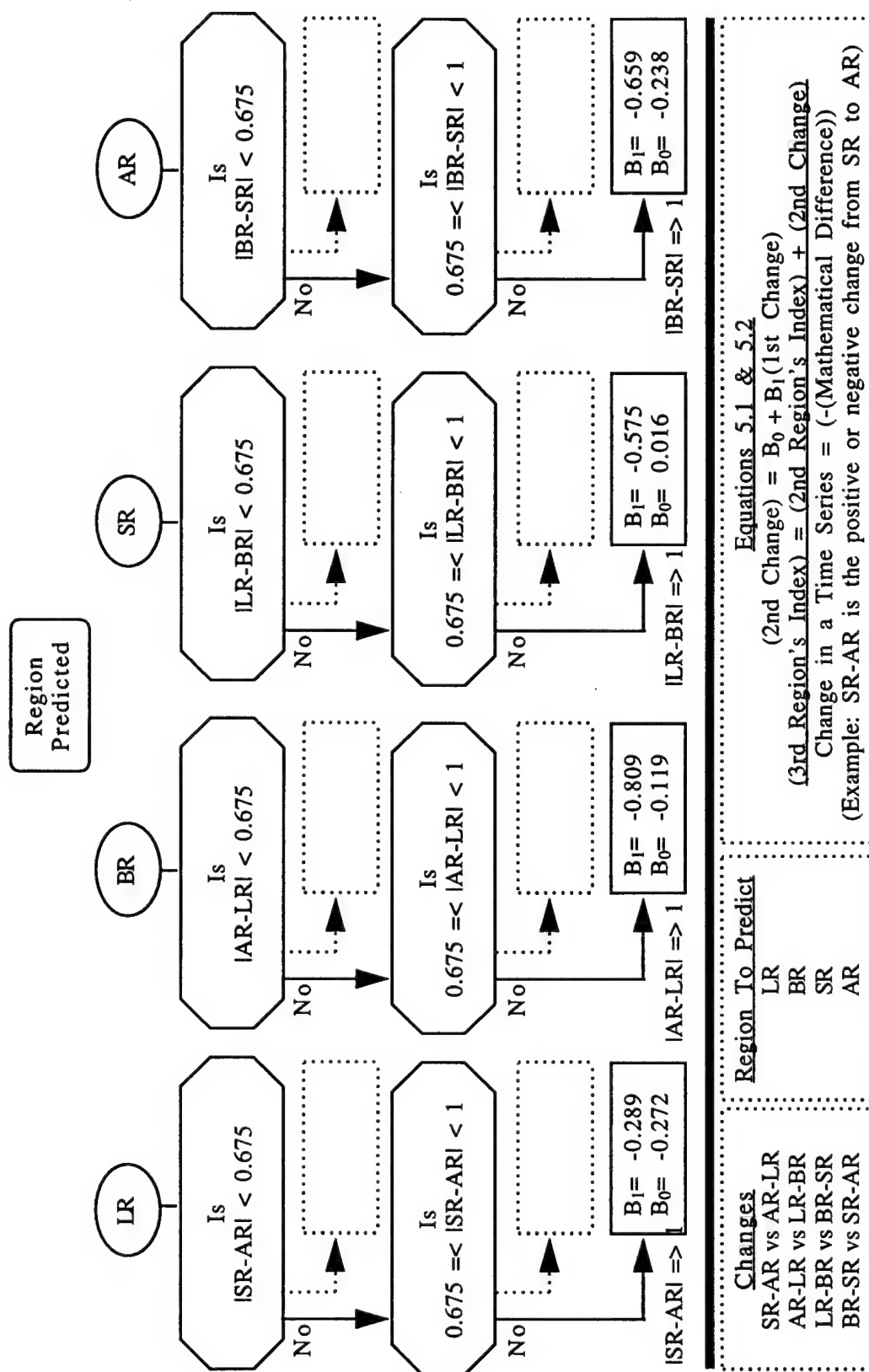


Fig. 56. Same as Figure 54 except showing the paths taken through the flowchart while producing the example forecasts listed in Table 24 for the year 1956. The dotted lines represent paths not taken.

the flowchart shown in Figure 54. The forecasted values are listed in Table 23 under the "Predicted" column headings.

The signs (or trends) of the predicted 2nd changes were correctly forecasted for all regions each year and their magnitudes were deemed respectable, at least when forecasting for the BR, SR, and AR regions. However, since the relationships are not perfectly linear, not all of the results for predicting the 3rd regional indices were desirable. But if an exact forecasted value for the region is required by a user, this method may still be worthy of use, at least for the BR, SR, and AR regions.

Trend Tool with Probability Table

The use of the regression method, which predicts actual values for the second change and third region's rainfall index, presents multiple risks for many users. With the second tool, users who are just interested in forecasting a trend for the upcoming rainy season may use the results listed in Table 24 for forecast purposes. For each region, the regression analyses in Figures 51-53 suggest that a trend exists which indicates that when the first change is positive, then the second change is negative, and vice versa. The observation counts for each quadrant of each graph in Figures 51-53 were used to compute the chance of being correct or incorrect using this method. As an example, using Figure 51a, there is a 73% chance (29 out of 40) of receiving a correct trend forecast using these data alone.

Table 24. Overall probability of receiving a correct trend forecast for each of the three sets of observations.

Observations Used	Region To Predict			
	LR	BR	SR	AR
All	67%	73%	80%	74%
> 0.675	71%	87%	82%	78%
> 1	68%	100%	81%	89%

As one can see from Table 24, as the number of observations decreases (as the data distribution is limited to its outward extremes), the probability of getting a correct forecast improves for the BR and AR regions but remains steady for the LR and SR regions. Therefore, if the data are greater than the absolute value of the probable error (0.675) or one standard deviation, users have a greater chance of receiving a correct trend forecast using this method.

Trend Tool with Decision Flowchart for Probabilities

The third tool is similar to the second but provides the user with a better indication of the probability for success or error. Since the two regional indices used to compute the first change are known, the information in Figures 51-53 (and in Tables 13, 17, and 21) may be used to more accurately indicate the probability of making a correct or incorrect forecast of the trend (positive or negative change) of the next change. Figure 57 is a flowchart diagram which users can easily follow to produce these forecasts when knowing the first two regional indices.

Using the data for 1956 in Table 22 as an example, Figure 58 shows the paths taken in the forecasting process to compute the probability of a correct or incorrect trend forecast for each of the four regions in 1956. The results are listed in Table 25 for both the years 1934 and 1956 and, as the data show, this method produced a correct trend forecast for all regions in both years. It not only provides users with a forecasted outlook but also, the probability of the forecast being correct or incorrect. Users can therefore balance this information with the risks they are willing to assume in their economic or planning endeavors.

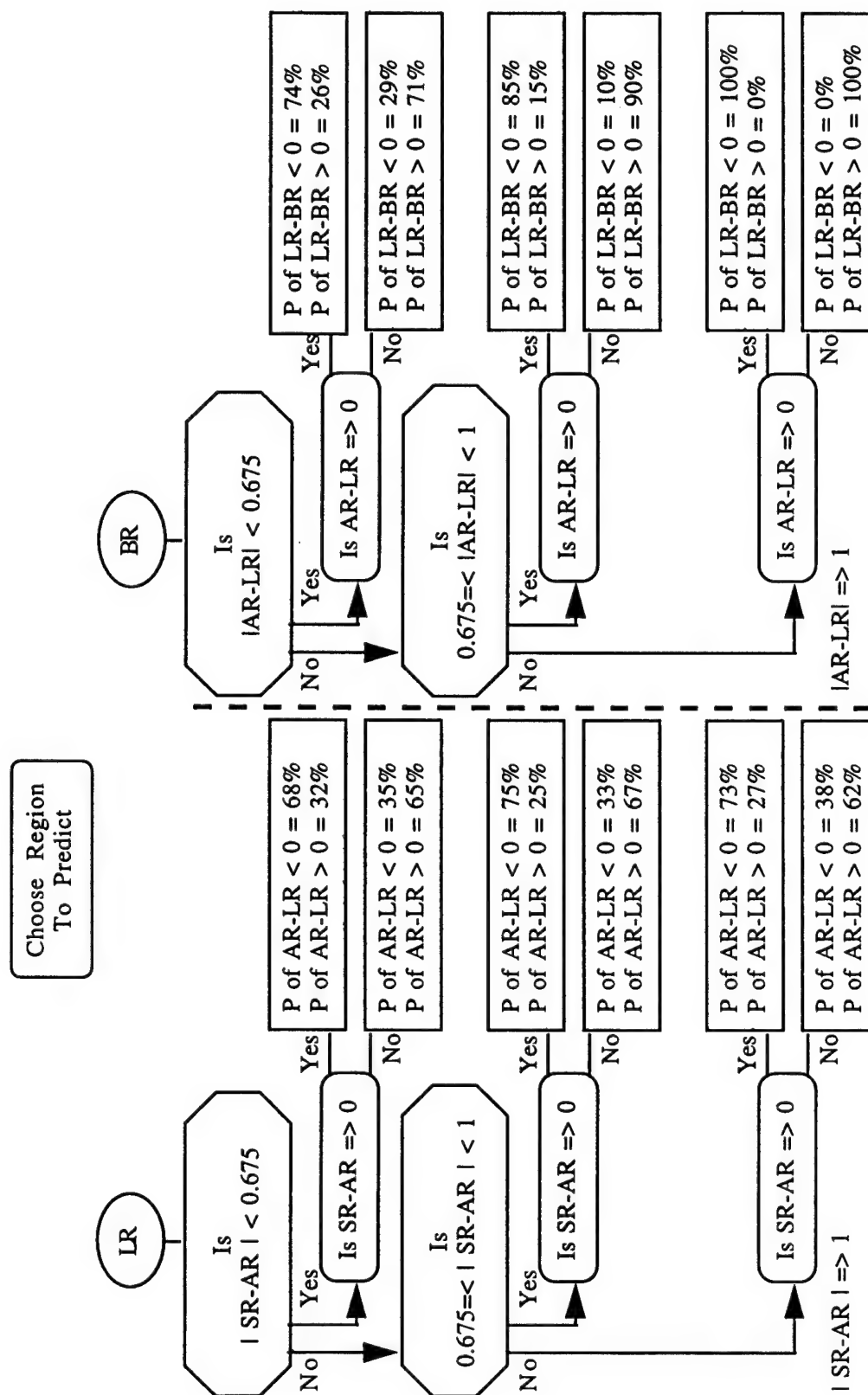


Fig. 57. Predictive flowchart to determine the probability (P) of the trend (or sign) of the second change when the first change is already known (the SR and AR regions are continued on the next page).

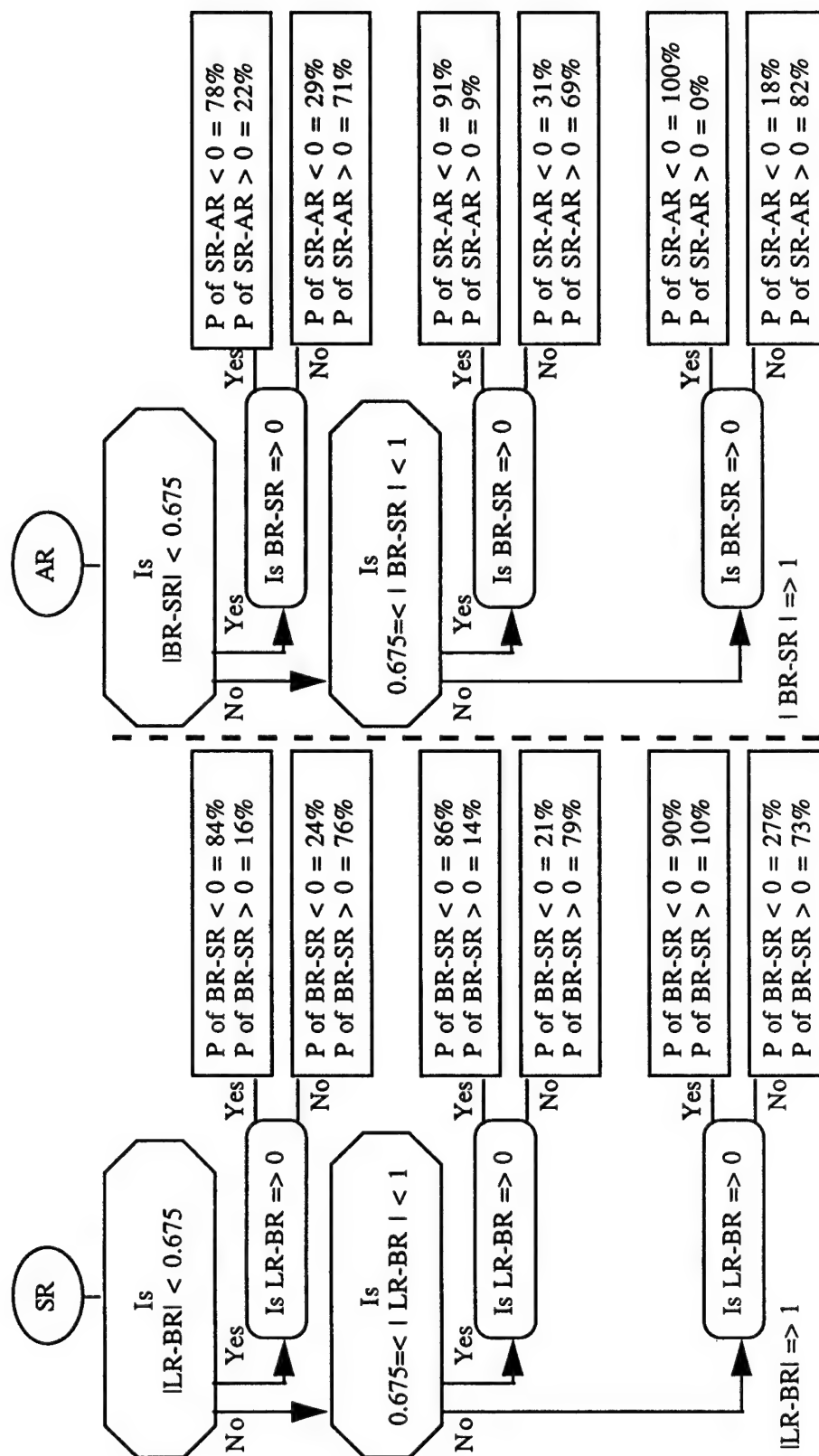


Fig. 57. Continued.

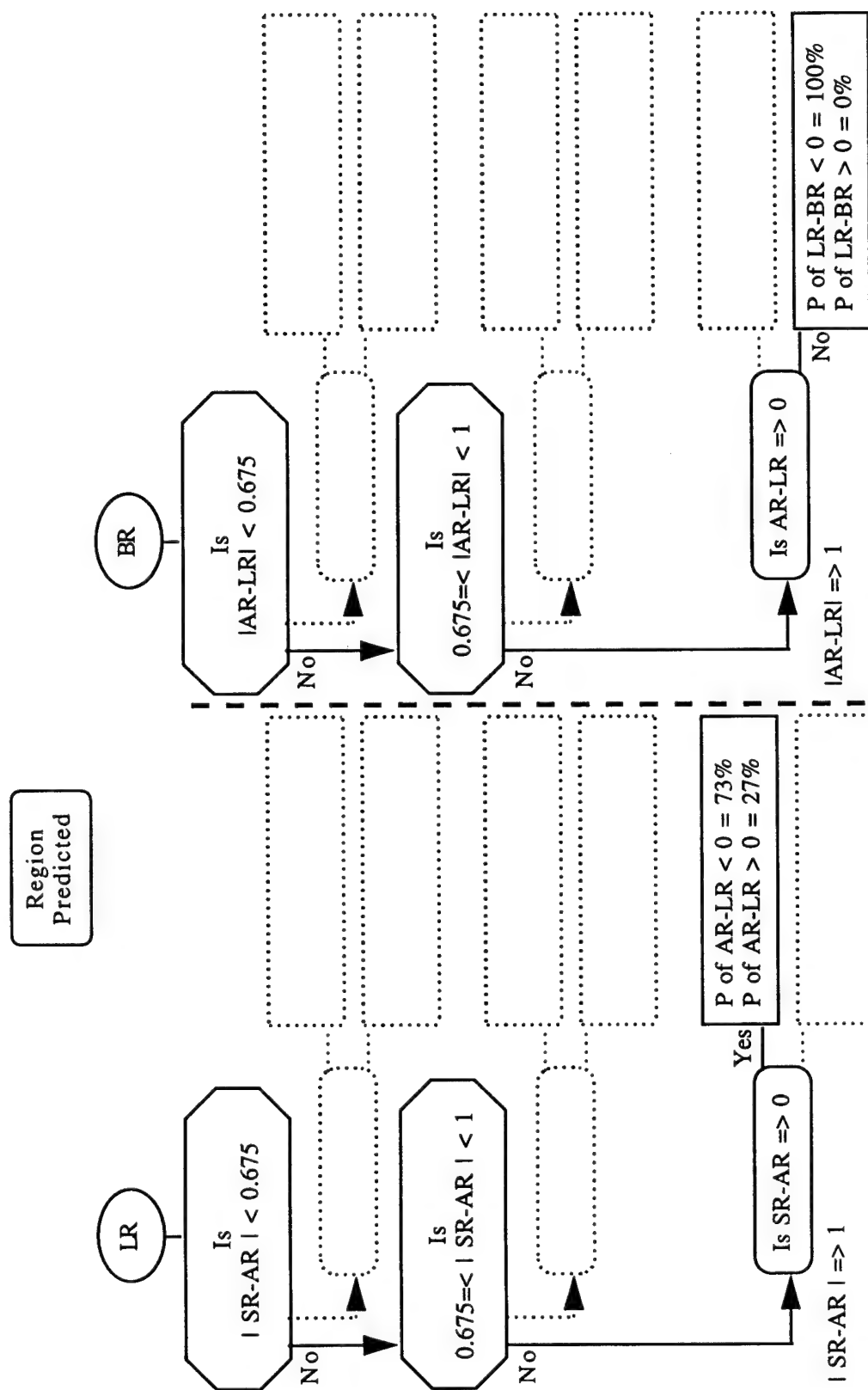


Fig. 58. Same as Figure 57 except showing the paths taken through the flowchart to determine the probabilities (P) of the trend (or sign) of the second change for the example data in Table 22.

Table 25. Example results from the trend tool decision flowchart showing the probabilities of getting a second change of opposite sign and, whether or not, the change was of opposite sign for the two example periods (1934 and 1956). The paths taken through the flowchart for the 1956 data are shown in Figure 58.

1934 Example				
Region Being Predicted	1st TS Change	2nd TS Change	Probability of 2nd Change Being of Opposite Sign	Was 2nd Change of Opposite Sign
LR	0.19	-0.86	67%	Yes
BR	-0.86	1.61	84%	Yes
SR	1.61	-1.41	90%	Yes
AR	-1.41	0.78	82%	Yes
1956 Example				
Region Being Predicted	1st TS Change	2nd TS Change	Probability of 2nd Change Being of Opposite Sign	Was 2nd Change of Opposite Sign
LR	1.30	-2.26	73%	Yes
BR	-2.26	3.40	100%	Yes
SR	3.40	-2.12	90%	Yes
AR	-2.12	0.29	82%	Yes

Improvement Tools Using Teleconnections

By examining the phases of several known teleconnections, it was found that a few of the relationships previously discovered could be improved upon to enable a more reliable forecast. Various aspects of these teleconnections are discussed as they relate to improvements in the forecasting ability of the relationships found.

1. ENSO Years: Previous researchers reported tendencies for the SR rainfall to be above normal during ENSO years and for the AR rainfall to be below normal. These results were confirmed in this study where it was found that of nine ENSO years, the SR rainfall was above normal for six of them, near normal for two of them, and below normal for one of them. During all nine ENSO years, the SOI during the SR season was in the negative or low/wet phase which supports the use of the ENSO years used in this study.

In the eight ENSO years with AR rainfall data, the rainfall was found to be below normal for six of the eight years. The SOI (during the AR

season) was positive in four of these years and negative the other four years. The conclusion was that SR rainfall is influenced more than AR rainfall by phases of the SOI, most probably since the ITCZ and Walker Circulation cells are aligned along the equator during the SR season, increasing the likelihood of direct on-shore flow into the region from the Indian Ocean.

When the rainfall changes between seasons were compared during ENSO years, the only set which showed significant improvement was between the LR→BR and BR→SR set which may be used to predict for the SR rainfall. The correlation between the sets improved from -0.68 using all years of data to -0.74 using only the ENSO years. However, the number of observations used to compute these correlations dropped from 40 to 9, respectively, resulting in the significance level of the relationship decreasing as well. When the data both during an ENSO year and when the previous change was greater than its probable error were compared, the correlation between the sets improved from -0.72 to -0.80. However, the number of observations also decreased resulting in the significance level of the relationship to decrease. Therefore, it was concluded that using these results in decision flowcharts for the SR region would not be statistically worthwhile.

2. Southern Oscillation. To explore whether or not previous results could be improved upon by knowing the current phase of the SOI, the correlations between the sets of changes were explored while using the CPC's SOI index. The average SOI during each rainfall season was computed by averaging the three monthly SOI indexes within each rainfall season. The data were then ranked according to the SOI index for each of the four rainfall regions with the top third of each corresponding to the SOI being in the high/dry phase and, the bottom third of each corresponding to the SOI being in the low/wet phase. The sets of changes were next examined according to the phase of the SOI during the season in which the next season's forecast would be made. For example, when examining the relationship between the LR→BR and BR→SR changes (to produce a forecast for the SR region), the average SOI during the three months of the BR season was used since it would be

during this season in which a forecast would be made. The results of these analyses showed no improvements for forecasts of the BR region's rainfall, slight improvements for the SR and AR region's rainfall, and very significant improvements for the LR region's rainfall.

When the rainfall changes between seasons for predicting the SR region's rainfall were compared, during periods in which the SOI was in its low/wet phase (during the BR season when the forecast would be made), the correlation coefficients strengthened by an average of 0.05. During periods in which the SOI was in its high/dry phase, the correlation coefficients strengthened by an average of 0.10. However, the number of observations used to compute these correlations decreased resulting in the significance level of the relationships to decrease as well (although it remained quite significant). For example, when the data both during a high/dry phase of the SOI and when the previous change was greater than its probable error were compared, the variance associated with this relationship increased from 52% to 69% over that associated with the relationship without considering the phase of the SOI. However, the significance level dropped from 0.000 to 0.010. Therefore, it was concluded that using these results in decision flowcharts for the SR region would not be statistically valid. However, users should be aware of these strengthened relationships during the extreme phases of the SOI.

When the rainfall changes for predicting the AR region's rainfall were compared using periods in which the SOI was in its low/wet phase (during the SR season when the forecast would be made), the correlation coefficients strengthened by an average of 0.05. However, just as with the SR region, the number of observations used to compute these correlations decreased resulting in the significance level of the relationship to decrease. Therefore, it was concluded that using these results to create separate decision flowcharts for the AR region would not be statistically worthwhile.

In earlier analyses, the weakest results were found when forecasting for the LR region. However, when the SOI was in its low/wet phase during the AR season, it was found the relationship between the

SR→AR and AR→LR changes increased significantly from previous results. For example, using all years of data, the correlation coefficient between the two sets of changes was -0.34. However, when using only years during which the SOI was in its low wet phase, the correlation improved to -0.77, and the variance associated with this relationship increased from 11% to 60%. Table 26 lists these improved correlations and the relationships are incorporated into forecast decision flowcharts for predicting the LR region's rainfall presented in the conclusions part of this study.

Table 26. Correlation values between the SR→AR and AR→LR changes using selected sets of observations and phases of the SOI.

Observations Selected	Correlation (r)	N	Probability Level	Variance Associated With
All Data	-0.34	39	0.035	11%
If $ISR \rightarrow ARI > 0.675$	-0.47	21	0.034	22%
If $ISR \rightarrow ARI > 1$	-0.45	19	0.051	21%
If SOI Low/Wet During AR	-0.77	12	0.003	60%
If SOI Low/Wet During AR & $ISR \rightarrow ARI > 0.675$	-0.87	5	0.052	75%

3. Radiational Forcing: Radiational forcing effects were explored to determine whether or not increased insolation influences the poleward progression of the ITCZ on an annual basis. Since no observational data exist for insolation measurements, modeled radiational forcing data as developed by Stevens (1997) were used. If varying amounts of insolation do influence the poleward progression of the ITCZ, the effects should be most evident on the BR region's rainfall since the band of maximum surface heating, moving with the solar declination, acts upon a larger land surface area while over the northern half of the continent.

Figure 59a shows insolation forcing effects over the BR region due to changing solar parameters. Since the solar data are monthly, the values

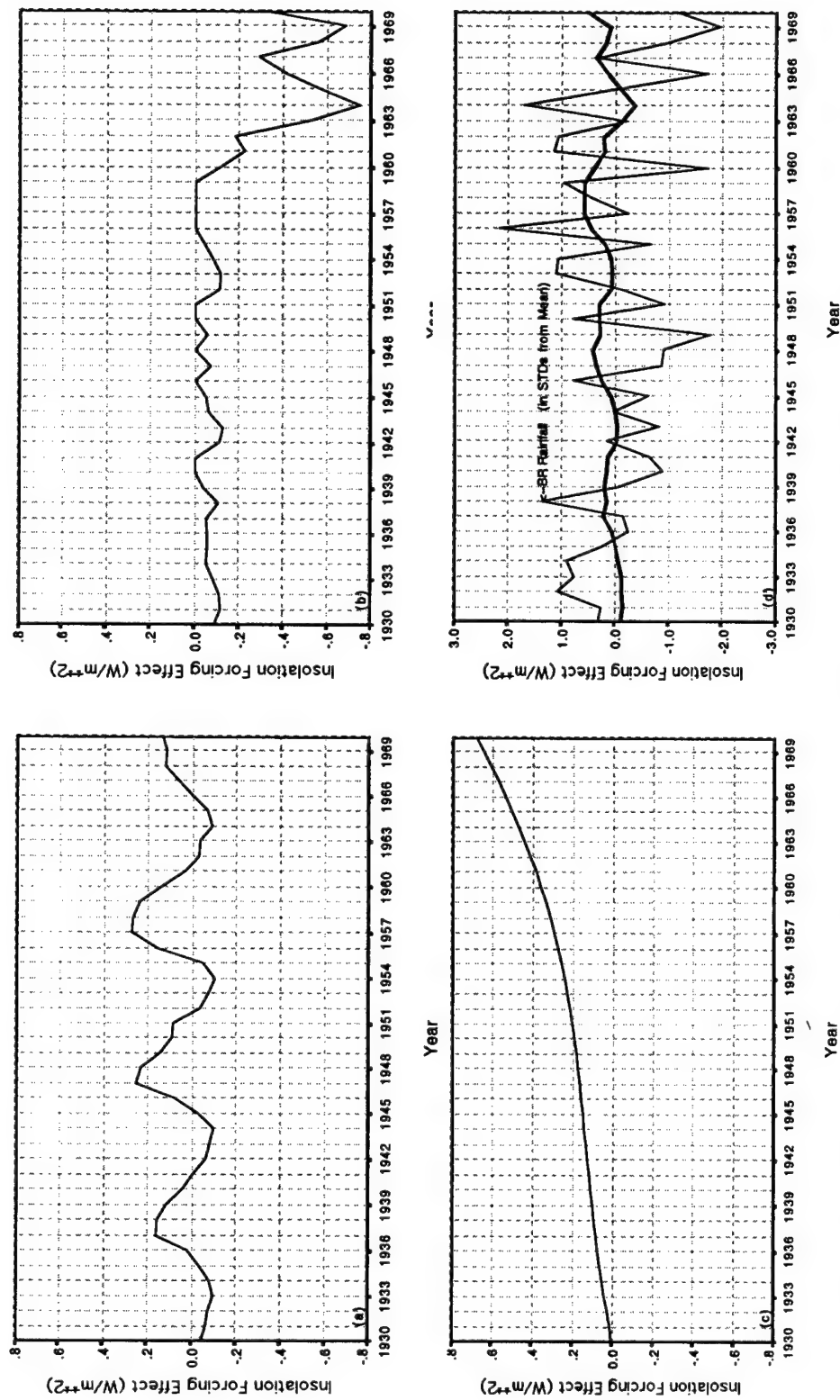


Fig. 59. Insolation forcing effects from (a) solar parameters, (b) stratospheric aerosols, (c) greenhouse gases, and (d) the combined effects of all three (heavy line) overlaid on top of the annual BR regional rainfall indices. No significant relationship is evident.

are the average of the three months: June-August. Figure 59b shows insolation forcing effects due to stratospheric aerosols (mostly volcanic) which only decrease insolation depending upon their atmospheric concentrations. These data are monthly for the 19.5°N latitude band since the insolation received ahead of the ITCZ system should influence its further progression. Just as with the solar data, the stratospheric aerosol data are the average of the three months during the BR season. In Figure 59c, insolation forcing effects are shown which are due to the increasing concentrations of greenhouse gases in the atmosphere (mainly CO₂). The annual value for 1930 was set to zero and incremented thereafter through the POR, thus depicting a steady increase in forcing. In Figure 59d, the effects of all three forcings are combined (through simple addition) and are shown along with the BR rainfall indices. Both Figure 59d and correlation analyses confirmed that no significant relationship was evident between the insolation forcing effects and the BR region's rainfall. Therefore, the conclusion is that there is insufficient evidence to support the theory that increased insolation ahead of the ITCZ's movement influences its poleward progression on an annual basis.

This same analysis was performed on the other three regions as well, using different latitude bands for the stratospheric aerosol forcing data. However, no significant relationships were found. In addition, when comparing the rainfall data with insolation forcing data, there seemed to be stronger relationships, although still not significant, when the greenhouse gas forcing component was removed. Since the scientific community is fairly certain that the greenhouse gas forcing is real, the only explanation offered is that, possibly, forcings due to tropospheric aerosols might offset the increased forcing due to greenhouse gases. While increasing concentrations of greenhouse gases increase insolation, tropospheric aerosols are thought to decrease it by acting as tiny microscopic mirrors in the atmosphere which deflect incoming solar radiation. However, this study did not use tropospheric aerosol forcing data since no reliability could be placed on the data over Eastern

Africa and, it was not an objective of this study to explore this relationship further.

The insolation data during the BR season (solar and stratospheric aerosol components only) were next ranked into thirds and used in correlation analyses between the LR→BR and BR→SR changes. As suspected, the correlations strengthened as the data distributions were limited toward their extremes (either the top or bottom thirds of the insolation data distribution). Using all years of data, the correlation between the sets was -0.68. Using only years within the top third of the insolation data, the correlation strengthened to -0.75. And, using only years within the bottom third of the insolation data, it strengthened further to -0.79. While these are notable increases, one must remember the insolation data is modeled data and no operational index of it exists for users to reference on a real time forecasting basis. Therefore, while this relationship is noteworthy for further research, it is not useful for inclusion in the forecast decision flowcharts developed in this work. However, users should be aware of this relationship.

4. The ASP Index: The extent of the poleward progression of the ITCZ into the NH was also examined by comparing the BR region's rainfall with the CPC's ASP index. It was theorized that if the ITCZ progressed further northward than its mean position during the BR season, the layer of tropical moisture following it would progress further northward as well. This would deepen the layer of moisture over the BR region (see Fig. 50), thereby, increasing the potential for convective activity.

Unfortunately, the ASP index data (which users can obtain directly over the internet from the CPC) are only available from 1950 to present, therefore, only 21 years of data were available for analysis (1950-1970). Correlation analyses between the ASP data and the BR region's rainfall revealed a -0.36 correlation, the sign of which was expected. With only 21 observations though, this relationship was only significant at the 10% level. In order for a -0.36 correlation to be significant at the 5% level for a sample from an unrelated population, a sample size of at least 30 would be required (Brooks and Carruthers, 1953). However, a

relationship found within a time series is only significant if it is found to be consistent throughout the entire time series. By assuming the ASP data and the BR region's rainfall data would have had the exact same relationship for the years 1930-1949, (for which ASP values were not available), one could effectively double the number of observations available for study. This new analysis revealed the probability level of the ($r = -0.36$) relationship improved in significance to 5% using 10 additional years of data and to under 2% for 20 additional years of data. This indicates there is likely to be a significant relationship between rainfall over the BR region and the ASP.

The ASP data were next sorted and divided into two groups: high (ASP $\Rightarrow 0.06$) and low (ASP < 0.06). When the ASP index was higher than its mean ($\Rightarrow 0.06$), the correlation between the LR \rightarrow BR and BR \rightarrow SR changes increased dramatically to over -0.94. This relationship is associated with 89% of the variance between the two changes and leads to a strong prediction capability for determining SR rainfall (since one could assume a near linear relationship). When the ASP indices were less than their mean, however, this relationship was not as significant.

A very significant result was discovered when the analysis was limited to both when the ASP index was higher than its mean ($\Rightarrow 0.06$) and, the absolute value of the LR \rightarrow BR change was greater than its probable error ($\Rightarrow 0.675$). The correlation between the LR \rightarrow BR and BR \rightarrow SR changes increased further to over -0.98. This relationship is associated with 96% of the variance between the two changes which leads to a very strong prediction for determining SR rainfall (since one could also assume a near perfect linear relationship).

Listed in Table 27 is a complete listing of the correlation values between the sets of changes using the selected categories of observations. The results in Table 27 are very significant since the ASP is in its high phase one out of every two years, on average, and it is both in its high phase and the LR \rightarrow BR change is greater than its probable error one in every three years, on average. Figures 60a and 60b show scatter graphs depicting these strong linear relationships. These very

Table 27. Correlation values between the LR→BR and BR→SR changes using selected sets of observations and phases of the ASP.

Observations Selected	Correlation (r)	N	Probability Level	Variance Associated With
All Data	-0.68	40	0.000	47%
If LR→BR > 0.675	-0.72	28	0.000	52%
If LR→BR > 1	-0.73	21	0.000	53%
If ASP < 0.06	-0.75	10	0.012	57%
If ASP > 0.06	-0.94	10	0.000	89%
If ASP > 0.06 & LR→BR > 0.675	-0.98	7	0.000	96%

positive results lead to the conclusion that the regression forecasting method works extremely well when forecasting for the SR region during years in which a high ASP index occurs. Since at least one of these conditions should occur 50% of the time, forecasters should use the following versions of equations 5.1 & 5.2 to forecast the value of the BR→SR change and a seasonal forecast of the SR region's rainfall.

When the ASP => 0.06, use:

$$(BR \rightarrow SR \text{ Change}) = 0.759 - 0.887(LR \rightarrow BR \text{ Change});$$

and when the ASP => 0.06 and the |LR→BR| Change => 0.675, use:

$$(BR \rightarrow SR \text{ Change}) = 1.003 - 0.902(LR \rightarrow BR \text{ Change}).$$

In addition, the observation counts listed in each quadrant of Figure 60 may also be used for trend forecasting purposes.

The results for predicting the AR region's rainfall were also enhanced during certain phases of the ASP. The correlation coefficient between the BR→SR and SR→AR changes with all years of data included was -0.63. However, this relationship strengthened to -0.71 when the ASP index was in its high phase and decreased to a non-significant -0.36 when the ASP was in its low phase. Since during the low phase of the ASP, the ITCZ is thought to progress further north during the BR season, other factors may influence these relationships. However, when the ASP is in its high phase, the ITCZ might not progress as far northward, and relationships between the changes may tend to

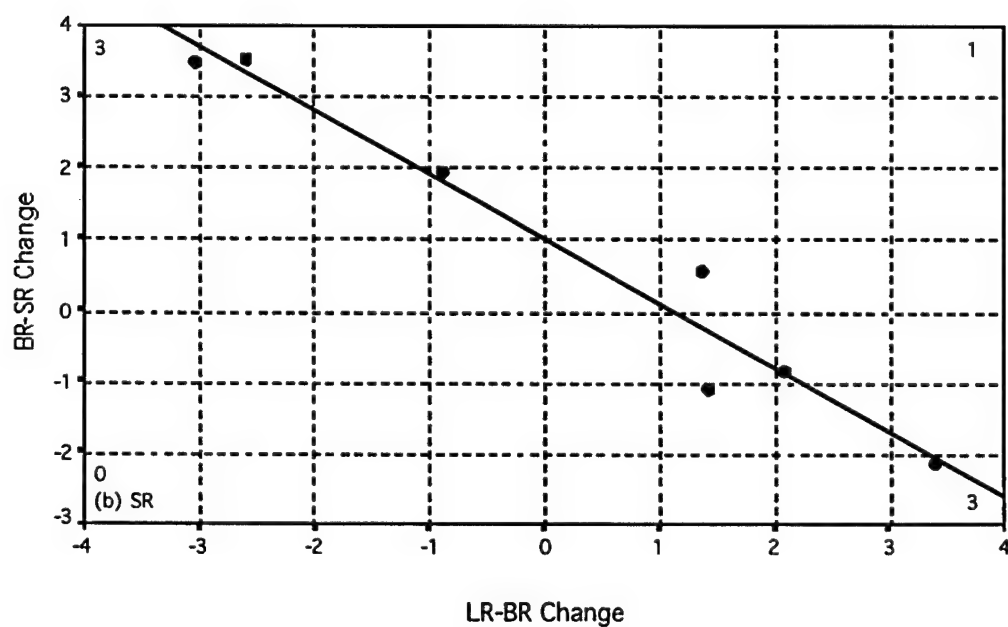
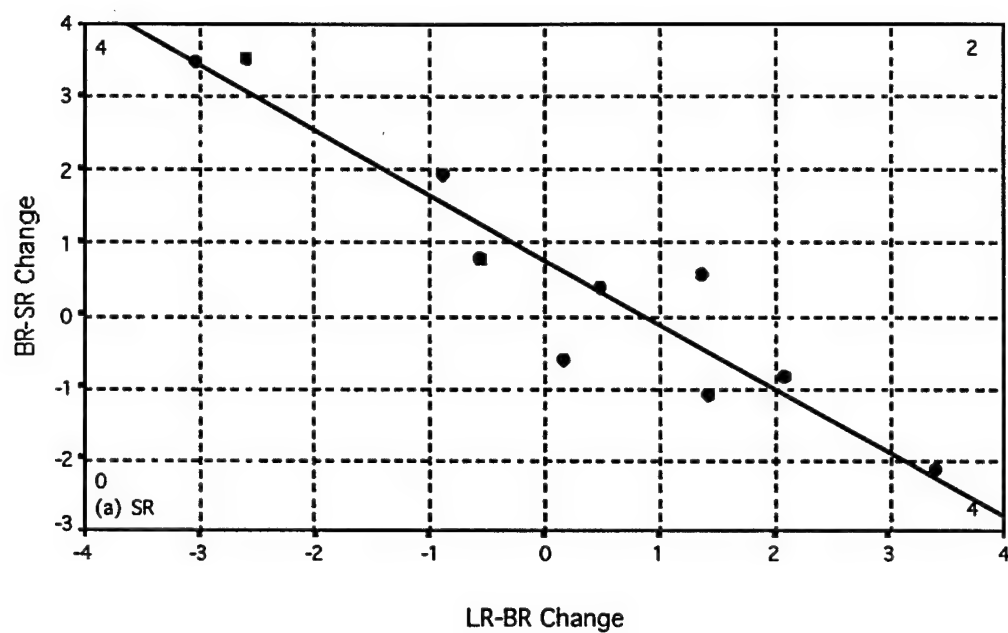


Fig. 60. Scatter graphs depicting the relationship between the LR→BR and BR→SR changes when (a) the ASP index is higher than its mean during the BR season and (b) when both the ASP index is higher than its mean and the absolute value of the LR→BR change is greater than its probable error.

strengthen. When the ASP index is in either its positive or negative phase during the BR season, forecasters should be aware of these relationships. The relationship strengthened further to -0.79 when both the ASP index was in its high phase and when the first change was greater than its probable error. However, the number of observations used to compute these correlations decreased resulting in the significance level of the relationship to decrease (although they were still very significant). Therefore, it was concluded that using these results to create separate decision flowcharts for the AR region would not be statistically worthwhile.

CHAPTER VII

USER FORECASTING DECISION FLOWCHARTS

In this chapter, decision flowcharts are presented which are deemed relevant and simple enough for users to produce seasonal rainfall forecasts for any of the four regions. The purpose of these tools is to enable users to reduce risks in potentially "poor" years and to maximize gains in potentially "good" years. Several different tools were offered throughout the study to provide users with a choice according to the degree of risk they are willing to assume. These choices are incorporated into the decision flowcharts presented here for each region, as well as choices to improve the predictive capacity of the forecast during certain phases of several known teleconnections.

All indices of teleconnected events used in these flowcharts are accessible to world-wide users via the Internet from the U.S. Climate Prediction Center. Users therefore only need to obtain the monthly rainfall indices for each region using the procedures outlined in this study. While many of the rainfall reporting stations used in the study may no longer report observations, users may compute monthly rainfall indices for each region from observations available to them. It is believed that as few as 10 widely-spaced rainfall reporting stations within each region may be used to form an index representative of the region's rainfall.

In order to choose the correct decision flowchart, users need to make several initial decisions. Figure 61 outlines the steps necessary to make these decisions when producing a seasonal rainfall forecast using the flowcharts presented in Figures 62-65.

Predictive Guidelines

Step 1

Choose the region for which to forecast
and reference the figure listed below for that region.
(reference Figure 3 for area map)

IR Fig. 62	BR Fig. 63	SR Fig. 64	AR Fig. 65
----------------------	----------------------	----------------------	----------------------



Step 2

Choose a method of forecasting within each figure.

Method 1 Regression	Method 2 Probability of Overall Trend	Method 3 Probability of the Trend Being Positive or Negative
-------------------------------	--	--



Step 3

Start with the general conditions or probabilities
for all cases.



Step 4

Follow the flowchart to improve the predictive capacity of the forecast
when specific conditions occur or during specific phases of known
teleconnections.

Fig. 61. Steps to produce a seasonal rainfall forecast.

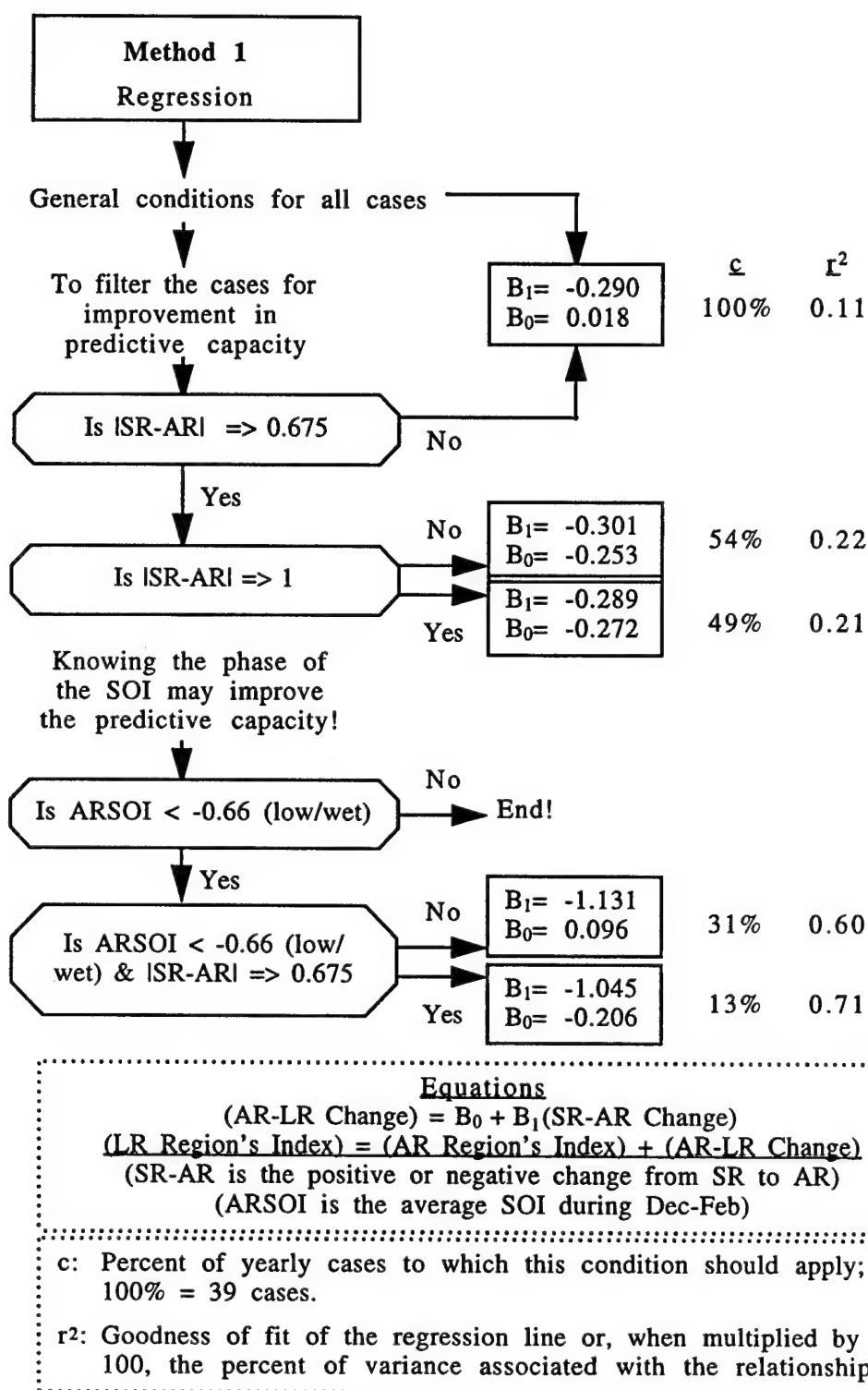
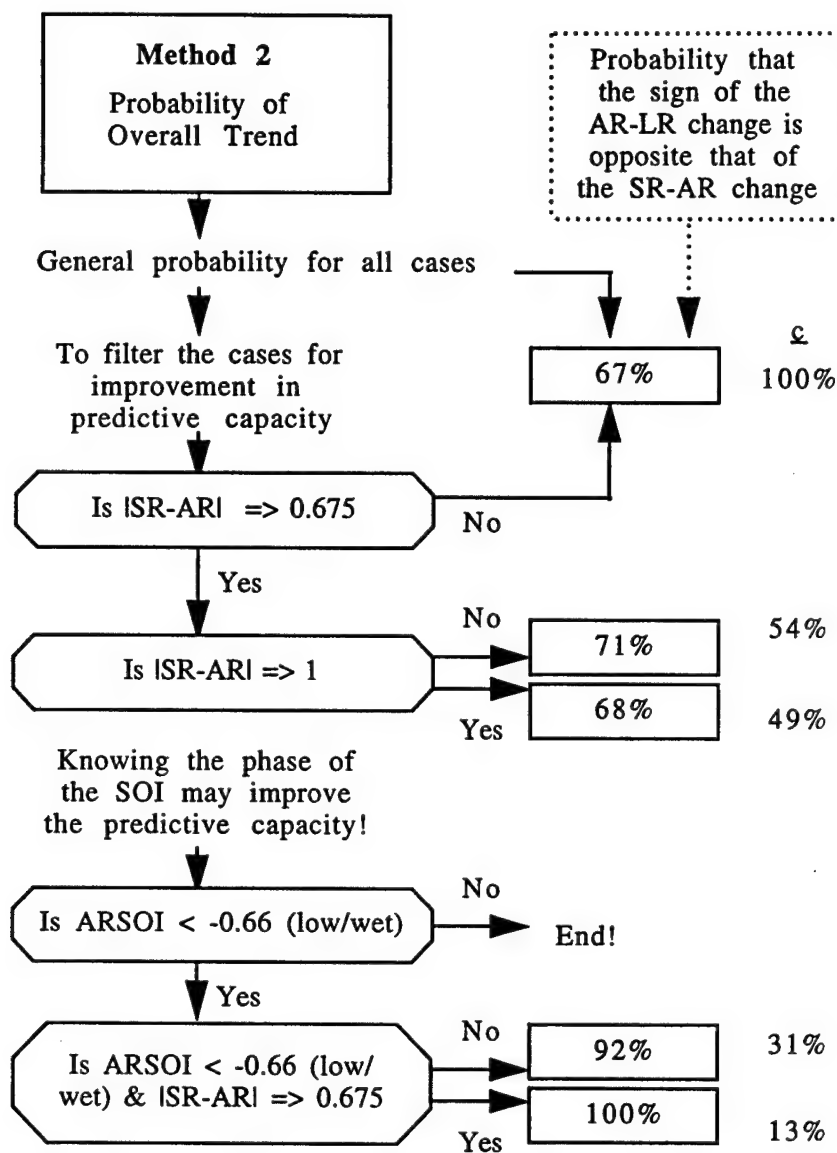


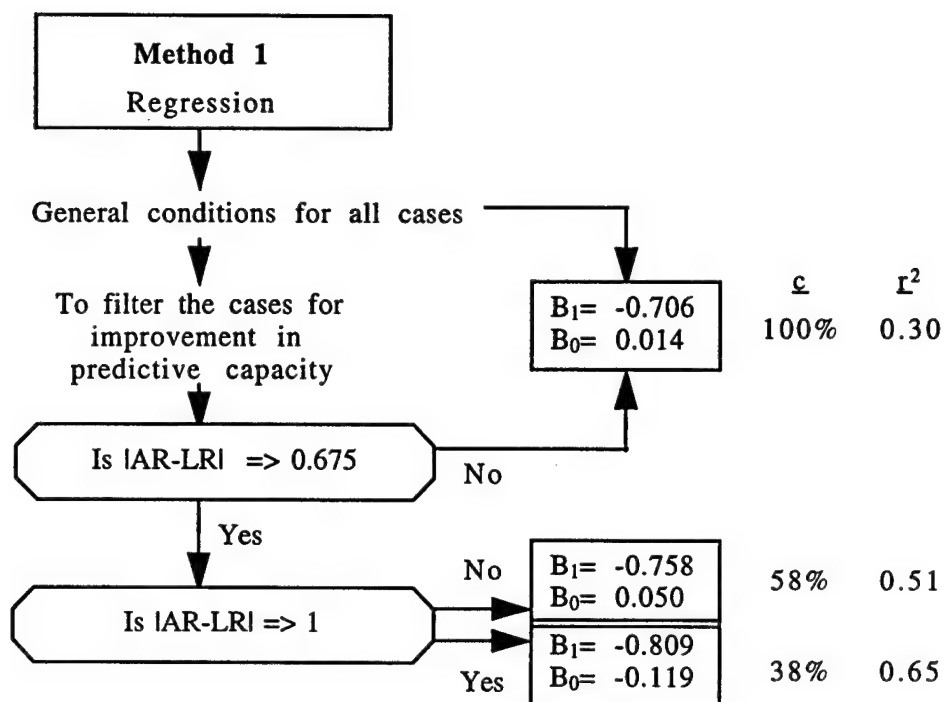
Fig. 62. Forecast decision flowchart for the LR region (or season).



(SR-AR is the positive or negative change from SR to AR)
(ARSOI is the average SOI during Dec-Feb)

c: Percent of yearly cases to which this condition should apply;
100% = 39 cases.

Fig. 62. Continued.



Equations

$$(AR-LR \text{ Change}) = B_0 + B_1(SR-AR \text{ Change})$$

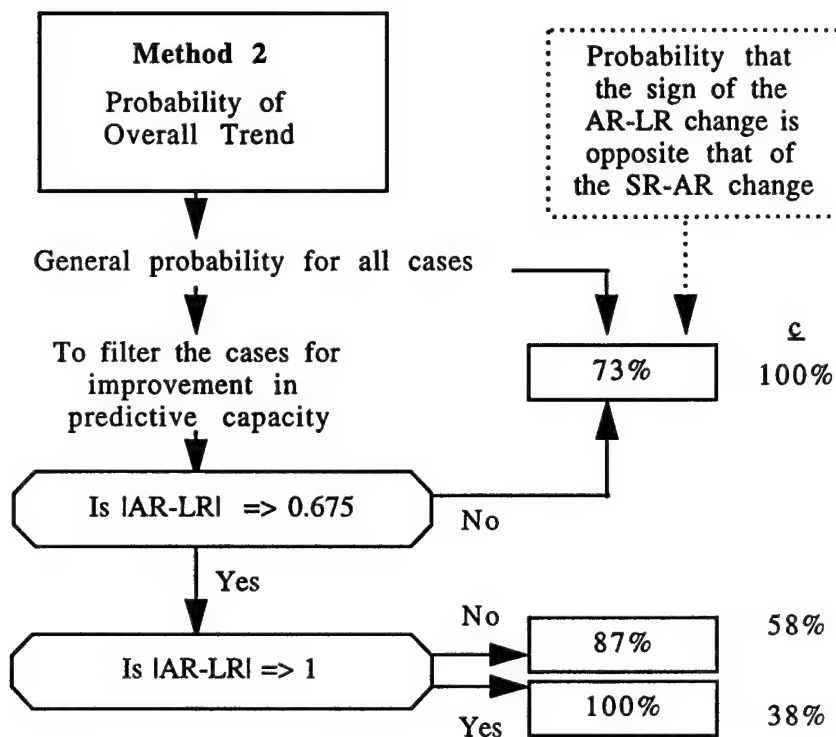
$$(LR \text{ Region's Index}) = (AR \text{ Region's Index}) + (AR-LR \text{ Change})$$

(AR-LR is the positive or negative change from AR to LR)

c : Percent of yearly cases to which this condition should apply;
100% = 40 cases.

r^2 : Goodness of fit of the regression line or, when multiplied by 100, the percent of variance associated with the relationship.

Fig. 63. Forecast decision flowchart for the BR region (or season).



(AR-LR is the positive or negative change from AR to LR)

c: Percent of yearly cases to which this condition should apply;
100% = 40 cases.

Fig. 63. Continued.

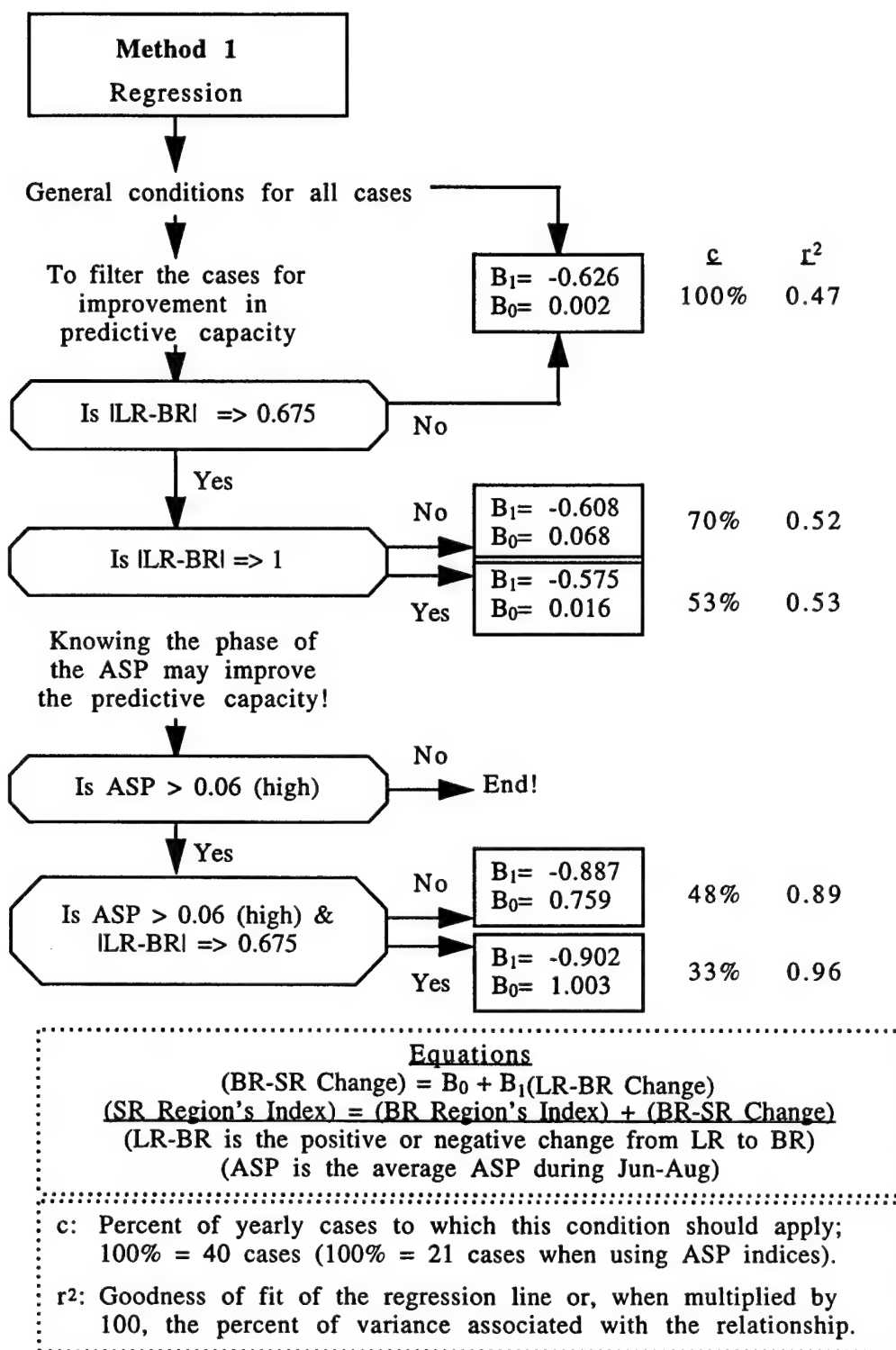


Fig. 64. Forecast decision flowchart for the SR region (or season).

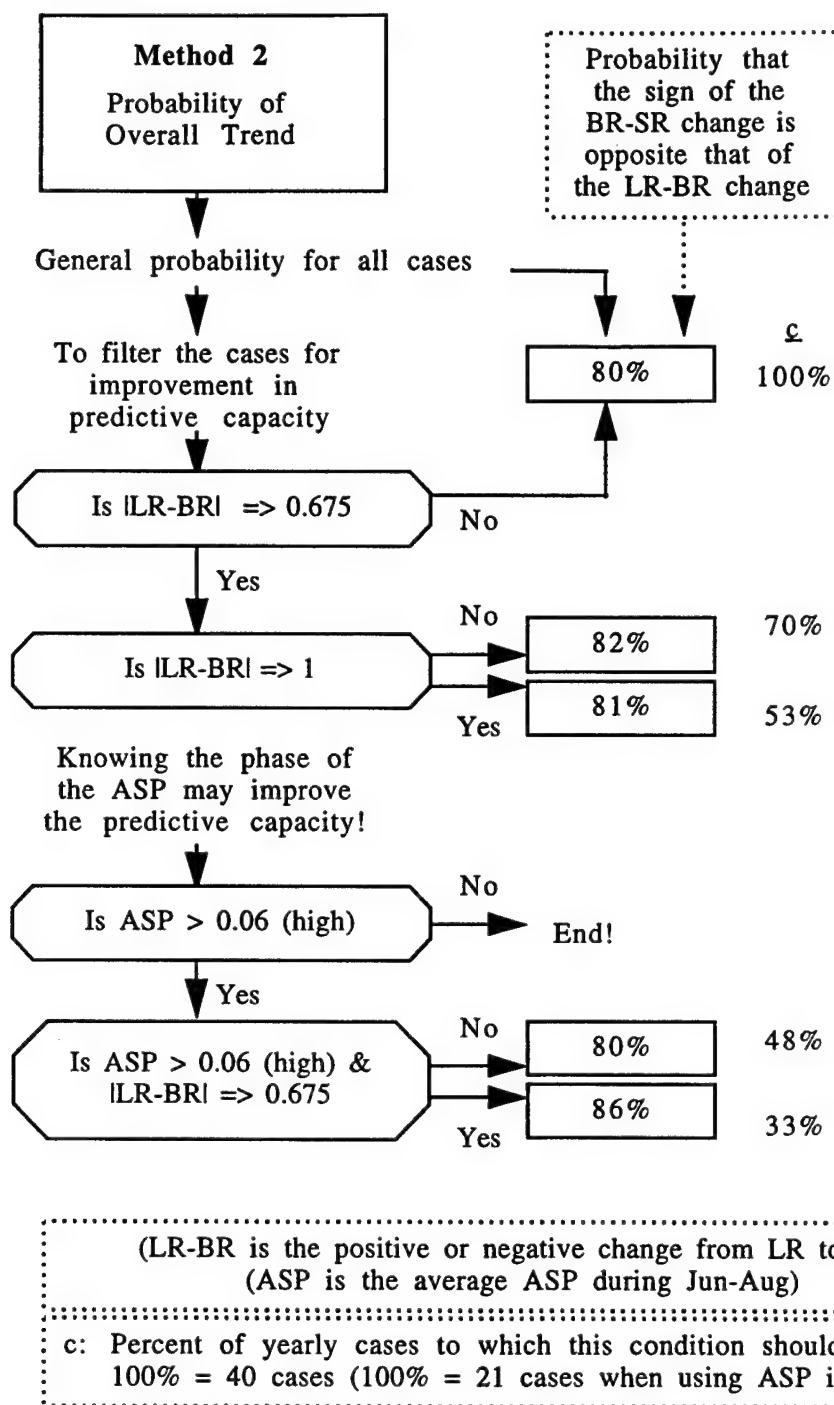
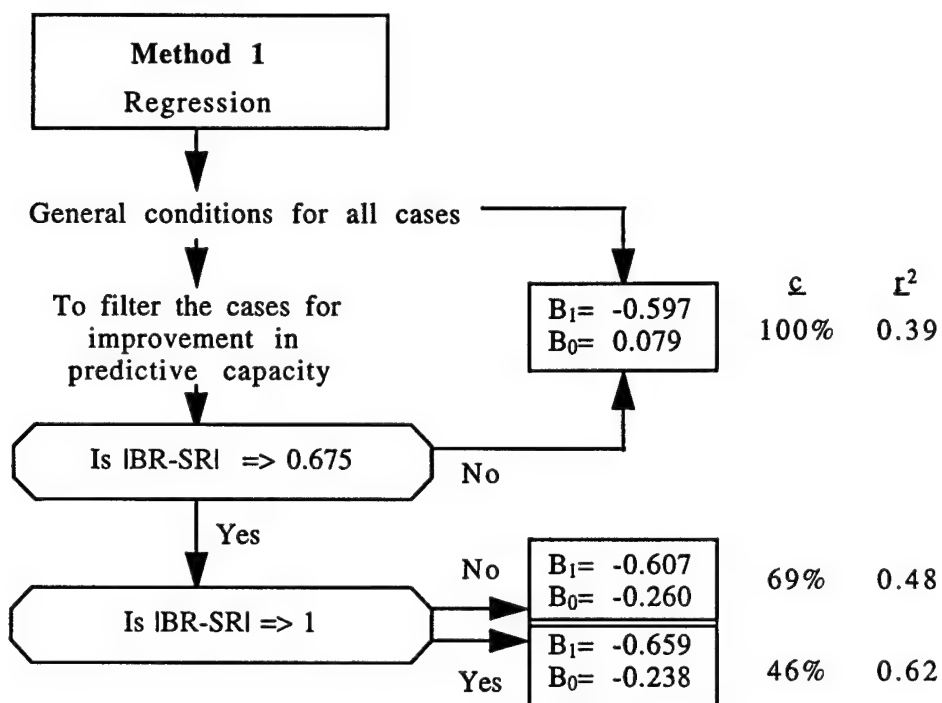


Fig. 64. Continued.



Equations

$$(SR-AR \text{ Change}) = B_0 + B_1(BR-SR \text{ Change})$$

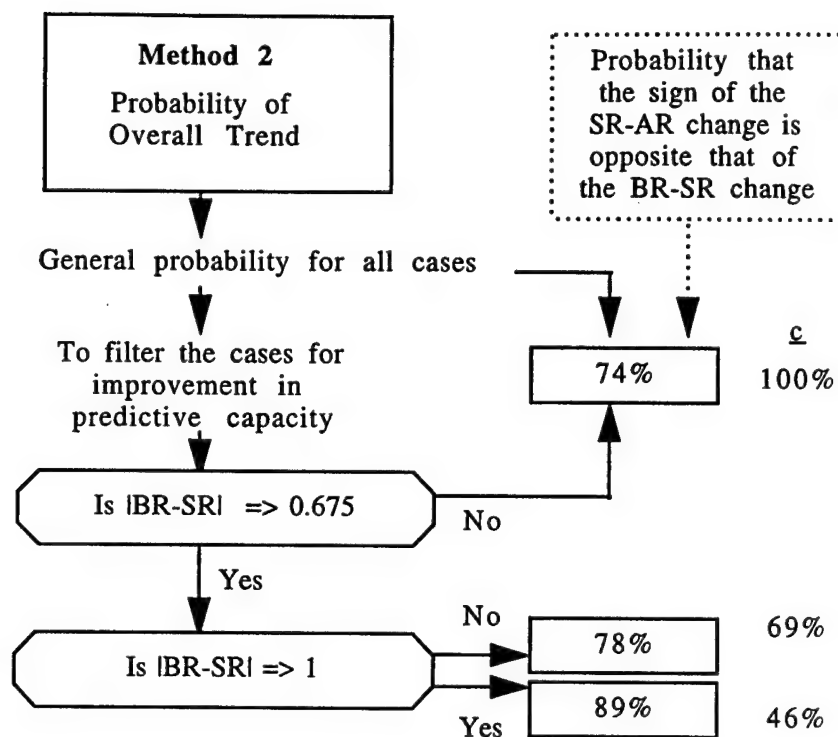
$$(AR \text{ Region's Index}) = (SR \text{ Region's Index}) + (SR-AR \text{ Change})$$

(BR-SR is the positive or negative change from BR to SR)

c : Percent of yearly cases to which this condition should apply;
100% = 39 cases.

r^2 : Goodness of fit of the regression line or, when multiplied by
100, the percent of variance associated with the relationship.

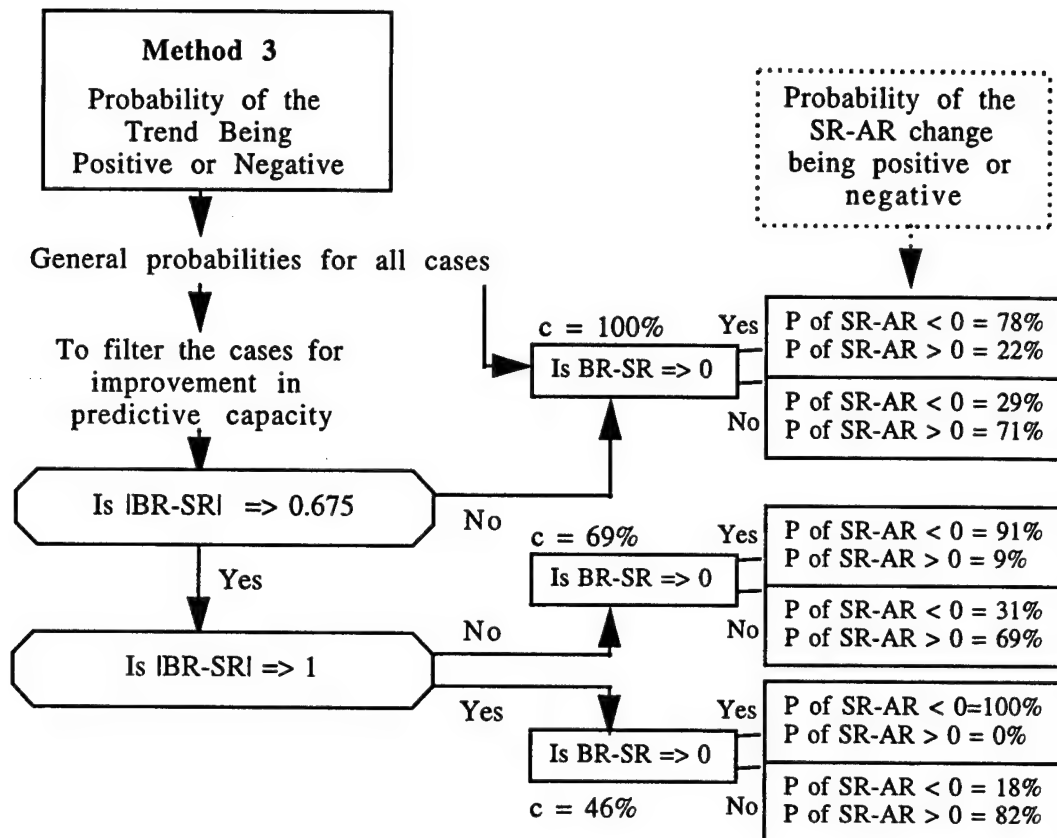
Fig. 65. Forecast decision flowchart for the AR region (or season).



(BR-SR is the positive or negative change from BR to SR)

c: Percent of yearly cases to which this condition should apply;
100% = 39 cases.

Fig. 65. Continued.



(BR-SR is the positive or negative change from BR to SR)
(SR-AR is the positive or negative change from SR to AR)

c: Percent of yearly cases to which this condition should apply;
100% = 39 cases.

Fig. 65. Continued.

CHAPTER VIII

CONCLUSIONS AND RECOMMENDATIONS

Conclusions

This study has shown the feasibility of forecasting seasonal rainfall three months in advance for ITCZ-associated rainfall over Eastern Africa. Using a time series analysis approach, the study examined regional rainfall based on preceding conditions and detected patterns of variability in the time series data. The study suggests that a continuity appears to exist with rainfall as the air mass following the ITCZ progresses through its annual cycle over the research area. It was found that this continuity leads to a reasonably dependable prediction of rainfall over the next region traversed by the same ITCZ system.

The region of Eastern Africa was divided, very selectively, into four seasonal rainfall patterns by choosing only stations which, on average, exhibited rainy seasons conforming to expected ITCZ-associated mechanisms (Objective 1). The data were analyzed using minimal statistical assumptions, and rainfall indices (which depict the average rainfall received during a rainy season) were developed for each region (Objective 2).

Time series visualizations of each region's rainfall were developed as well as those of ITCZ-associated rainfall (as the ITCZ traversed each region in sequential order). Each region's rainfall was examined using time series analyses to determine any trends over the POR that may be attributable to climate change, however, no trends were found. In addition, the time series of ITCZ-associated rainfall data was also examined, but again, no trends were found (Objective 3). However, all of the six values greater than two standard deviations above the mean did occur in the latter half of the POR. This may suggest that the intensity of rainfall events within the area may be increasing, along with possible global warming.

By using a first-difference transformation on the ITCZ-associated rainfall time series data, the study was able to identify predictive relationships within the data. The change (or first-difference transformation of the time series) between rainfall indices for two regions traversed sequentially by the ITCZ was found to be highly negatively correlated with the previous change (between the indices of the two previous regions traversed by the same ITCZ system). Therefore, it was concluded that knowing the rainfall indices for the first two regions can lead to a prediction of the rainfall index for the next region traversed (Objective 4). This effectively produces a seasonal rainfall forecast three months in advance for the average rainfall over each region.

Three methods for producing these seasonal forecasts were found to be relevant for use with the data. Each method is dependent upon the amount of risk users are willing to assume for receiving an incorrect forecast. The first method uses linear regression and produces a forecast for an actual amount of rainfall (on average) over each region. However, this method assumes a perfect linear relationship among the data which does not exist. This method is deemed reliable under some circumstances though, if the user is willing to assume the risk and accept varying degrees of incorrect forecasts a certain percentage of the time.

The second method of forecasting uses the trend relationship between the two sets of changes. Regression analyses showed that a trend exists which indicates that when one change is negative, then the next change tends to be positive, and vice versa. This method reveals the probability of knowing the sign (positive or negative) of the upcoming change between indices. Therefore, this method produces a predictive outlook type of forecast which estimates the probability of the forecast being correct or incorrect.

The third method improves upon the second since the first change would be already known. When producing a forecast, the rainfall indices of both the region currently being traversed by the ITCZ and of the last region traversed would be known. Therefore, by knowing the

sign (positive or negative) of the change between them, the probability of the next change being positive or negative can be calculated.

Additionally, it was found that these relationships could be improved upon when the first change was large, or when it fell into the outer extremes of its data distribution (Objective 5). For example, the relationships showed a tendency to strengthen when the absolute value of first change exceeded its probable error or one standard deviation.

It was shown that the use of these methods produced positive results when forecasting for the BR, SR, and AR rainfall regions. However, the method was shown to be less useful while forecasting for the LR region, most probably, since the amount of moisture which enters the air mass as the ITCZ traverses into the Southern Hemisphere is both unknown and influenced by multiple synoptic factors. In other words, the continuity associated with the rainfall seems to end as the ITCZ traverses over its most southern extent.

It was also found that the relationships discovered could be improved upon for specific regions during periods associated with teleconnected events (Objective 6). By examining the current phase of the Southern Oscillation when the forecast for the next region was being made, it was demonstrated that the results improved for the AR and SR regions and, improved significantly for the LR region when the Southern Oscillation was in its low/wet phase during the Austral summer. The conclusion is that when the SOI is in its low/wet phase during the Austral summer, the AR region's rainfall tends to be below average, which indicates the lack of synoptic scale features entering the region from the Indian Ocean.

Each region's rainfall was also compared with modeled insolation forcing data to determine if increased insolation over northeastern Africa (and the Sahel) caused the ITCZ to progress further poleward on an interannual basis (Objective 7). However, no significant results were found. However, the study also used the CPC's ASP index as an indicator of the large scale surface pressure fields over northeastern Africa and southern Asia during the Boreal Summer (also Objective 6). Relationships were found which improved the forecasting ability for

the SR and AR seasons very dramatically. During the high phase of the ASP, a near-perfect linear relationship was found for predicting the SR region's rainfall. In addition, the ASP data and the BR rainfall were found to be significantly negatively correlated. The conclusion is that when the ASP index is high, the ITCZ does not progress as far northward as when the index is low; therefore, the intensity of the BR rainfall is less and the BR→SR change is more closely related to the previous LR→BR change.

Predictive guidelines in the form of decision flowcharts were developed which are deemed relevant and simple enough for users to produce seasonal rainfall forecasts for individual regions. The purpose of these tools is to enable users to reduce risks in potentially "poor" years and maximize gains in potentially "good" years. Several different tools were offered throughout the study to provide users with a choice according to the degree of risk they are willing to assume. Complete forecast decision flowcharts for each region are developed in Chapter VII which users can follow to produce seasonal rainfall forecasts three months in advance for each region. All indices of teleconnected events used in the flowcharts may be obtained by users via the internet from the CPC (Objective 8).

The decision flowcharts were developed for use not only by meteorologists but also many other professions involved in decision making such as agricultural economics and water resource management. The potential for research using this methodology is tremendous, and in terms of economic applications, refined research is still necessary along with the inclusion of expertise from other disciplines. It has been shown that this method of producing seasonal rainfall climate forecasts works. Therefore, the next step is to inform users of its capabilities. In addition, this effort should be part of a larger process to educate both users and scientists on each others needs and capabilities, so that any impediments on the use of such climate forecasts can be overcome.

Recommendations

The objective of this study was to examine the interseasonal variability of Eastern Africa rainfall on the hypothesis that it is a major climatic phenomenon exhibiting large scale, well-organized characteristics occurring fairly regularly. As such, it should therefore be susceptible to a reasonable degree of empirical and semi-objective analysis for predictability purposes. The results were positive and it is hoped this research will stimulate and encourage additional research into these phenomena in not only Eastern Africa but other tropical regions around the globe.

This study was intended to be user oriented and it is hoped that the forecasting flowcharts provided in Chapter VII will be put to immediate use in the region by a variety of users. However, any scientific study which is supported and refined through continued research has a stronger basis for its application. Therefore, the following recommendations for further research should be considered to improve upon the results found:

1. This study identified stations within each region that presented the most identifiable patterns of ITCZ-associated rainfall. However, local forecasters may be able to adjust the size of each region or buffer zones in between them to maximize the statistical relationships found for their own particular applications.
2. Local forecasters also need to apply both the forecasting tools provided in this study as well as local forecasting techniques which may apply to smaller scale regions. It must be remembered that the study deleted some stations from the original analyses whose annual rainfall patterns did not conform to what was expected from ITCZ-associated rainfall. Therefore, forecasters for these locations (most of which were located either near the coast or in high terrain) need to identify whether or not synoptic or terrain influences affect their local climate. If so, they need to supplement the application of the forecasting tools provided in this study with their own local forecasting knowledge.
3. Due to the large scale climatic and smaller scale synoptic influences which affect the low-level moisture transport into the

region, this forecasting methodology may only work in Eastern Africa. However, it may also apply in other tropical regions with similar ITCZ movements, air mass characteristics, and climatic controls. Suggested areas of study to examine this possibility are West Africa, the Australian interior, the Indian subcontinent, and the Amazon Basin of South America. If this same relationship were found in West Africa, a side benefit of providing seasonal rainfall forecasts may include improved Atlantic tropical storm forecasts, since current researchers believe them to be significantly correlated with the amount of rainfall received over West Africa.

4. Stronger relationships were found when forecasting for the SR and AR regions during extreme phases of the SOI. However, due to the limited number of years available on which to base the comparisons, the significance of the relationships decreased. As a result, it was concluded it would not be statistically valid to incorporate these into the forecast decision flowcharts. However, these relationships should be further examined using additional years of data in order to confirm the strengthened relationships found.

5. The ASP indices data and the BR rainfall data were concluded to be significantly correlated with each other. However, the lack of 30 years of ASP data limited the statistical significance of this relationship. This relationship should be examined further using all available years of ASP data (1950-present).

6. Very significant results were found when forecasting for the SR region when the ASP was in its positive phase during the Boreal summer. These results should be investigated synoptically, using current data, to further enhance the forecasting ability when using this methodology.

REFERENCES

- Adams, M. E., 1983: Nile water: a crisis postponed, *Economic Development & Cultural Change*, 31 (4), 639-643.
- Barnston, A. G., and R. E. Livezey, 1987: Classification, seasonality and persistence of low-frequency atmospheric circulation patterns. *Mon. Wea. Rev.*, 115, 1083-1126.
- Bhatt, N. S., 1989: Circulation regimes of rainfall anomalies in the African-South Asian monsoon belt. *J. Climate*, 2, 1133-1144.
- Bradley, R. S. 1988: The explosive volcanic eruption signal in the northern hemisphere continental temperature records. *Clim. Change*, 12, 221-243.
- Brooks, C. E. P., and N. Carruthers, 1953: *Handbook of Statistical Methods in Meteorology*. Her Majesty's Stationery Office, 412 pp.
- Butzer, K. W., G. L. Isaac, J. L. Richardson, C. Washbourn-Kamau, 1972: Radiocarbon dating of East African lake levels. *Science*, 175, 1069-1076.
- Cadet, D. L., and B. C. Diehl, 1984: Interannual variability of surface fields over the Indian Ocean during recent decades. *Mon. Wea. Rev.*, 112, 1921-1935.
- Critchfield, H. J., 1983: *General Climatology*. Prentice Hall, 453 pp.
- Crowley, T. J., and G. R. North, 1991: *Paleoclimatology*. Oxford University Press, 349 pp.
- Duncan, D. E., 1996: Volcanoes. *Life*, 261, 52-63.
- Dyer, T. G. J., 1979: Rainfall along the east coast of southern Africa, the southern oscillation, and the latitude of the subtropical high pressure belt. *Quart. J. Roy. Meteor. Soc.*, 105, 445-451.
- El-Fandy, M. G., Z. H. Ashour, and S. M. Taiei, 1994: Time series models adoptable for forecasting Nile floods and Ethiopian rainfalls. *Bull. Amer. Meteor. Soc.*, 75, 83-94.
- Farmer, G., 1988: Seasonal forecasting of the Kenya coast short rains. *J. Climatol.*, 8, 489-497.
- Faure, H., and M. Leroux, 1990: Are there solar signals in the African monsoon and rainfall? *Phil. Trans. R. Soc.*, A 330, 575.
- Findlater, J., 1971: Observational aspects of the low-level cross-equatorial jet stream, *Pure Appl. Geophys.*, 115, 1251-1262.
- Fleer, H. E., 1981: Teleconnections of Rainfall Anomalies in the Tropics. *Monsoon Dynamics*, Cambridge University Press, 5-18.
- Flohn, H., 1965: *Studies on the meteorology of tropical Africa*. Bonner Meteorologische Abhandlungen, Bonn, 57 pp.

- Flohn, H., 1983: Der Katastrophenregen 1961/62 und die Wasserbilanz des Viktoria-See-Gebietes. *Wiss. Ber. Meteor. Inst. Karlsruhe*, 4, 17-34.
- Flohn, H., 1986: Indonesian droughts and their teleconnections. *Berliner Geogr. Studien*, 20, 251-265.
- Flohn, H., 1987: Rainfall teleconnections in northern and northeastern Africa. *Theor. Appl. Climatology*, 38, 191-197.
- Geary, R. C., 1935: The ratio of the mean deviation to the standard deviation as a test of normality. *Biometrika*, 27, 310.
- Griffiths, J. F., 1962: *The climate of East Africa*. The Natural Resources of East Africa, East African Literature Bureau, 20 pp.
- Griffiths, J. F., 1972: *Climates of Africa*. World Survey of Climatology, 10, 604 pp.
- Griffiths, J. F., 1990: *The ASEAN User's Manual for the ASEAN Climatic Atlas and Compendium of Climatic Statistics*. ASEAN Secretariat, Jakarta, 430 pp.
- Grotjahn, R., 1993: *Global Atmospheric Circulations, Observations and Theories*. Oxford University Press, 430 pp.
- Hadley, G., 1735: Concerning the cause of the general trade winds. *Phil. Trans.*, 29, 58-62.
- Hastenrath, S., 1986: On climate prediction in the tropics. *Bull. Amer. Meteor. Soc.*, 67, 697-702.
- Hastenrath, S., 1995: Recent advances in tropical climate prediction. *J. Climate*, 8, 1519-1532.
- Hastenrath, S., A. Nicklis, and L. Greischar, 1993: Atmospheric-hydrospheric mechanisms of climate anomalies in the western equatorial Indian Ocean. *J. Geophys. Res. Oceans*, 98 (C11), 20219-20235.
- Hays, J. D., J. Imbrie and N. Shackleton, 1976: Variations in Earth's orbit: pacemaker of the ice ages. *Science*, 194, 1121-1132.
- Hsu, D. F., and J. M. Wallace, 1976: The global distribution of the annual and semiannual cycles in precipitation. *Mon. Wea. Rev.*, 109, 2080-2092.
- Huschke, R. E., 1959: *Glossary of Meteorology*. American Meteorological Society, 638 pp.
- Hutchinson, M. F., H. A. Nix, and J. P. McMahon, 1995: *Africa: A Topographical and Climatic Database*. Centre for Resource and Environmental Studies. Australian Nat. Univ., Ver. 1.0, CDROM.
- Hutchinson, P., 1992: The southern oscillation and the prediction of 'Der' season rainfall in Somalia. *J. Climate*, 5, 525-531.
- Imbrie, J., and J. Z. Imbrie, 1980: Modeling the climatic response to orbital variations. *Science*, 207, 943-953.
- Janowiak, John E., 1988: Investigation of interannual rainfall variability in Africa. *J. Climate*, 1 (3), 240-255.

- Johnson, D. H., 1962: Rainfall in East Africa. *Quart. J. Roy. Meteorol. Soc.*, **88**, 1-19.
- Kapala, A., K. Born, and H. Flohn, 1994: Monsoon anomaly or an El Nino event at the equatorial Indian Ocean? Catastrophic rains 1961/62 in East Africa and their teleconnections. *Proceedings of the International Conference on Monsoon Variability and Prediction*, WMO/TD-No. 619, 119-126.
- Kazarian, R., 1977: Possible link noted between monsoons in India and winds over Kenya. *Environmental Conservation*, **4** (4), 301.
- Kidson, J. W., 1977: African rainfall and its relation to the upper air circulation. *Quart. J. Roy. Meteor. Soc.*, **103**, 441-456.
- Klein, W. H., 1983: Objective specification of monthly mean surface temperature from mean 700 mb heights. *Mon. Wea. Rev.*, **111**, 674-691.
- Kulshrestha, S. M., 1995: Climate change studies: need for a refocusing. *Current Science*, **68** (12), 1208-1213.
- Kutzbach, J. E., 1981: Monsoon climate of the early Holocene: climatic experiment using the Earth's orbital parameters for 9000 years ago. *Science*, **214**, 59-61.
- Kutzbach, J. E., 1983: Monsoon rains of the late Pleistocene and early Holocene: Patterns, intensity and possible causes of changes. Variations in the Global Water Budget. *Dordrecht*, 371-389.
- Lorenz, E. N., 1967: *The Nature and Theory of the General Circulation of the Atmosphere*. WMO/TD-No. 218, 115 pp.
- Lutgens, F. K., and E. J. Tarbuck, 1986: *The Atmosphere - An Introduction to Meteorology*. Prentice-Hall, 492 pp.
- Meehl, G. A., 1987: The annual cycle and interannual variability in the tropical Pacific and Indian Ocean regions. *Mon. Wea. Rev.*, **115**, 27-50.
- National Climatic Data Center, 1994: *Global Tropical/Extratropical Cyclone Climatic Atlas*. Ver. 1.0, CDROM.
- Newell, R. E., J. W. Kidson, D. C. Vincent, and G. J. Boer, 1972: *The General Circulation of the Tropical Atmosphere and Interaction with Extratropical Latitudes*. Vol. 1, MIT Press, 258 pp.
- Nicholson, S. E. and H. Flohn, 1980: African environmental and climatic changes and the general atmospheric circulation in the late Pleistocene and Holocene. *Climate*, **2**, 313-348.
- Nicholson, S. E., 1981: Rainfall and atmospheric circulation during drought periods and wetter years in West Africa. *Mon. Wea. Rev.*, **109**, 2191-2208.
- Nicholson, S. E., 1986a: The nature of rainfall variability in Africa south of the equator. *J. Climatol.*, **6**, 515-530.
- Nicholson, S. E., 1986b: The spatial coherence of African rainfall anomalies: interhemispheric teleconnections. *J. Climate and Appl. Meteor.*, **25**, 1365-1381.

- Nieuwolt, S., 1977: *Tropical Climatology-An Introduction to the Climates of the Low Latitudes*. John Wiley and Sons, 207 pp.
- Ogalllo, L. J., 1979: Rainfall variability in Africa. *Mon. Wea. Rev.*, 107, 1133-1139.
- Penland, C., and T. Magorian, 1993: Prediction of Nino 3 sea surface temperatures using inverse modeling. *J. Climate*, 6, 1067-1076.
- Prell, W. and E. Van Campo, 1986: Coherent response of Arabian Sea upwelling and pollen transport to late Quaternary monsoonal winds. *Nature*, 323, 526-528.
- Quinn, W. H., D. O. Zopf, K. S. Short, and R. T. W. Yang Kuo, 1978: Historical trends and statistics of the Southern Oscillation, El Nino, and Indonesian droughts. *Fish. Bull.*, 76, 663-678.
- Ramage, C. S., 1995: *Forecasters Guide to Tropical Meteorology*. AWS/TR-95/001, 392 pp.
- Rasmusson, E. M., and T. H. Carpenter, 1982: Variations in tropical sea surface temperature and surface wind fields associated with the southern oscillation/El Nino. *Mon. Wea. Rev.*, 110, 354-384.
- Reverdin, G., D. L. Cadet, and D. Gutzler, 1986: Interannual displacements of convection and surface circulation over the equatorial Indian Ocean. *Q. J. Royal Met. Soc.*, 112, 43-67.
- Riehl, H., 1954: *Tropical Meteorology*. McGraw-Hill, 406 pp.
- Rowell, D. P., J. M. Ininda and M. N. Ward, 1994: The impact of global sea surface temperature patterns on seasonal rainfall in East Africa. *Proceedings of the International Conference on Monsoon Variability and Prediction*, WMO, 822 pp.
- Sear, C. B., P. M. Kelly, P. D. Jones, and C. M. Goodess, 1987: Global surface-temperature responses to major volcanic eruptions. *Nature*, 330, 365-376.
- Shanin, M., 1985: *Hydrology of the Nile Basin*. Elsevier, 203 pp.
- Stevens, M. J., 1997: *Optimal Estimation of Surface Temperature Response to Natural and Anthropogenic Climate Forcings Over the Past Century*. Dissertation, Texas A&M Univ., 157 pp.
- Stommel, H., and E. Stommel, 1981: The year without a summer. *Sci. Amer.*, 240, 176-186.
- Stone, R. C., G. L. Hammer, and T. Marcussen, 1996: Prediction of global rainfall probabilities using phases of the southern oscillation index. *Nature*, 384, 252-255.
- Stothers, R. B., 1984: The great Tambora eruption in 1815 and its aftermath. *Science*, 224, 1191-1198.
- Street-Perrott, F. A., and A. T. Grove, 1976: Environmental and climatic implications of late Quaternary lake-level fluctuations in Africa. *Nature*, 261, 385-390.

Street-Perrott, F. A. and N. Roberts, 1983: Fluctuations in closed-basin lakes as an indicator of past atmospheric circulation patterns. *Dordrecht*, 331-345.

Street-Perrott, F. A., J. F. Mitchell, D. S. Marchand and J. S. Brunner, 1990: Milankovich and albedo forcing of the tropical monsoons: A comparison of geological evidence and numerical simulations for 9000 yBP. *Transactions of the Royal Society of Edinburgh - Earth Sciences.*, 407-427.

Tadesse, T., 1994: Summer monsoon seasonal rainfall of Ethiopia in ENSO episodic years. *National Meteorological Services Agency Agromet Bulletin*, 2, 48-55.

Trenberth, K. E., 1997: The definition of El Nino. *Bulletin of the Amer. Met. Soc.*, 78 (12), 2771-2777.

Tyson, P. D., 1984: The atmospheric modulation of extended wet and dry spells over South Africa. *J. Climatol.*, 4, 621.

Tyson, P. D., T. G. J. Dyer, and M. N. Mametse, 1975: Secular changes in South African rainfall: 1880-1972. *Quart. J. Roy. Meteor. Soc.*, 101, 817.

United Nations, 1970: *Integrated River Basin Development: Report of a Panel of Experts*. Rev. Ed., United Nations, 552 pp.

United States Air Force Environmental Technical Applications Center, 1992: *DTED (Digital Terrain Elevation Data) Study*, USAFETAC/PR-92/002, Air Weather Service, 54 pp.

Van Riper, J. E., 1971: *Man's Physical World*, McGraw-Hill, 302 pp.

Walker, G., 1924: Correlation in seasonal variations of weather. *Mem. India Meteor. Dept.*, 24, 75-332.

Waterbury, J., 1979: *Hydropolitics of the Nile Valley*, Syracuse University Press, 296 pp.

Webster, P. J., and H. R. Chang, 1988: Equatorial energy accumulation and emanation regions: impacts of a zonally varying basic state. *J. Atmos. Sci.*, 45, 803-829.

Winstanley, D., 1985: Africa in drought: a change of climate? *Weatherwise*, 38 (2), 74-81.

APPENDIX A

STATION LOCATION TABLES AND GRAPHS FOR EACH REGION

Table A-1. Location listing for stations within the Long Rains (LR) region. Station numbers correspond to the location numbers printed on Figures 27 and A-1.

Station #	Station Name	Latitude	Longitude
1	Arusha	-3.33	36.62
2	Bagamoyo	-4.30	37.50
3	Bukoba	-1.33	31.82
4	Embu	-0.50	37.45
5	Entebbe	0.00	32.40
6	Fataki	2.00	30.60
7	Fort Hall	0.70	37.00
8	Fort portal	0.60	30.30
9	Garissa	-0.47	39.63
10	Igabiho Estate	-1.80	31.60
11	Kagondo Mission	-1.60	31.70
12	Kampala	0.32	32.62
13	Kibosho Mission	-3.30	37.30
14	Kisumu	-0.10	34.75
15	Kitui	-1.30	38.00
16	Kome Mission	-2.30	32.40
17	Lokitaung	4.20	35.50
18	Lushoto Agric.	-4.80	38.30
19	Machakos	-1.50	37.20
20	Makindu	-2.28	37.83
21	Marsabit	2.30	37.90
22	Masindi	1.68	31.72
23	Mazumbai Estate	-4.80	38.50
24	Mbarara	-0.62	30.65
25	Meru	0.08	37.65
26	Mombasa	-4.03	39.62
27	Moshi met.	-3.40	37.30
28	Moyale	3.53	39.05
29	Musoma	-1.50	33.80
30	Nairobi/Kabete	-1.30	36.80
31	Nairobi/Kenyatt	-1.32	36.92
32	Nairobi/Wilson	-1.32	36.82
33	Namasagali	1.00	32.90
34	Rombo Mission	-3.20	37.60
35	Tarime	-1.40	34.40
36	Tororo	0.68	34.17
37	Voi	-3.40	38.57

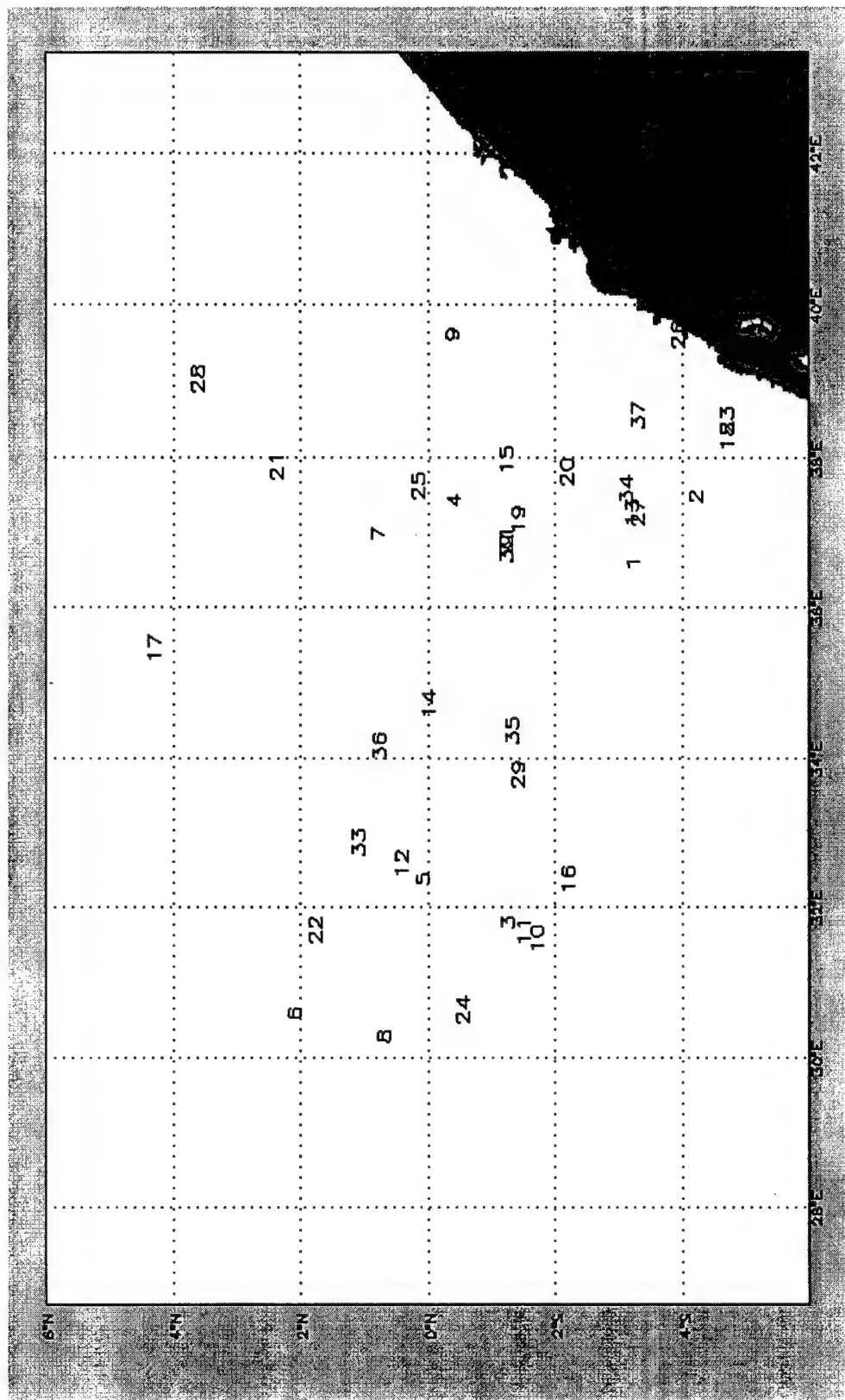


Fig. A-1. Graph depicting the location of stations within the Long Rains (LR) region.
Table A-1 presents a listing of station information.

Table A-2. Location listing for stations within the Boreal Rains (BR) region. Station numbers correspond to the location numbers printed on Figures 28 and A-2.

Station #	Station Name	Latitude	Longitude
1	Abdel Magid	14.80	32.80
2	Abu Deleiq	15.90	33.80
3	Abu Quta	14.90	32.70
4	Addis Ababa	8.98	38.80
5	Adi Ugri	14.10	38.80
6	Agordat	15.60	37.90
7	Aroma	15.83	36.15
8	Asmara	15.28	38.92
9	Bahar Dar	11.60	37.40
10	Bara	13.70	30.30
11	Barakat	14.30	33.50
12	Barakat(HQ)	14.30	33.50
13	Bolein	13.90	33.50
14	Dubeiba	14.90	33.00
15	El Geteina	14.80	32.30
16	El Masid	15.20	32.90
17	Er Rahad	12.70	30.60
18	Fangak	9.00	30.80
19	Fashashoya	13.40	32.50
20	Fatisa	14.60	32.20
21	Futeis	14.50	33.10
22	Gambela	8.20	34.50
23	Gedaref	14.03	35.40
24	Ghadambaliya	14.00	34.90
25	Hag Abdullah	13.90	33.60
26	Harar Meda	8.73	39.00
27	Hawata	13.40	34.60
28	Jebel Aulia	15.20	32.50
29	Jebelein	12.50	32.80
30	Kamlin	15.00	33.10
31	Kassawi	14.70	32.90
32	Kemeir	14.90	32.70
33	Keren	15.80	38.50
34	Khartoum	15.60	32.55
35	Kodok	9.80	32.10
36	Kologi	10.50	30.60
37	Kosti	13.17	32.67
38	Kurmuk	10.80	34.40
39	La'ota	15.20	32.90
40	M.C.K. 169	14.90	33.10
41	Manaqil	14.20	33.00
42	Medina S.G.B.	14.30	33.30
43	Melut	10.30	32.10

Table A-2 Continued.

Station #	Station Name	Latitude	Longitude
44	Qoz Khadra	12.60	31.70
45	Qundal(Sid)	13.70	33.50
46	Qurashi	14.70	33.20
47	Rashad	11.87	31.05
48	Renk	11.75	32.78
49	Roseires	11.80	34.30
50	Rufa'a	14.70	33.30
51	Sennar	13.55	33.62
52	Shabasha	14.10	32.20
53	Sherkeila	12.80	31.40
54	Showak	14.22	35.85
55	Sibu Sire	9.00	36.90
56	Sudeira	15.10	32.80
57	Tabat	14.60	33.00
58	Tabat K55	14.60	33.10
59	Talodi	10.60	30.40
60	Talodi M. A.	10.60	30.50
61	Tuleih	14.40	33.30
62	Umm Udam	14.60	33.10
63	Umm Gerr	13.80	32.40
64	Umm Gir	14.30	33.20
65	Umm Ruwaba	12.80	31.20
66	Wad Bilal	14.60	33.30
67	Wad El Haddad	13.80	33.50
68	Wad Hussein	14.60	33.10
69	Wad Nimr	14.50	32.10
70	Wad Nu'man	14.10	33.40
71	Wonji	8.50	39.30

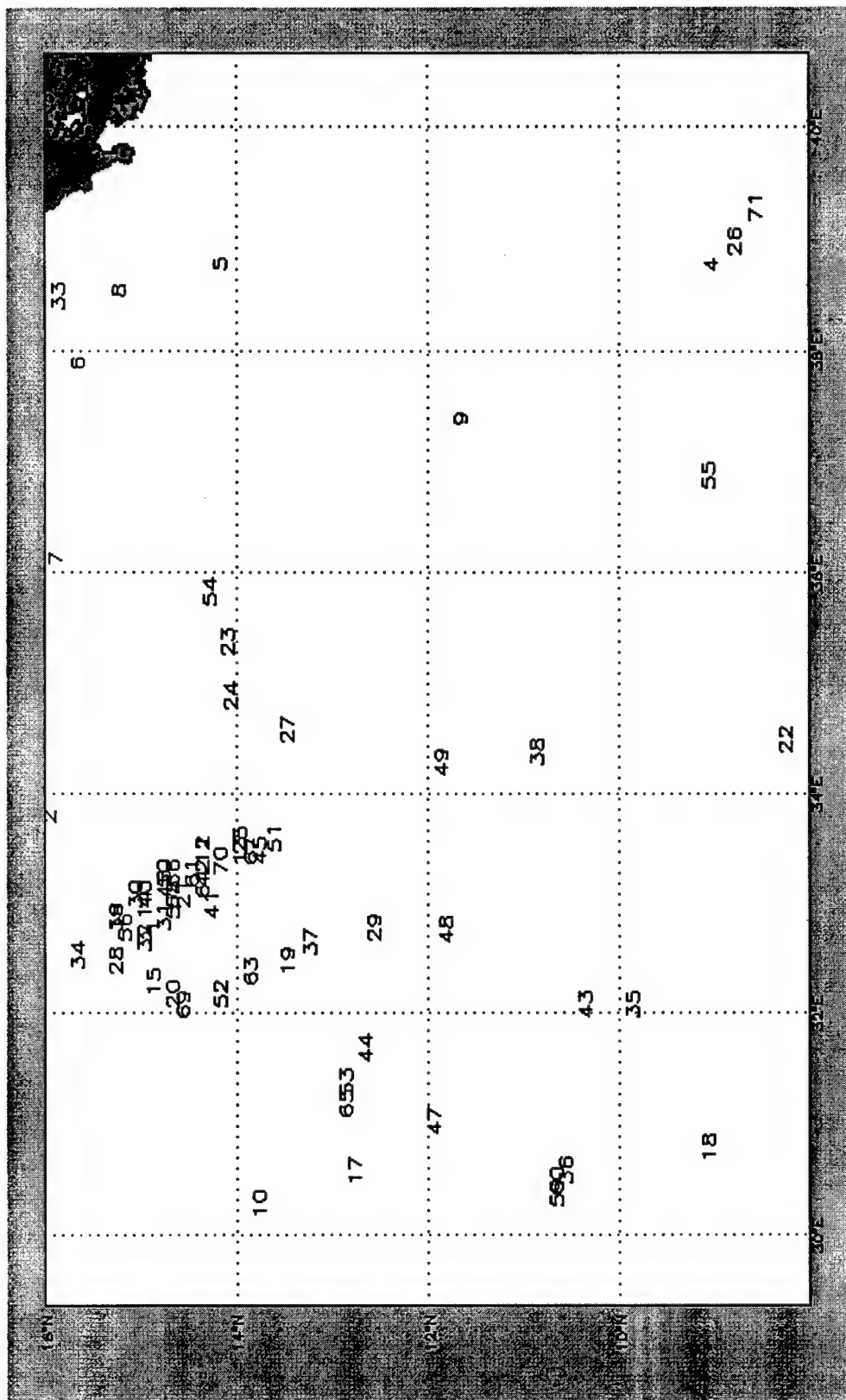


Table A-3. Location listing for stations within the Short Rains (SR) region. Station numbers correspond to the location numbers printed on Figures 29 and A-3.

Station #	Station Name	Latitude	Longitude
1	Arusha	-3.33	36.62
2	Bukoba	-1.33	31.82
3	Embu	-0.50	37.45
4	Fataki	2.00	30.60
5	Fort Hall	0.70	37.00
6	Fort Portal	0.60	30.30
7	Garissa	-0.47	39.63
8	Igabiro Estate	-1.80	31.60
9	Kagondo Mission	-1.60	31.70
10	Kampala	0.32	32.62
11	Kitui	-1.30	38.00
12	Kome Mission	-2.30	32.40
13	Machakos	-1.50	37.20
14	Makindu	-2.28	37.83
15	Marsabit	2.30	37.90
16	Masindi	1.68	31.72
17	Mbarara	-0.62	30.65
18	Meru	0.08	37.65
19	Moyale	3.53	39.05
20	Musoma	-1.50	33.80
21	Nairobi/Kabete	-1.30	36.80
22	Nairobi/Kenyatta	-1.32	36.92
23	Nairobi/Wilson	-1.32	36.82
24	Namasagali/B.G.	1.00	32.90
25	Rombo Mission	-3.20	37.60
26	Tarime	-1.40	34.40
27	Voi	-3.40	38.57



Fig. A-3. Graph depicting the location of stations within the Short Rains (SR) region.
Table A-3 presents a listing of station information.

Table A-4. Location listing for stations within the Austral Rains (AR) region. Station numbers correspond to the location numbers printed on Figures 30 and A-4.

Station #	Station Name	Latitude	Longitude
1	Alto Molocue	-15.60	37.60
2	Atondwe Mission	-15.30	30.30
3	Chasefu	-11.90	33.10
4	Chibwa	-11.10	31.40
5	Chicoa	-15.40	32.20
6	Chinsali	-10.50	32.00
7	Chipata	-13.55	32.58
8	Chitambo	-12.90	30.60
9	Chiuta	-15.50	33.20
10	Cuamba	-14.82	36.53
11	Entre rios	-14.90	37.40
12	Eregoiile	-16.00	37.10
13	Feira	-15.60	30.40
14	Fingoe	-15.10	30.80
15	Furancungo	-14.90	33.60
16	Ifakara	-8.10	36.60
17	Ilondola Mission	-10.90	31.80
18	Isoka	-10.12	32.63
19	Kala	-8.10	31.00
20	Kapati	-9.70	30.70
21	Kasama	-10.22	31.13
22	Kayambi	-9.40	31.90
23	Kilwa	-8.70	39.40
24	Lichinga	-13.28	35.25
25	Lindi	-10.00	39.70
26	Lituhi	-10.50	34.60
27	Liuli	-11.00	34.60
28	Liwale	-9.70	37.90
29	Lundazi	-12.28	33.20
30	Madibira Mission	-8.20	34.80
31	Mahenge	-8.60	36.70
32	Malangali	-8.50	34.90
33	Maniamba	-12.70	34.90
34	Marrupa	-13.73	37.55
35	Masasi	-10.70	38.80
36	Maua	-13.80	37.10
37	Mbala	-8.85	31.33
38	Mbesuma	-10.00	32.10
39	Mbeya	-8.93	33.47
40	Milo	-9.80	34.60
41	Montepuez	-13.10	39.00
42	Mpika	-11.90	31.43
43	Mporokoso	-9.40	30.10

Table A-4 Continued.

Station #	Station Name	Latitude	Longitude
44	Msoro	-13.60	31.90
45	Muecate	-14.90	39.60
46	Mueda	-11.60	39.50
47	Mulobola	-10.60	31.00
48	Musekera	-9.30	33.60
49	Nachingwea	-10.35	38.75
50	Namapa	-13.70	39.80
51	Nametil	-15.70	39.30
52	Nampula	-15.10	39.28
53	Njombe	-9.30	34.70
54	Nove Freizo	-14.80	36.50
55	Petauke	-14.25	31.28
56	Ribaue	-14.90	38.20
57	Rosa Mission	-9.60	31.40
58	Santa Maria	-11.10	30.00
59	Serenje	-13.23	30.22
60	Shiwa Ngandu	-11.10	31.70
61	Songea	-10.68	35.58
62	Tunduru	-11.10	37.30
63	Utete	-8.00	38.70
64	Vila Coutinho	-14.50	34.30
65	Vila Vasco Da Gama	-14.90	32.20
66	Zumbo	-15.62	30.43

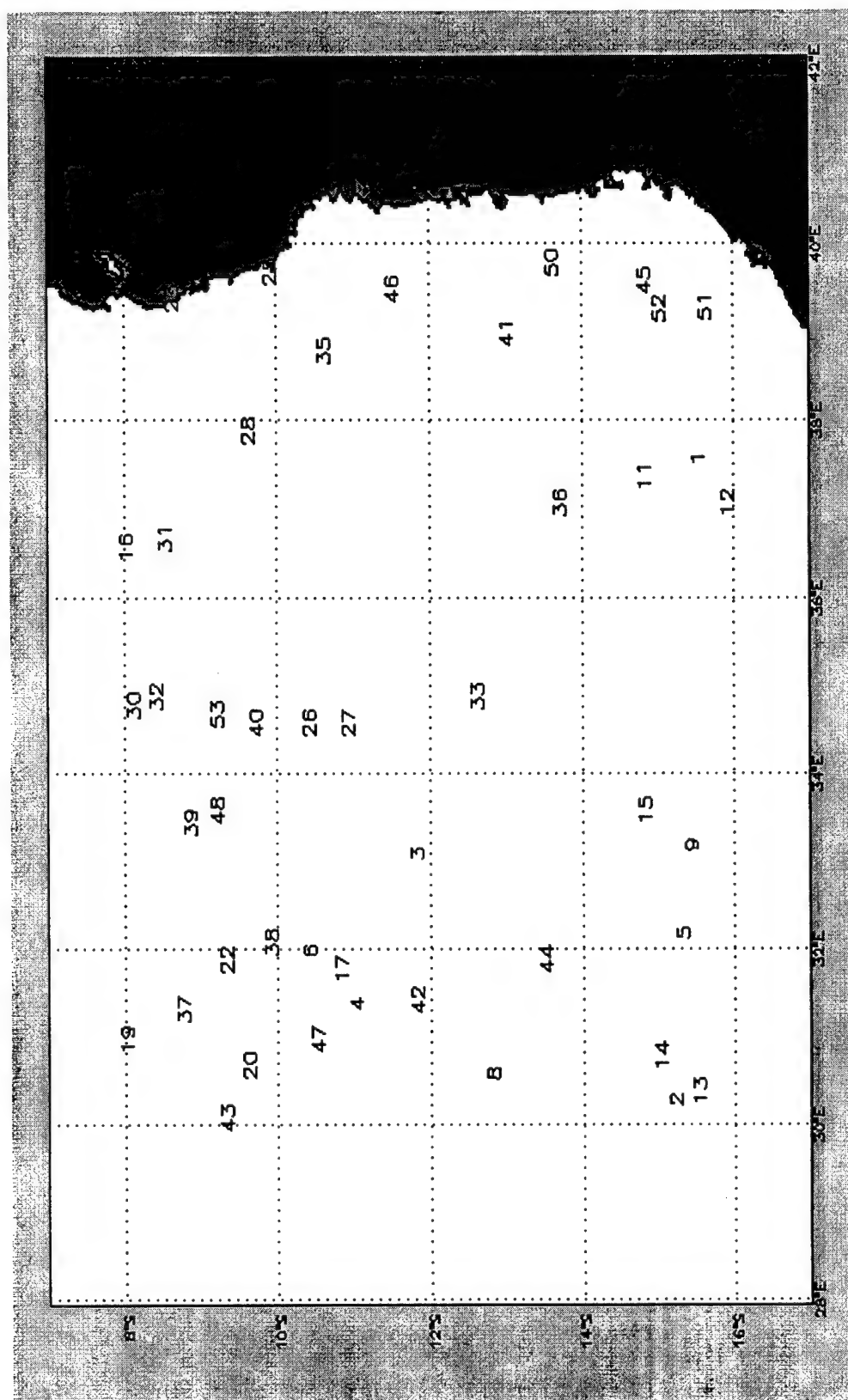


Fig. A-4. Graph depicting the location of stations within the Austral Rains (AR) region.
Table A-4 presents a listing of station information.

APPENDIX B
CORNU CRITERION PROBABILITY LIMITS

Table B-1. Cornu Criterion probability limits for n=10 through n=41.

Sample Size	Upper 1%	Upper 5%	Lower 5%	Lower 1%
10	0.940	0.911	0.714	0.664
11	0.936	0.907	0.715	0.668
12	0.932	0.904	0.717	0.671
13	0.927	0.900	0.719	0.674
14	0.923	0.896	0.720	0.677
15	0.918	0.892	0.722	0.680
16	0.914	0.888	0.724	0.683
17	0.911	0.886	0.725	0.685
18	0.908	0.884	0.726	0.688
19	0.906	0.881	0.728	0.690
20	0.903	0.879	0.728	0.693
21	0.900	0.877	0.730	0.695
22	0.898	0.875	0.732	0.697
23	0.896	0.874	0.733	0.699
24	0.894	0.872	0.734	0.700
25	0.892	0.870	0.735	0.702
26	0.890	0.869	0.736	0.704
27	0.889	0.867	0.737	0.705
28	0.887	0.866	0.738	0.707
29	0.886	0.865	0.739	0.708
30	0.884	0.864	0.740	0.710
31	0.883	0.863	0.740	0.711
32	0.882	0.862	0.741	0.712
33	0.880	0.861	0.742	0.713
34	0.879	0.860	0.743	0.714
35	0.878	0.859	0.743	0.716
36	0.877	0.858	0.744	0.717
37	0.876	0.857	0.745	0.718
38	0.875	0.856	0.745	0.719
39	0.874	0.856	0.746	0.720
40	0.873	0.855	0.746	0.721
41	0.872	0.854	0.747	0.722

APPENDIX C

THEORY ON THE 1961 SHORT RAINS HEAVY RAINFALL EVENT

The 1961 SR season datum was deleted from this research since it was such an extreme outlier. This study suspects the 1961 event was associated with a rare sequence of events across the Pacific and Indian Oceans which occurred over a time span of two to three years. Since these events did not relate directly to the objectives of this study, they are presented separately in this appendix. The purpose is to only suggest that these events may have contributed to the extreme 1961 event and to encourage research on the subject.

In Figure C-1, solar insolation was near a record peak in 1958 and extremely high for several years thereafter. In Figure C-2, stratospheric aerosols were very low in 1958 and 1959, thus allowing a maximum of insolation in the equatorial region. This increased heating may have led to increased warming of the Equatorial Pacific warm pool. During El Nino years, this warm pool would be released back across the Eastern Pacific toward the South American coast. However, if an El Nino event does not occur, some of this warm water is thought to continue westward and mix into the warm upper layer flow of the thermohaline circulation (Fig. C-3).

Since no El Nino event or reversal of the Walker Circulation occurred in 1958 or 1959, it is suggested that this warm water may have moved very slowly with the thermohaline circulation into the Indian Ocean taking 2-3 years to reach the western side. It is further theorized that this warm water may have contributed to the heavy SR rain event of 1961 over Eastern Africa and also the heaviest recorded monsoon-associated rainfall over the Indian subcontinent within this past century.

Again, this theory is only presented here as a suggestion for further research. Little research exists to confirm this finding, however, all evidence found in this study supports it.

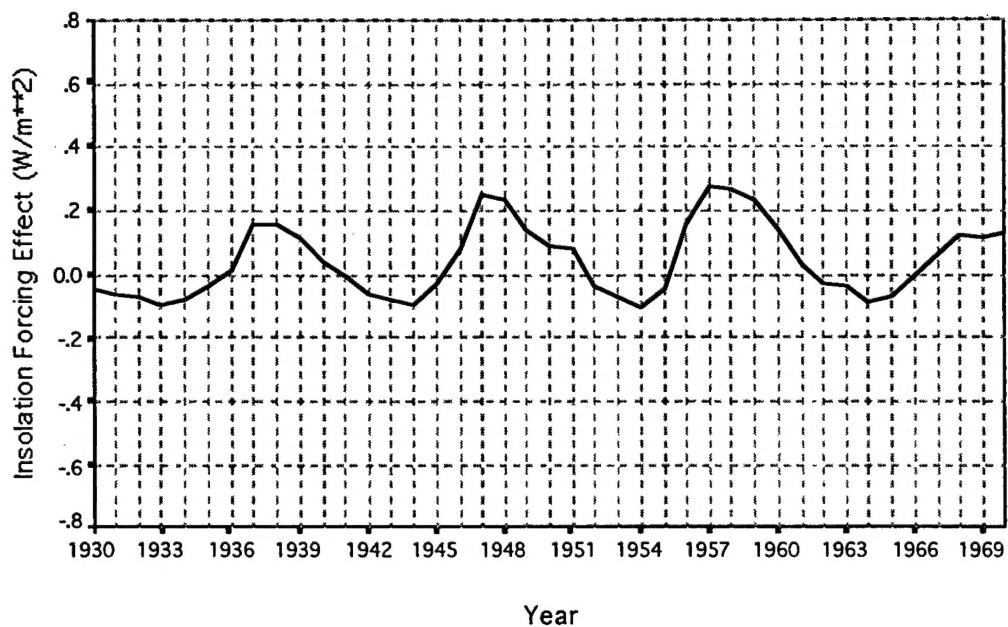


Fig. C-1. Insolation forcing effects from solar parameters.

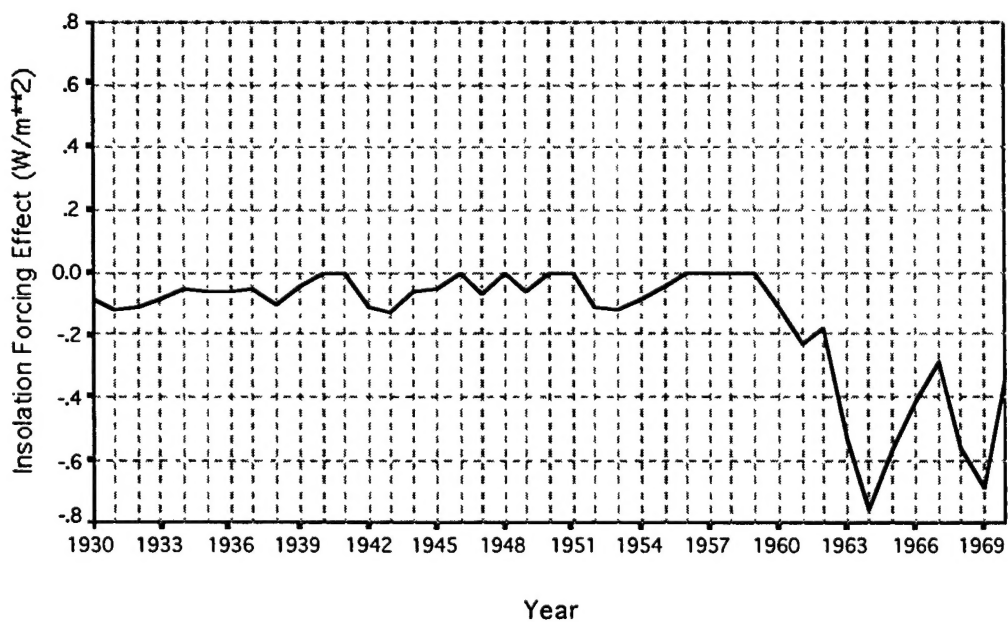


Fig. C-2. Insolation forcing effects from stratospheric aerosols (mostly of volcanic origin).

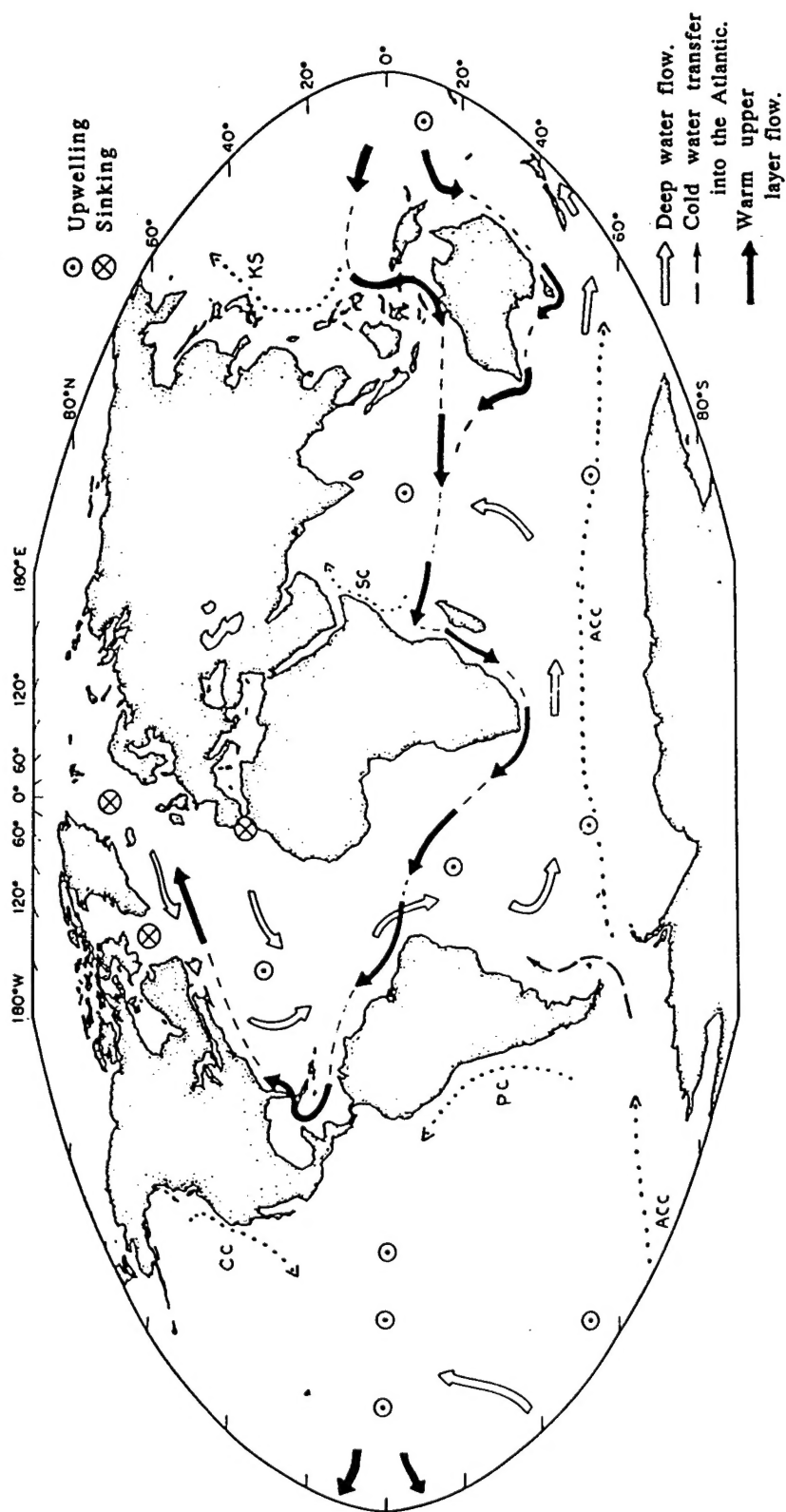


Fig. C-3. The motion of the global scale thermohaline circulation (adapted from Grotjahn, 1993).

VITA

The author, Ronald Paul Lowther, is the son of Leroy and Katherine Lowther of San Antonio, Texas, and was born on February 13, 1957, in Fort Knox, Kentucky. Ron graduated from Judson High School in 1975 in Converse, Texas, and, in November of 1975, he enlisted in the United States Air Force (USAF).

Undergraduate education was received at San Antonio College, the Community College of the Air Force, New Mexico State University, and Chapman College. Ron graduated from the latter institution with a Bachelor of Science degree in Computer Science in February, 1983. In July, 1983, he was commissioned in the USAF and sent to the Naval Post-Graduate School for a one year non-degree meteorological program. After many prestigious assignments, he graduated from Texas A&M University with a Master of Science degree in Meteorology in May, 1989.

Currently holding the rank of Major, Ron is assigned to the U. S. Air Force Institute of Technology (AFIT) and is presently attending Texas A&M University to complete this doctoral study. Upon leaving this institution, he will be assigned to the U. S. Air Force Combat Climatology Center, which is co-located with the National Climatic Data Center in Asheville, North Carolina.

Ron is married to the former Sue Ju Fang of Taipei, Taiwan. They have two of the best children anyone could ask for: Jeffrey, born October 13, 1979, and James, born December 10, 1981. As his father moves on to another assignment, Jeffrey will follow in his father's footsteps by becoming an Aggie majoring in Civil Engineering at Texas A&M University. Ron's permanent address is 5139 Redding Drive, San Antonio, Texas, 78219, U.S.A.